Zachos, J.C., Kroon, D., Blum, P., et al., 2004
Proceedings of the Ocean Drilling Program, Initial Reports Volume 208

8. Site 1267[1]

Shipboard Scientific Party[2]

INTRODUCTION

Site 1267 (proposed Site WALV-11B) is located in the Angola Basin near the base of the northwestern flank of Walvis Ridge. At a water depth of 4356 m, the site is 100 m shallower than Deep Sea Drilling Project (DSDP) Site 527 just 10 km to the east, where previous drilling recovered a 341-m-thick section of Neogene, Paleogene, and Maastrichtian sediment. Sediments at Site 527 vary from clays to carbonate-rich oozes and chalks. The Pliocene–Pleistocene section consists of nannofossil oozes and extends to ~100 meters below seafloor (mbsf). The Oligocene–Miocene sequence, primarily carbonate-poor clays, is condensed and contains an unconformity. The Paleocene–Eocene sequence appears complete and consists of nannofossil oozes and chalks and a clay layer. However, only a portion of the Paleocene/Eocene Thermal Maximum (PETM), including a 70-cm-thick clay layer, was recovered at this site (Thomas and Shackleton, 1996; Thomas et al., 1999). A continuous Cretaceous/Paleogene (K/P) boundary was also recovered at DSDP Site 527 (Moore, Rabinowitz, et al., 1984). The basal *Parvularugoglobigerina eugubina* Zone in the Tertiary is well represented (25 cm), and faunas are well preserved. The sediments immediately above basement are of late Maastrichtian age. Site 527 was rotary cored, and, as a consequence, recovery was poor (25%–75%) and much of the core suffered from severe drilling disturbance, particularly the unlithified Neogene and Paleogene oozes.

Our main objective for this site was the recovery of undisturbed sediments recording critical intervals in the early Cenozoic, specifically the K/P boundary, and the following recovery of biota from the mass extinction, the PETM, and the period of global cooling and growth of polar ice caps across the Eocene/Oligocene (E/O) boundary into the earliest Oligocene (early Oligocene Glacial Maximum). We planned to recover 100% of the sedimentary section in multiple holes to make it

[1]Examples of how to reference the whole or part of this volume.
[2]Shipboard Scientific Party addresses.

Ms 208IR-108

possible to establish a cyclostratigraphy and develop an astronomically tuned timescale. We aimed to fully document events across the critical intervals as well as short-lived events such as the mid-Paleocene biotic event (PBE) and episodes of climate fluctuation during the early Eocene Climatic Optimum. Site 1267 is located in water ~400 m shallower than at Site 1262, the deep anchor of the Leg 208 depth transect, and is located close to the calcite compensation depth (CCD), making the site suitable to document fluctuations in the depth of the CCD over the early Cenozoic.

We chose a location where the Neogene section is thin (estimated at ~100 m) to facilitate recovery of much of the Paleogene section using the advanced piston corer (APC) rather than the extended core barrel (XCB). Site 1267 is located on a slightly elevated area on the basin floor where the Paleogene sequence appears to be thickest (GeoB 01-039; common depth point 3566) (Figs. F1, F2). Seismic profiles show two distinct packages of reflectors in the basin, a thin upper package (0–105 ms two-way traveltime [TWT] below seafloor) with low-amplitude reflectors and a thicker lower package of slightly higher-amplitude reflectors (105–280 ms TWT below seafloor) (Fig. F2). The upper package is interpreted as a moderately condensed interval of Neogene calcareous oozes and clays, and the lower package is interpreted as upper Maastrichtian to lower Eocene calcareous oozes and chalks. Two prominent reflectors dissect the lower package. The upper reflector, $R_{P/E}$ (240 ms TWT below seafloor), represents the Paleocene/Eocene (P/E) boundary clay layer estimated at ~216 mbsf (velocity = 1.8 m/ms), whereas the deeper reflector, $R_{K/P}$ (310 ms TWT below seafloor), represents the K/P boundary contact at an estimated depth of ~279 mbsf.

In two holes at Site 1267, we used the APC and XCB systems to obtain nearly 100% of a 330-m-thick sequence of upper Maastrichtian to Pleistocene sediment (see "Leg 208 Summary" chapter). The APC system produced less distorted core than was obtained with the rotary coring system during drilling of Site 527. The upper Maastrichtian and Paleocene–lower Eocene sections are moderately expanded. The middle–upper Eocene, upper Oligocene, and middle Miocene are represented by condensed clay-rich layers. The P/E boundary was recovered using the APC in both holes at ~205 mbsf with no obvious coring disturbance. The K/P boundary was recovered using the XCB in both holes at 283.5 mbsf with minimal coring disturbance (i.e., minor biscuiting).

F1. Locations of Site 1267 and alternate sites, p. 28.

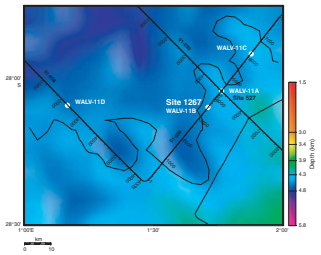

F2. Site 1267 and DSDP Site 527 along line GeoB 01-039, p. 29.

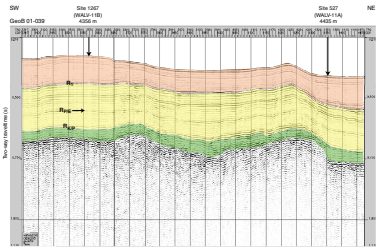

OPERATIONS

Transit to Site 1267

The 43-nmi transit to Site 1267 (proposed Site WALV-11B) was accomplished in 4.4 hr at an average speed of 9.8 kt. The vessel was positioned over the site by 0940 hr on 21 April 2003. The corrected precision depth recorder depth estimate was 4378.4 meters below rig floor (mbrf).

Coring intervals, times, nominal recovery rates, core barrels that required drillover to be released from the sediment, and the deployments of the Advanced Piston Corer Temperature (APCT) tool, Tensor core orientation tool, and nonmagnetic core barrel are listed in Table T1.

T1. Coring summary, p. 60.

Hole 1267A

Hole 1267A was initiated with the bit at 4365.0 mbrf. The seafloor depth estimated by the recovery of the first core barrel was established at 4356.6 mbrf. Piston coring advanced to 236.1 mbsf, where the formation became too indurated to continue with the APC. The bit was advanced by recovery on the last two cores because of incomplete strokes (Cores 208-1267A-24H and 25H). The hole was deepened with the XCB system to the target depth of 312.1 mbsf, which included a sample of the critical P/E and K/P boundary intervals. Active heave compensation was not used because of the fast rate of penetration (average rate of penetration = ~24 m/hr).

The Interstitial Water Sampler (IWS) was deployed for a second time following the conclusion of coring in this hole. The tool was lowered on the coring line to 312.1 mbsf and met with partial success. The internal data logger recorded 2.5 hr of data. The temperature, pressure, and differential pressure data were good, but the system failed to obtain a water sample. An internal software problem was suspected.

Hole 1267B

The bit was pulled clear of the seafloor at 2135 hr on 23 April, and the vessel was offset 20 m south. After obtaining a bottom water temperature with the APCT at 4360 mbrf, Hole 1267B was initiated, with the bit positioned 5 m shallower than its position during the initial mudline attempt at Hole 1267A. The seafloor depth calculated from the 3.1 m of recovery was 4366.4 mbrf. Piston coring advanced to 231.1 mbsf, and the hole was deepened with the XCB to the total approved depth of 329.0 mbsf.

The IWS was lowered on the coring line to 2267 mbrf on two runs to test the water sampler. The first run, between cutting Cores 208-1267B-19H and 20H, was not successful. The pressure fitting in the transducer manifold leaked and caused the sensors to fail. The second deployment was between Cores 208-1267B-32X and 33X. This time, the IWS was successful in obtaining a full set of data on all channels and recovering a water sample. At the conclusion of coring, the IWS was deployed for the last time during the leg. This time, the tool was run on the coring line to the bottom of the hole (329.0 mbsf). The data logger recorded 2.5 hr of temperature and pressure data. A software update appeared to have fixed the sampling program, but no water sample was secured because of a broken soldered joint on the servo motor.

The total cored interval at Site 1267 was 641 m, and the recovered interval was 637 m (average nominal recovery = 99%).

Six downhole temperature measurements (Hole 1267A: 37–123 mbsf) and one bottom water temperature measurement (Hole 1267B) with the APCT yielded an initial temperature gradient estimate of 4.3°C/100 m.

The drill string was recovered, and the beacon was retrieved. The coring line was coated with preservative, and the bottom-hole assembly was deconstructed. After the hydrophones and thrusters were secured, the vessel departed on the long journey to Rio de Janeiro at 1648 hr on 26 April.

COMPOSITE DEPTH

Magnetic susceptibility (MS) and sediment lightness (L*) data collected from Holes 1267A and 1267B at 2.5-cm intervals were used to construct the composite section for Site 1267 (Figs. F3, F4). The MS data were primarily used for core-to-core correlation and to construct the composite section. The depth offsets that define the composite section for Site 1267 are given in Table T2.

The composite data show that the cores from Site 1267 provide a continuous sequence down to 267 meters composite depth (mcd), the base of the last APC core in Hole 1267B (Core 208-1267B-26H; upper Paleocene). The hole-to-hole correlation in the interval between 63 and 75 mcd (Cores 208-1267A-7H and 8H and 208-1267B-8H) is ambiguous due to sediment disturbances. The XCB-cored interval between 267 and 368 mcd is characterized by five gaps in the composite record. The composite depth section below 267 mcd was constructed by using the average growth rate of 13% of the overlying 0- to 267-mcd interval (Fig. F5). Following construction of the composite depth section for Site 1267, a single spliced record was assembled from the aligned core intervals from the two parallel holes (Table T3).

Cores that had been significantly stretched, squeezed, or disturbed by the coring process were not used for the splice. The P/E boundary interval in the composite was taken from Core 208-1267B-23H (231.5 mcd); the K/P boundary interval in the composite was taken from Core 208-1267A-31X (320.3 mcd). The Site 1267 splice can be used as a guide to sample a single sedimentary sequence between 0 and 367.5 mcd and was used to plot other data sets from this site.

LITHOSTRATIGRAPHY

Two holes were cored at Site 1267. Hole 1267A was cored to a depth of 348.8 mcd (311.9 mbsf), and Hole 1267B was cored to 367.8 mcd (329.0 mbsf). The major lithologies consist of various proportions of nannofossil ooze and clay with minor components including foraminifers, volcanic ash, and hematite. Near the bottom of the hole, chalk and porcellanite were encountered. The lithostratigraphic units and subunits at Site 1267 are very similar to those defined at Site 1262, as these sites differ in water depth by only 400 m; however, Site 1267 is marked by less dissolution and congruently higher sedimentation rates than those found at Site 1262.

On the basis of variations in lithologic observations and physical property measurements, we divided the sequence into three major lithostratigraphic units, with Units II and III further subdivided based on additional lithologic characteristics (Table T4; Fig. F6). These observations and measurements are summarized in plots illustrating variation with depth: whole-core magnetic susceptibility, natural gamma radiation (NGR), and sediment density from the multisensor track (MST) (Fig. F7); sediment L*, chromaticity (a* and b*), and carbonate content (Fig. F8); smear slide components (Fig. F9); split-core measurements of grain and bulk density, porosity, and compressional wave (*P*-wave) velocity (Figs. F10, F11); and interstitial water Mn and Fe contents (Fig. F12).

F3. MS data, p. 30.

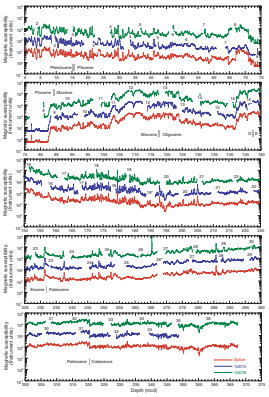

F4. Color reflectance data, p. 31.

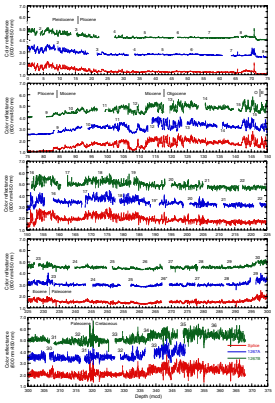

T2. Composite depth scale, p. 62.

F5. Mbsf vs. mcd growth rates, p. 32.

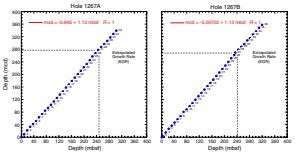

T3. Splice tie points, p. 63.

T4. Lithostratigraphic subdivisions, p. 64.

F6. MS, NGR, carbonate concentration, and L*, p. 33.

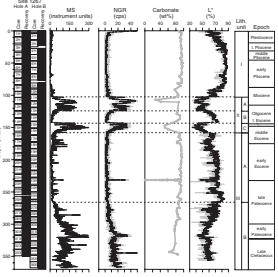

Description of Lithostratigraphic Units

Unit I

Interval: Sections 208-1267A-1H-1 through 10H-7, 0 cm; Sections 208-1267B-1H-1 through 11H-3
Depth: Hole 1267A: 0.0–93.4 mbsf (0.0–102.5 mcd); Hole 1267B: 0.0–91.7 mbsf (0.0–102.3 mcd)
Age: Pleistocene to Miocene
Lithology: nannofossil ooze and foraminifer-bearing nannofossil ooze

Unit I consists dominantly of nannofossil ooze with 92.6 wt% carbonate, which is reflected by relatively low MS and NGR, and light-colored sediments (Figs. F7, F8). Sediments are light brown to very pale brown or light gray, and color alternates on scales of 10–50 cm (Fig. F13). Darker-colored sediment is generally associated with more clay rich lithologies, reflecting periods characterized by a shallower lysocline and CCD in the South Atlantic Ocean. Unit I at Site 1267 is lithologically similar to Unit I at Site 1262 except that the unit thickness at Site 1267 is almost twice that of Site 1262. Difficulties in stratigraphic correlation between Cores 208-1267A-7H and 208-1267B-8H suggest disturbance, although we observed no obvious evidence of downslope transport in these cores.

Physical properties in the uppermost 50 mcd of Unit I differ from the interval below (50–100 mcd). Downhole, increasing bulk density and decreasing porosity in the upper 50 m of Unit I reflect sediment compaction (Fig. F10). Grain density shows a steplike increase from ~2.6 to 2.7 g/cm^3 at ~50 mcd. Below this level, Unit I is marked by relatively high grain density and porosity and low bulk density. In the lower part of Unit I (~82–102.3 mcd), sediments become slightly more clay rich, as indicated by a small increase in MS and a decrease in L* (Fig. F6). Discrete measurements of density (moisture and density bulk density) correlate well with gamma ray attenuation bulk density measured with the MST (Fig. F11). A weak correlation exists between bulk density and grain density and, similar to Site 1262, a good linear correlation (r^2 = 0.8) exists between increasing bulk density and decreasing porosity. A relatively good correlation (r^2 = 0.69) exists between bulk density and *P*-wave velocity.

Unit II

Interval: 208-1267A-10H-7, 0 cm, through 15H-7, 48 cm; Sections 208-1267B-11H-3 through 16H-5, 30 cm
Depth: Hole 1267A: 93.4–141.9 mbsf (102.5–155.6 mcd); Hole 1267B: 91.7–142.4 mbsf (102.3–157.8 mcd)
Age: Miocene to middle Eocene
Lithology: clay, hematite-bearing clay, nannofossil clay, clay-bearing nannofossil ooze, nannofossil ooze, and foraminifer-bearing nannofossil ooze.

Unit II consists of an upper and lower subunit dominated by clay and separated by a middle subunit of nannofossil ooze. Similar to Site 1262, MS and NGR values are high, whereas L* is low in the clay-rich subunits (Subunits IIA and IIC), reflecting low carbonate content (48.0 and 54.6 wt%, respectively). Subunit IIB is marked by high carbonate concentra-

F7. MS, NGR, and GRA bulk density, p. 34.

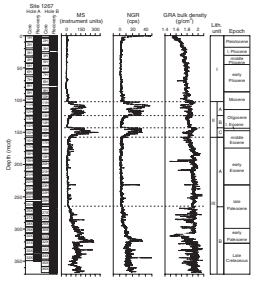

F8. Lightness, carbonate, and chromaticity, p. 35.

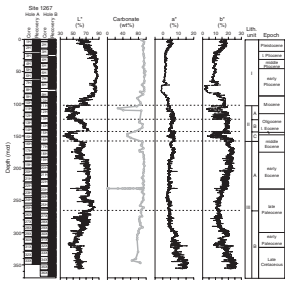

F9. Smear slide components, p. 36.

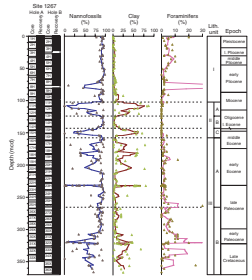

F10. Grain density, bulk density, porosity, and *P*-wave velocity, p. 37.

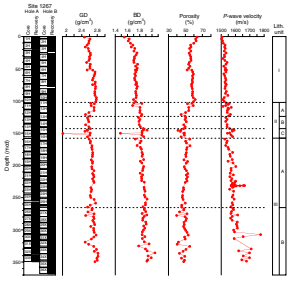

tion (83.5 wt%), which gives rise to lower MS and NGR and higher sediment L* values (Fig. F6). Unlike the sequence at Site 1262, carbonate concentration in Unit II at Site 1267 never decreases to 0 wt%, indicating less dissolution at the shallower water depth of Site 1267. Unit II is thicker at Site 1267 (55.5 mcd) than at Site 1262 (44.2 mcd), but nonetheless, biostratigraphy at both sites suggests that Unit II is a highly condensed interval with pervasive downslope transport, reworking, and dissolution (see "Biostratigraphy," p. 9).

Subunit IIA

Interval: 208-1267A-10H-7, 0 cm, through 12H-CC, 10 cm; Sections 208-1267B-11H-3 through 13H-3, 140 cm
Depth: Hole 1267A: 93.4–113.3 mbsf (102.5–123.3 mcd); Hole 1267B: 91.7–112.0 mbsf (102.3–124.0 mcd)
Age: Miocene to Oligocene
Lithology: clay-bearing nannofossil ooze, nannofossil clay, and hematite-bearing clay

The contact between Unit I and Subunit IIA is abrupt and marked by a pronounced increase in MS and NGR and a decrease in sediment L*. Subunit IIA consists of clay-rich lithologies oscillating on a decimeter scale: dark brown hematite-bearing clay with abundant pinkish blebs of clay-bearing nannofossil ooze, light brown clay-bearing nannofossil ooze, and brown nannofossil clay. Carbonate content is low, averaging 48.0 wt%. Color variations in Subunit IIA reflect alternating concentrations of clay, nannofossils, hematite, and zeolite. *Braarudosphaera* is present in the clay-bearing nannofossil ooze of Core 208-1267A-10H (94.4–103.9 mbsf).

Subunit IIB

Interval: 208-1267A-12H-CC, 10 cm, through 14H-5, 95 cm; 208-1267B-13H-3, 140 cm, through 15H-2, 50 cm
Depth: Hole 1267A: 113.3–129.9 mbsf (123.3–143.0 mcd); Hole 1267B: 112.0–128.6 mbsf (124.0–143.0 mcd)
Age: Oligocene to late Eocene
Lithology: nannofossil ooze, foraminifer-bearing nannofossil ooze, and clayey nannofossil ooze.

Subunit IIB is more carbonate rich than Subunits IIA and IIC (average = 83.5 wt%). Lithologies vary among light brown to gray nannofossil ooze, foraminifer-bearing nannofossil ooze, and medium brown to gray clayey nannofossil ooze. Unlike Site 1262, where clear evidence of turbidites was found in Subunit IIB, Site 1267 appears to have been less affected by downslope transport. Nonetheless, biostratigraphy indicates intensive downslope transport and reworking. The E/O boundary, although not clearly defined at this site, likely occurs near the base of Subunit IIB and is marked by an upward transition from brown clay to light brown nannofossil ooze (Fig. F14). Across the boundary interval, MS, NGR, and bulk density exhibit an upward decrease, whereas sediment L* increases from the Eocene into the Oligocene.

Subunit IIC

Interval: 208-1267A-14H-5, 95 cm, through 15H-7, 48 cm; 208-1267B-15H-2, 50 cm, through 16H-5, 30 cm
Depth: Hole 1267A: 129.9–141.9 mbsf (143.0–155.6 mcd); Hole 1267B: 128.6–142.4 mbsf (143.0–157.8 mcd)

F11. Physical property measurements, p. 38.

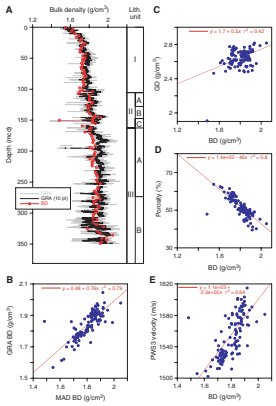

F12. Chromaticity, Mn and Fe, and grain density, Hole 1267A, p. 39.

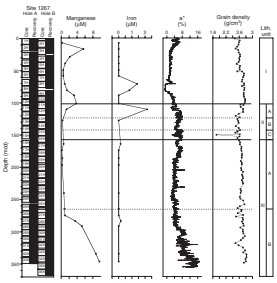

F13. Digital images and cyclic patterns of sedimentation, p. 40.

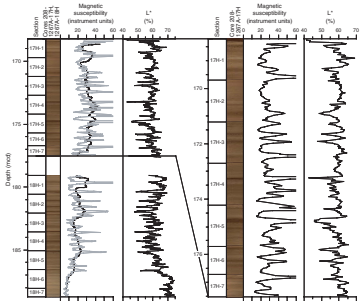

F14. Digital image, MS, NGR, and L* across the E/O boundary, p. 41.

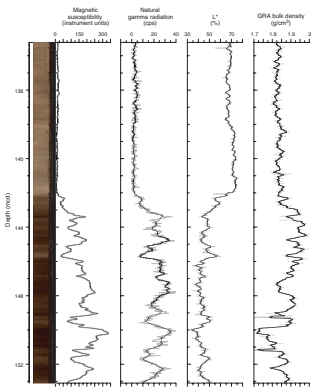

Age: late Eocene to middle Eocene
Lithology: clayey nannofossil ooze, clay-bearing nannofossil ooze, ash-bearing nannofossil clay, and ash-bearing clay

Subunit IIC is composed of clay-bearing and clayey nannofossil ooze at the top and bottom of the subunit, with ash-bearing clay more prominent in the center of the subunit. Subunit IIC is distinguished from Subunit IIB by its lower carbonate content (average = 54.6 wt%), higher MS, NGR, and bulk density, and decreased sediment L*.

Unit III

Interval: 208-1267A-16H-1, 0 cm, through 33X-CC, 38 cm; 208-1267B-16H-5, 30 cm, through 36X-CC, 37.5 cm
Depth: Hole 1267A: 149.9–312.3 mbsf (158.3–349.2 mcd); Hole 1267B: 142.4–329.2 mbsf (157.8–367.9 mcd)
Age: middle Eocene to Maastrichtian
Lithology: nannofossil ooze and chalk, nannofossil and ashy clay, clay-bearing nannofossil ooze and chalk, and clay-bearing foraminifer nannofossil chalk

Unit III is a carbonate-rich lithology composed primarily of nannofossil ooze with varying abundances of clay, foraminifers, and volcanic glass. It was divided into two subunits based mainly on clay content and degree of induration. Subunit IIIA has higher carbonate and lower clay content than Subunit IIIB. Sediments become progressively indurated downhole from ooze to chalk, with the first chalk occurring at ~300 mcd.

Subunit IIIA

Interval: 208-1267A-16H-1, 0 cm, through 25H-6, 80 cm; 208-1267B-16H-5, 30 cm, through 26X-3, 65 cm
Depth: Hole 1267A: 141.9–234.9 mbsf (158.3–265.6 mcd); Hole 1267B: 142.4–234.7 mbsf (157.8–265.4 mcd)
Age: middle Eocene to late Paleocene
Lithology: nannofossil ooze, clay-bearing nannofossil ooze, and nannofossil clay

Subunit IIIA consists predominantly of nannofossil ooze with variable, although generally low, clay content. Lithologies oscillate on a decimeter to meter scale between light gray-brown nannofossil ooze and medium gray clay-bearing nannofossil ooze, with attendant variations in MS and color parameters. In the upper part of this unit, nannofossil clay is present in some of the thin dark horizons. Similar to Subunit IIA at Site 1262, large pinkish white blebs, which may be associated with burrowing or diagenetic alteration, occur sporadically throughout the unit. Cyclicity is apparent macroscopically and in records of MS and color reflectance, especially in the upper part of Subunit IIIA (Fig. **F13**).

Subunit IIIA contains the P/E boundary, a carbonate-free interval formed during a severe dissolution event in response to a shoaling of the lysocline and CCD in the earliest Eocene (Fig. **F15**). This boundary interval, similar in lithologic and physical properties to the boundary sequence at Site 1262, was recovered at 231.6 mcd in both Holes 1267A and 1267B (Sections 208-1267A-22H-7, 33 cm, and 208-1267B-23H-3, 102 cm). Carbonate content decreases from ~85 wt% in a nannofossil ooze to 0 wt% immediately above the contact, where the lithology

F15. Digital images, MS, carbonate, and a* across the P/E boundary, p. 42.

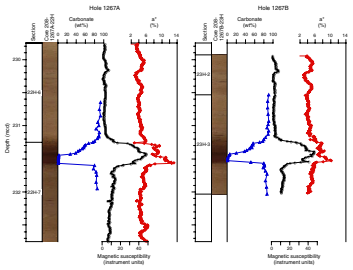

changes to a 15-cm-thick dark red clay layer. Chromaticity a* (green-red) increases sharply above the boundary toward greater red values and then decreases gradually to baseline values over a 35-cm interval (Fig. F15). This is followed by a stepped increase in carbonate and decrease in MS as sediment gradually grades back to nannofossil ooze. *P*-wave velocity also changes across this interval, yet not in concert with other measures (Fig. F16). The maximum *P*-wave velocity lags behind the increase in MS and decrease in carbonate, with the velocity maximum occurring at 10 cm above the MS maximum.

A similar but less intense early Eocene dissolution event is represented by a thin reddish clay layer ~25 m above the P/E boundary (Fig. F17). This interval was recovered in Sections 208-1267A-20H-3 and 208-1267B-20H-7 and 20H-CC, but it is clearly incomplete in Hole 1267B. In addition to macroscopic characteristics, it is recognized in physical property records by an increase in MS and a* (Fig. F17). This clay-rich interval was observed at all of the Leg 208 sites except Site 1264, where sediments of this age were not recovered.

Subunit IIIB

Interval: 208-1267A-25H-6, 80 cm, through 33X-CC, 38 cm; 208-1267B-26X-3, 65 cm, through 36X-CC, 37.5 cm
Depth: Hole 1267A: 234.9–312.3 mbsf (265.6–349.2 mcd); Hole 1267B: 234.7–329.2 mbsf (265.4–367.9 mcd)
Age: late Paleocene to Maastrichtian
Lithology: nannofossil ooze, nannofossil chalk, clay-bearing nannofossil chalk, clay-bearing foraminifer nannofossil chalk, nannofossil clay, and rare foraminifer-nannofossil–bearing ashy clays

Subunit IIIB is composed of nannofossil ooze, nannofossil clay, ashy clay, and nannofossil chalk with variable nannofossil, foraminifer, clay, and ash content. Subunit IIIB is similar to Subunit IIIB at Site 1262 but with slightly more varied clay, ash, and chalk content. This variability is also observed in physical properties such as MS, NGR, and *P*-wave velocity (Figs. F6, F10).

The K/P boundary was recovered in both holes (intervals 208-1267A-31X-3, 75 cm, and 208-1267B-32X-4, 80 cm). Despite disruption and biscuiting by XCB coring and slight rotation directly at the K/P boundary, the transition is well represented in both physical property measurements and lithologic characteristics. Below the boundary, light reddish brown and brown clay-bearing nannofossil chalk alternate on a 0.5-m scale, a cyclicity that is recorded in both sediment lightness and chromaticity. Within the darker lithology, bioturbational features are well preserved with both subhorizontal and vertical structures present. In addition, rare foraminifer-nannofossil–bearing ashy clays are present as isolated blebs in some of the darker layers. At the boundary (Fig. F18), light reddish brown clay-bearing foraminifer nannofossil chalk grades upward into a distinctive 3- to 4-cm light gray nannofossil foraminifer chalk that contains minor amounts of ash (or is slightly silicified). This layer is abruptly overlain by a 2- to 3-cm-thick dark red to reddish brown Fe oxide–bearing foraminifer nannofossil chalk that is not bioturbated. A light reddish brown clay-bearing nannofossil chalk, which is mottled by dark red burrows, overlies this thin transition interval. The MS values increase abruptly across the K/P boundary (320.5 mcd) as sediment L* decreases, reflecting a higher abundance of Fe oxide in the overlying Paleocene sediments. This does not appear to corre-

F16. *P*-wave velocity across the of P/E boundary, p. 43.

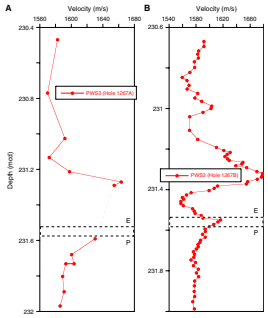

F17. Digital images, MS, and a* for the red clay layer, p. 44.

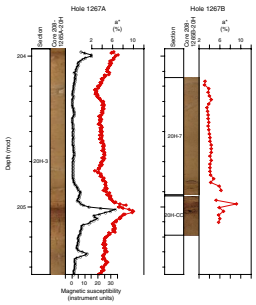

F18. Digital images, MS, and L* of the K/P boundary, p. 45.

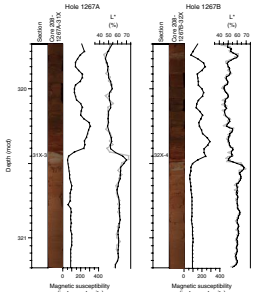

late directly with clay content, which does not change dramatically at the boundary; however, clay does increase progressively upsection, as does the abundance of foraminifers. Clay content then decreases again toward the upper boundary of Subunit IIIA.

Lithification increases in the lower part of Subunit IIIA, leading to a dominance of nannofossil chalk. Rarely, nannofossil ooze is partially silicified with the development of porcellanite. In addition, discrete ash layers are present that are composed of abundant Fe oxides and highly altered volcanic glass. These layers are represented by spikes in the NGR record (e.g., interval 208-1267A-32X-3, 123 cm) (Fig. F6).

BIOSTRATIGRAPHY

At Site 1267, Pleistocene through upper Maastrichtian sediments were recovered. Nannofossils are present in almost all samples, showing generally moderate preservation with reworking and dissolution in the upper Eocene through Miocene and dissolution in the Maastrichtian (Fig. F19). Planktonic foraminifers are present in moderate to high abundances and with variable preservation because of dissolution in the Pliocene sediments through upper middle Eocene and Maastrichtian. Reworked specimens are common in the Pleistocene and Miocene through the middle Eocene (Fig. F19). Benthic foraminifers are rare and have good preservation in some parts of the section, but in the lower Pliocene through the upper lower Eocene and the middle upper Paleocene, benthic foraminifers, large echinoid spines, and ostracodes are reworked and transported downslope from water depths of no less than ~600–1500 m.

Shipboard examination of calcareous nannofossils and planktonic foraminifers permits preliminary zonal and stage assignments (Fig. F19; Tables T5, T6, T7, T8). Biochronological ages plotted against mcd delineate overall sedimentation rates (Fig. F20) (see "Age Model and Mass Accumulation Rates," p. 25).

The Pleistocene–uppermost Miocene and lower Eocene–upper Maastrichtian (including the P/E and K/P boundaries) are biostratigraphically complete at shipboard resolution, but the middle Miocene–upper middle Eocene sediments are difficult to zone because of massive reworking and severe dissolution, and they are condensed or interrupted by unconformities. An "unconformity" corresponding to the earliest late Miocene through early Miocene (~10.5–22.8 Ma) occurs between 108 and 113 mcd in Core 208-1267A-11H. Sediments between 113 and 115 mcd are early Miocene, and sediments between 115 and 129 mcd cannot be dated precisely and might be Oligocene in age. Sediments between 130 and 146 mcd are earliest Oligocene (~31.7–32.9 Ma), and the highly condensed sequence between 115 and 130 mcd thus represents ~8–9 m.y. Sediments between 146 and 151 mcd are problematic because of severe dissolution and massive reworking, and they could be either earliest Oligocene or late Eocene in age. Thus, the E/O boundary cannot be identified unequivocally. At 151 mcd, sediments are ~42.3 Ma (middle Eocene). The interval between 146 and 151 mcd thus represents a large part of the late and late middle Eocene.

Benthic foraminifers indicate generally lower abyssal depths (>3000 m) from the late Paleocene through the Pleistocene, although the paleodepths of some samples could not be ascertained because of intensive downslope transport, reworking, and dissolution. The paleodepth was transitional between upper and lower abyssal (~3000 m) in the middle

F19. Planktonic foraminiferal and calcareous nannofossil biozonations, p. 46.

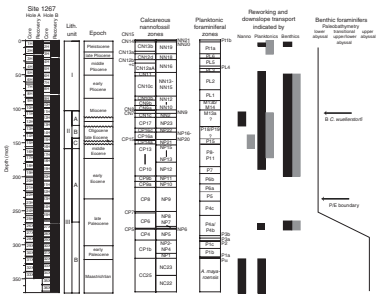

T5. Selected calcareous nannofossil datums, p. 65.

T6. Range and abundance of calcareous nannofossils, p. 67.

T7. Selected planktonic foraminiferal datums, p. 68.

T8. Range and abundance of planktonic foraminifers, p. 69.

F20. Sedimentation rates, p. 47.

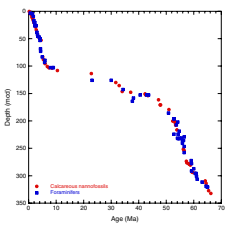

part of the Paleocene and upper abyssal (<3000 m) during the Maastrichtian through early Paleocene.

Calcareous Nannofossils

Calcareous nannofossil assemblages contained in core catcher samples for all holes and additional samples taken at critical intervals in Hole 1267A were examined. Depth and age estimates of key biostratigraphic markers are shown in Table T5; Table T6 shows a distribution chart of the core catcher samples. Nannofossils have good to moderate preservation throughout the section and are always present except for some intervals in Core 208-1267A-12H and a few centimeter-thick intervals in Core 22H just above the P/E boundary. Paleogene assemblages show dissolution of placoliths and overgrowth of discoasterids with secondary calcite.

Pleistocene (0–17 mcd)

The recovered section represents an almost complete record of the upper Pleistocene (Zone CN15/NN21) through the Pliocene/Pleistocene boundary in Cores 208-1267A-1H through 2H. The complete succession of Pleistocene nannofossil assemblages is present, including the events based on the size change of *Gephyrocapsa*. The Pliocene/Pleistocene boundary is between the lowest occurrence of medium *Gephyrocapsa* spp. and the highest occurrence of *Discoaster brouweri* in Sample 208-1267A-2H-5, 65 cm, and Section 2H-CC (16.2–19.0 mcd) and is placed at 17.1 mcd in agreement with planktonic foraminiferal data (see "Planktonic Foraminifers," p. 13).

Pliocene (17–85 mcd)

Pliocene assemblages consist mainly of reticulofenestrids, sphenoliths, and discoasterids. Helicoliths belonging to the genus *Amaurolithus* (*Amaurolithus delicatus* and *Amaurolithus primus*) are common, and ceratholiths belonging to the genus *Ceratolithus* (*Ceratolithus rugosus*) are rare. The middle and upper Pliocene assemblages are dominated by small placoliths (2–4 µm), mainly small *Reticulofenestra* spp., and *Pseudoemiliania lacunosa* (Cores 208-1267A-3H through 5H). *D. brouweri, Discoaster brouweri* var. *triradiatus, Discoaster pentaradiatus, Discoaster surculus, Discoaster tamalis,* and *Discoaster asymmetricus* are consistently present in the middle–upper Pliocene (17.1–25.6 mcd). The middle/lower Pliocene boundary is placed at 25.6 mcd in agreement with the planktonic foraminiferal data. An expanded lower Pliocene section is present between 25.6 and 84.2 mcd (Sections 208-1267A-5H-4 through 8H-CC), corresponding to Zones CN11 and CN10 (NN15–NN13). The discoasterid assemblage is characterized by *D. surculus, D. pentaradiatus, Discoaster variabilis* gr., *A. delicatus,* and *A. primus* and by common *Scyphosphaera* spp. The Miocene/Pliocene (M/P) boundary is well constrained between Section 208-1267A-8H-CC (83.5 mcd) and Sample 9H-1, 120 cm, (85.7 mcd), based on the presence of the marker *Ceratolithus acutus* in Sections 9H-1 and 9H-2 together with very rare specimens of *Ceratolithus larrymayeri.* Both species have distinct short ranges that straddle the M/P boundary in the equatorial Atlantic Ocean and Mediterranean Seas (Raffi et al., 1998).

Miocene–Oligocene (85–147 mcd)

Uppermost Miocene sediments could be placed in the interval encompassing Subzones CN10a–CN8b, but the absence of the marker species *Discoaster quinqueramus* and *Discoaster berggrenii* prevented the recognition of the Zone CN10/CN9 (NN12/NN11) and Subzone CN9a/Zone CN8 (NN11/NN10) boundaries. The uppermost Miocene ceratolith marker *Nicklithus amplificus* occurs between Samples 208-1267A-10H-2, 40 cm, and 10H-5, 40 cm (95.5–100.8 mcd), placing these sediments in Subzone CN9bB. The lowermost occurrence of *Amaurolithus* spp. between Samples 208-1267A-10H-7, 10 cm, and 10H-7, 100 cm, indicates the Subzone CN9bA/CN9a boundary. Just below this interval, preservation of nannofossils deteriorates and dissolution affects the assemblages.

The marker for Subzone CN8b, *Discoaster loeblichii,* is present in a short interval with a partially dissolved assemblage in Section 208-1267A-10H-7. The sediments in Core 208-1267A-11H contain an unconformity marked by reworked material because assemblages typical for several upper Miocene zones (CN8a, CN7, and CN3–CN2) are present in a few samples in the upper five sections of the core between intervals barren of nannofossils. Assemblages of lower Miocene Subzone CN1c (NN2) occur in Sections 208-1267A-11H-6, 11H-7, and 11H-CC. Within Core 208-1267A-12H, nannofossil assemblages occur in scattered intervals, are strongly dissolved, and do not contain diagnostic markers. The rare species present (*Dictyococcites bisectus, Sphenolithus predistentus, Sphenolithus moriformis,* and *Cyclicargolithus* spp.) indicate a possible Oligocene age. The uppermost occurrence (top [T]) of *Reticulofenestra umbilicus* is between Samples 208-1267A-13H-3, 110 cm, and 13H-4, 110 cm (129.1–130.6 mcd), indicating an early Oligocene age. The T of *Ericsonia formosa* is between Section 208-1267A-13H-CC and Sample 14H-1, 40 cm (134.4–136.5 mcd). The assemblages in these samples mainly consist of *R. umbilicus, Isthmolithus recurvus, Dictyococcites* spp., *Reticulofenestra dictyoda, Discoaster tani,* and *Discoaster deflandrei*. Section 208-1267A-14H-CC (145.9 mcd) is problematic because of dissolution and reworking and might be either lower Oligocene or upper Eocene.

Eocene (147.0–231.6 mcd)

The uppermost nonreworked occurrences of the last Paleogene representatives of the rosette-shaped discoasters *Discoaster saipanensis* and *Discoaster barbadiensis* are between Section 208-1267A-14H-CC and Sample 15H-1, 76 cm (145.8–146.9 mcd), and ~1 m of upper Eocene sediment might be present in the uppermost part of Core 15H. The absence of *I. recurvus* and *Calcidiscus protoannulus,* however, indicates that we cannot recognize the E/O boundary and that most of the upper Eocene is not present. The T of *Chiasmolithus grandis* (37.1 Ma) between Samples 208-1267A-15H-1, 76 cm, and 15H-2, 100 cm (146.9–148.6 mcd), suggests a possible middle Eocene age for this interval, but most of the middle Eocene is missing. Below ~149 mcd, the middle through lower Eocene Zones NP16–NP10 (CP13–CP9) were recognized. Nannofossils are abundant throughout this interval, and preservation varies from moderate to good with dissolved and overgrown discoasterids and *Tribrachiatus orthostylus*. The assemblages mainly consist of the marker species of the lower Eocene zones including abundant *T. orthostylus,*

Discoaster lodoensis, D. barbadiensis, D. saipanensis, Sphenolithus radians, and common *Discoaster diastypus.*

Paleocene/Eocene Boundary Interval (221–236 mcd)

The P/E boundary (231.5 mcd) is characterized by the lowermost occurrences of *Rhomboaster cuspis* and *Rhomboaster calcitrapa*. Poorly preserved specimens of *Rhomboaster* occur between Samples 208-1267A-22H-7, 20 cm, and 22H-7, 26 cm (231.45–231.51 mcd). The 10-cm interval directly above the P/E boundary is barren of calcareous nannofossils. The uphole decrease in relative abundance of *Fasciculithus,* which is relatively common in the uppermost Paleocene, occurs where *Zygrhablithus bijugatus* increases uphole in relative abundance between Samples 208-1267A-22H-6, 60 cm, and 22H–6, 105 cm (230.35–230.80 mcd). The uppermost occurrence of fasciculiths is between Samples 208-1267A-22H-4, 40 cm, and 22H-6, 10 cm (227.1–229.8 mcd). Specimens belonging to the *Rhomboaster-Tribrachiatus* plexus are poorly preserved because of calcite recrystallization. Overgrowth of specimens of the *Rhomboaster-Tribrachiatus* plexus hampered identification of *Tribrachiatus contortus* and *Tribrachiatus bramlettei*. Thus, the lowermost occurrence (bottom [B]) of *T. orthostylus* (between Samples 208-1267A-20H-5, 30 cm, and 20H-6, 30 cm; 207.2–208.3 mcd) and the B of *D. diastypus* (between Samples 21H-4, 20 cm, and 21H-5, 30 cm; 215.4–217.0 mcd), the marker of the base of Subzone CP9a, have been used to approximate the Subzone CP9b/CP9a (NP11/NP10) and Zone NP10/NP9 boundaries.

Paleocene (231.6–320.4 mcd)

The major components of the upper Paleocene assemblages are *Discoaster* spp. *Toweius* spp., *Coccolithus pelagicus, Prinsius* spp., *Chiasmolithus* spp., *Sphenolithus* spp., *Fasciculithus* spp., *Heliolithus* spp., and *Ericsonia* spp. Nannofossil assemblages are generally diverse and moderately to well preserved. Most of the important primary and secondary markers (Table **T5**) of the upper Paleocene are present from the top of Core 208-1267A-22H through the top of Core 29H (~231.5–296.7 mcd). The B of *Heliolithus kleinpellii* between Section 208-1267A-26X-CC and Sample 27X-1, 41 cm (277.5–278.5 mcd), indicates the presence of the PBE.

The boundary between the upper and lower Paleocene can be approximated with the B of *Sphenolithus primus* between Section 208-1267A-28X-CC and Sample 29X-1, 23 cm (294.8–296.7 mcd), and is placed at 296.6 mcd, in agreement with planktonic foraminiferal data. In the lower Paleocene, the absence of *Ellipsolithus macellus* in the lower part of its range prevents the recognition of the Zone CP3/CP2 (NP4/NP3) boundary. *E. macellus* has its lowermost continuous occurrence in Zone CP5 (NP6). Reworked Cretaceous specimens occur from Cores 208-1267A-25H-CC through the middle part of 31X and from Sections 208-1267B-26X-CC through the middle part of 32X-CC (~267–295 mcd).

Upper Cretaceous/Lower Paleocene Boundary Interval (312.0–368.0 mcd)

The lowermost Paleocene is characterized by moderately well preserved assemblages. The B of *Cruciplacolithus tenuis* s.s. (64.5 Ma) and

the B of *Cruciplacolithus primus* (64.8 Ma) occur between Samples 208-1267A-30X-5, 20 cm, and 30X-6, 60 cm (312.9–314.8 mcd), and 31X-1, 99 cm, and 31X-2, 60 cm (318.7–319.3 mcd), respectively. The assemblages are mainly composed of *Prinsius dimorphosus, C. pelagicus, Neochiastozygus* spp., *Cruciplacolithus* spp., and *Zeugrhabdothus sigmoides*. The K/P boundary interval is marked by a mass extinction of Cretaceous nannofossil taxa, together with a significant increase in the abundance of *Thoracosphaera* spp., the B of *Biantholithus sparsus* (between Samples 208-1267A-31X-3, 68 cm, and 31X-3, 69 cm; 320.38–320.39 mcd), and the co-occurrence of *Markalius inversus* and *Cyclagelosphaera reinhardtii*.

The upper Maastrichtian nannofossil assemblages (Zones CC26–CC25 and NC23–NC22–NC21) show dissolution and fragmentation, and *Micula staurophora, Micula murus, Prediscosphaera grandis, Lithraphidites quadratus, Lithraphidites carniolensis, Arkhangelskiella cymbiformis, Eiffellithus turriseiffelii,* and *Watznaueria barnesae* are the major components. The B of *Micula prinsii* (which occurs in Zone CC26) is between Sample 208-1267A-31X-7, 133 cm, and Section 31X-CC (327.0–327.3 mcd). The B of *M. murus* is between Samples 208-1267A-32X-3, 40 cm, and 32X-5, 100 cm (332.3–335.91 mcd), and that of *L. quadratus* occurs between Section 208-1276B-35X-CC and Sample 36X-1, 33 cm (358.3–358.5 mcd).

Planktonic Foraminifers

Planktonic foraminifers were examined in all core catcher samples from Holes 1267A and 1267B and in additional samples from the cores through such critical intervals as the Pliocene/Pleistocene, M/P, P/E, and K/P boundary intervals (Tables T7, T8). The preservation and abundance vary throughout the record. Miocene and Oligocene samples between 67.1 and 182.6 mcd (Sample 208-1267A-7H-3, 32–34 cm, through Section 208-1267B-18H-CC) show severe dissolution, with Section 208-1267A-12H-CC being barren. Paleocene–Eocene assemblages are well preserved. Preservation deteriorates in the Maastrichtian (321.3–337.1 mcd; Sample 208-1267A-32X-4, 10–11 cm, through Section 208-1267B-33X-CC). Reworking is common in the Pleistocene (0–18 mcd) and from the middle Miocene through the uppermost lower Eocene (108–177 mcd).

Pleistocene (0–17 mcd)

Sample 208-1267A-1H, 0–1 cm (0.01 mcd), contains specimens of the Pliocene species *Globigerinoides extremus,* indicating reworking and/or downslope transport. Pleistocene assemblages in Cores 208-1267A-1H and 208-1267B-1H through 2H (0.6–12.3 mcd) consist of a mixture of well-preserved subtropical and temperate planktonic foraminifers. Common species are *Globorotalia crassaformis, Globorotalia truncatulinoides, Globorotalia tumida, Globoconella inflata, Globigerinoides ruber, Globigerinoides sacculifer, Globigerina (Zeaglobigerina) rubescens, Globigerinella siphonifera, Hirsutella scitula,* and *Neogloboquadrina pachyderma* (dextral). Cursory sampling in Cores 208-1267A-1H and 2H and 208-1267B-1H and 2H indicates that the presence of Pliocene planktonic foraminifers in Pleistocene sediments is largely restricted to an interval near the mudline. Thus, the Pliocene/Pleistocene boundary is provisionally approximated by the uppermost in situ occurrence of *G. extremus* between Samples 208-1267A-2H-5, 32–34 cm (15.9 mcd), and 2H-

7, 32–34 cm (18.4 mcd), and is placed at 17.1 mcd, in agreement with calcareous nannofossil data (see "Calcareous Nannofossils," p. 10).

Pliocene (17–85 mcd)

Pliocene tropical/subtropical age-diagnostic taxa are missing because the environmental conditions were temperate. *G. crassaformis, Globoconella puncticulata, Globoconella conomiozea, Globoconella conoidea,* and *G. inflata* dominate the assemblage. Data from this site confirm that the uppermost occurrences of *G. conomiozea* and *G. conoidea* are diachronous, as reported by Boersma (1984). Although warm-water species are generally rare, *G. ruber, G. sacculifer,* and *Globigerinoides trilobus* are present throughout the Pliocene. The base of Zone PL6 is approximated by the uppermost appearance of *Globoturborotalita woodi* between Samples 208-1267A-3H-3, 32–34 cm (25.1 mcd), and 3H-5, 32–34 cm (28.1 mcd). This datum and the uppermost appearances of *Globigerina decoraperta* (2.7 Ma) between Samples 208-1267A-3H-3, 32–34 cm (25.1 mcd), and 3H-5, 32–34 cm (28.1 mcd), are used to approximate the middle/upper Pliocene boundary, in agreement with the calcareous nannofossil data.

The base of Zone PL3 and the lower/middle Pliocene boundary were approximated by the uppermost occurrence of *Neogloboquadrina acostaensis* between Section 208-1267B-5H-CC (45.8 mcd) and Sample 208-1267A-5H-5, 32–34 cm (48.6 mcd). The M/P boundary (B of *Sphaeroidinella dehiscens* and *Globigerinoides conglobatus*) is between Sections 208-1267A-8H-CC (83.5 mcd) and 9H-CC (92.1 mcd).

Miocene–Oligocene (85–147 mcd)

Uppermost Miocene Subzone M13a and the Subzone M13b/Zone M14 boundary have been recognized. The upper Miocene sequence from 5.3 to 8.94 Ma seems to be complete despite the rapidly deteriorating preservation downhole. A zonation and age estimate of Miocene sediments older than 8.94 Ma, defined by the B of *G. extremus* between Sample 208-1267A-10H-6, 32–34 cm (101.8 mcd), and Section 10H-CC (104.0 mcd), is impossible because of the strong dissolution. Sediments deposited between 8.9 and 23.1 Ma are condensed in only 14 m, suggesting the presence of an "unconformity" that is placed in Core 208-1267A-11H based on nannofossil evidence (see "Calcareous Nannofossils," p. 10). Sections 208-1267B-11H-CC and 12H-CC are largely barren, containing rare reworked middle Eocene acarininids and morozovellids.

The transition from the lower Miocene into the upper Oligocene could not be recognized with confidence using planktonic foraminifers because of dissolution, and the entire Oligocene sequence is condensed in 30 m. The intense carbonate dissolution extends from the middle to lower Miocene well into the Oligocene, and the highest Oligocene sample identified with confidence is Section 208-1267B-13H-CC (128.5 mcd). The poorly preserved assemblage in this sample consists solely of dissolution-resistant taxa such as *Subbotina angiporoides, Globorotalides suteri, Catapsydrax* spp., and *Globigerina euapertura.* The presence of *S. angiporoides* constrains this sample to lower Oligocene Zones P18 and P19 (>30 Ma), indicating that the upper Oligocene is not present.

Eocene (147–231.6 mcd)

Sections 208-1267A-14H-CC (145.9 mcd) and 208-1267B-15H-CC (150.0 mcd) are problematic because they contain assemblages that are winnowed and highly fragmented. The presence of *Globigerinatheka* spp. and the absence of *Acarinina* spp. may indicate that this assemblage belongs to Zone P15, but the sedimentological character of this sample suggests reworking comparable to that seen in the lower Oligocene at Site 1266. Moreover, the absence of uppermost Eocene marker taxa indicates that the E/O boundary is not preserved, in agreement with the nannofossil data.

The close proximity (~10 m) of the T of *Globigerinatheka index* (34.3 Ma) and the T of *Morozovella aragonensis* (43.6 Ma) points to the presence of a highly condensed interval or unconformity; the latter is indicated by the more detailed nannofossil data that indicate that most of the upper and upper middle Eocene is not represented in the sedimentary record. Intense dissolution and a dearth of tropical marker taxa hindered precise age determination for Section 208-1267A-15H-CC (155.6 mcd), but the co-occurrence of rare diminutive specimens of *M. aragonensis* and *Globigerinatheka kugleri* constrains this sample to lower–middle Eocene Zones P10 and P11 (43.6–49.0 Ma).

Although preservation improves downhole, the assemblages in Sections 208-1267A-16H-CC (167.3 mcd) and 17H-CC (177.7 mcd) suffer from varying degrees of dissolution and minor amounts of reworking. Primary constituents of these moderately preserved assemblages are *Morozovella caucasica, M. aragonensis, Acarinina spinuloinflata,* and *"Globigerinatheka" senni,* as well as rare specimens of *Subbotina inaequispira* and *Turborotalia frontosa*. Section 208-1267A-16H-CC is loosely assigned to Zones P9 and P10, whereas Section 17H-CC is assigned to the uppermost lower Eocene (Zone P9), in agreement with calcareous nannofossil data.

Preservation improves significantly downhole. Section 208-1267B-18H-CC (182.6 mcd) contains common *M. aragonensis* and *M. caucasica* but no *Acarinina bullbrooki* and *A. spinuloinflata*. This faunal association is indicative of Zone P8. Sections 208-1267A-18H-CC (188.9 mcd) and 208-1267B-19H-CC (193.3 mcd) contain rare specimens of both *Morozovella formosa* and *M. aragonensis,* indicating that this interval belongs to Zone P7. Other taxa in these assemblages include *Morozovella lensiformis, Morozovella gracilis, Morozovella subbotinae, Acarinina coalingensis, Acarinina soldadoensis,* and *Igorina broedermanni*.

The combination of the presence of *M. lensiformis* and the absence of *M. aragonensis* in Sections 208-1267A-19H-CC and 208-1267B-20H-CC qualifies this interval (199.1–205.1 mcd) as Subzone P6b. Sections 208-1267A-20H-CC through 208-1267B-21H-CC (209.5–216.3 mcd) are assigned to Subzone P6a. The general scarcity of *Morozovella velascoensis* in the lowermost Eocene of this region makes recognition of the P5/P6a zonal boundary difficult. Hence, the upper part of the *Morozovella acuta* stratigraphic range is substituted to approximate the top of Zone P5. The use of this alternative datum places the top of Zone P5 between Sections 208-1267B-21H-CC (216.3 mcd) and 208-1267A-21H-CC (221.0 mcd) at ~219 mcd.

Paleocene/Eocene Boundary Interval (221–236 mcd)

The P/E boundary interval spans Zone P5. Investigation of six closely spaced (~12 cm) samples across the clay layer that marks the P/E

boundary shows that preservation decreases downhole through the lowermost Eocene into the clay layer. Planktonic foraminifers are virtually absent between 231.37 and 231.53 mcd (Samples 208-1267A-22H-7, 12–13 cm, through 28–29 cm). Intense dissolution has left only extremely rare specimens of *A. soldadoensis, A. coalingensis, Acarinina "chascanona,"* and *M. subbotinae.* Preservation improves and the relative abundance of planktonic foraminifers increases significantly in Sample 208-1267A-22H-7, 37–38 cm (231.62 mcd). This moderately preserved assemblage is composed of morozovellids, acarininids, subbotinids, and rare globanomalinids. The benthic extinction event that demarcates the P/E boundary (231.53–231.62 mcd) is correlative with this change in preservation. Much like other P/E boundary records recovered during Leg 208, the Site 1267 record contains no *M. velascoensis* or related "excursion" taxa (e.g., Kelly et al., 1996). The bottom of this critical interval coincides with the base of Zone P5 in the uppermost Paleocene, is delimited by the uppermost occurrence of *Globanomalina pseudomenardii* between Sections 208-1267A-22H-CC (232.9 mcd) and 208-1267B-23H-CC (238.2 mcd), and is placed at ~236 mcd.

Paleocene (231.6–320.4 mcd)

Preservation among upper Paleocene assemblages is variable but generally moderate. All the standard Paleocene biozones are recognized in the recovered section. The base of Subzone P4c (56.5 Ma), as delimited by the B of *A. soldadoensis,* falls between Sections 208-1267A-24H-CC (254.2 mcd) and 208-1267B-25H-CC (261.4 mcd) at an estimated depth of ~258 mcd (Fig. **F19**). Sections 208-1267A-26X-CC (277.5 mcd) and 208-1267B-27X-CC (278.3 mcd) contain a relatively high abundance of *Igorina tadjikstanensis,* indicative of the mid-Paleocene biotic event in the lower part of Biozone P4a.

The Subzone P3b/P4a boundary is marked by the B of *G. pseudomenardii* between Sections 208-1267B-28X-CC (288.1 mcd) and 208-1267A-28X-CC (294.8 mcd) at an estimated depth of ~291 mcd. The boundary between the upper and lower Paleocene (Danian) is correlative to the base of Subzone P3a, marked by the B of *Morozovella angulata* between Sections 208-1267B-29X-CC (296.6 mcd) and 208-1267A-29X-CC (305.6 mcd); a placement of this boundary at 296.6 mcd would best agree with calcareous nannofossil data (see **"Calcareous Nannofossils,"** p. 10). The base of Zone P2, based on the B of *Praemurica uncinata,* is between Sections 208-1267A-29X-CC (305.6 mcd) and 208-1267B-30X-CC (306.9 mcd), at ~306.21 mcd. Zone P2 is underlain conformably by Subzone P1c based on the B of *Praemurica inconstans* and the B of *Globanomalina compressa* between Sections 208-1267B-30X-CC (306.9 mcd) and 31X-CC (315.8 mcd).

Upper Cretaceous/Lower Paleocene Boundary Interval (312.0–368.0 mcd)

Core catcher samples bracketing the K/P boundary were supplemented by sampling in Core 208-1267A-31X. Assemblages are generally moderately well preserved, although some Maastrichtian faunas exhibit strong dissolution.

The base of Subzone P1b, delimited by the B of *Subbottina triloculinoides,* is tentatively placed at 318.95 mcd (Fig. **F19**), suggesting that this subzone is much more expanded than it is in Hole 1262B. The base of Subzone P1a is tentatively placed between Samples 208-1267A-31X-

3, 21–30 cm (320.0 mcd), and 50–51 cm (320.2 mcd), suggesting that Subzone P1a is also more expanded at Site 1267 than at Site 1262. Large, reworked specimens of Maastrichtian foraminifers are present in Zone Pα (320.2–320.4 mcd), and Zone P0 was not recognized.

The Danian "dwarfed" assemblages in Subzones P1a and P1b show fragmentation and some overgrowth, and they consist primarily of diminutive forms of *Praemurica taurica, Parasubbotina pseudobulloides, Parasubbotina eobulloides, Globanomalina planocompressa, Globoconusa daubjergensis, Eoglobigerina eobulloides, Guembelitria cretacea, Woodringinia hornerstownensis, Chiloguembelina midwayensis,* and *Chiloguembelina morsei*.

The presence of *Abathomphalus mayaroensis, Contusotruncana contusa,* and *Heterohelix striata* in Sample 208-1267B-31X-3, 74–75 cm (320.4 mcd), signifies the Maastrichtian. The K/P boundary (Fig. **F19**) is situated between Samples 208-1267A-31X-3, 70–71 cm, and 74–75 cm (320.40–320.44 mcd). Assemblages of the *A. mayaroensis* Zone contain *Globotruncana falsostuarti, Globotruncana aegyptiaca, Pseudotextularia elegans,* and *Racemiguembelina fructicosa,* in addition to the species mentioned above, and occur down through 367.97 mcd in Section 208-1267B-36X-CC at the bottom of the hole.

Benthic Foraminifers

All core catcher samples from Hole 1267A, mudline samples from Holes 1267A and 1267B, Sections 208-1267B-1H-CC and 11H-CC through 36X-CC, and additional samples in the P/E and K/P boundary intervals were semiquantitatively investigated for benthic foraminifers (Table **T9**).

T9. Selected benthic foraminifers, p. 70.

In intervals above 52 mcd, between 193.0 and 267.2 mcd, and below 278.3 mcd, benthic foraminifers are rare, strongly outnumbered by planktonic foraminifers, and generally well preserved. Between 52.0 and 193.0 mcd (Section 208-1267A-5H-CC through Sample 19H-3, 10–11 cm) and between 267.2 and 278.3 mcd (Sections 208-1267A-25H-CC through 208-1267B-27X-CC), samples have common to abundant benthic foraminifers with highly variable preservation because of dissolution, downslope transport, and reworking. Indicators of downslope transport are abundant large siphonodosariid species (e.g., *Siphonodosaria pomuligera*), large nodosariids, large specimens of *Gyroidinoides* spp., *Oridorsalis umbonatus, Globocassidulina subglobosa,* and the agglutinant species *Spiroplectammina spectabilis* and *Vulvulina spinosa*. Abraded specimens of *Cibicidoides havanensis, Cibicidoides grimsdalei,* and *Cibicidoides eocaenus* are common in samples between 92.1 and 160.7 mcd (Sections 208-1267A-9H-CC through 208-1267B-16H-CC), as in coeval samples from Site 1266. *Plectofrondicularia paucicostata* occurs in samples at 145.9 mcd (Section 208-1267A-14H-CC) and 188.9 mcd (Section 18H-CC) and is abundant in the former. Section 208-1267B-11H-CC (108.6 mcd) and Sample 208-1267A-22H-7, 28–29 cm (231.5 mcd), are barren.

Benthic foraminiferal assemblages from Site 1267 indicate deposition at lower abyssal depths (>3000 m) between 0 and 243.3 mcd (Sample 208-1267B-1H, 0–1 cm, through Section 208-1267A-23H-CC). Between 249.9 and 288.1 mcd (Sections 208-1267B-24H-CC through 28X-CC), assemblages indicate deposition at transitional upper to lower abyssal depths, and below 296.7 mcd through the bottom of the hole at 368.0 mcd, they indicate lowermost upper abyssal depths (~3000 m). The

paleodepths for samples from Site 1267 are not significantly different from those of coeval samples at Site 1262.

Assemblages in samples between 0 and 104.0 mcd (Sample 208-1267B-1H-1, 0–2 cm, through Sections 208-1267A-10H-CC) resemble those presently living in the Walvis Ridge area at depths below ~4200 m (Schmiedl et al., 1997), including common *Nuttallides umbonifera, Epistominella exigua, Alabaminella weddellensis, Pyrgo* spp., *Pullenia* spp., *O. umbonatus, Stainforthia complanata,* and *G. subglobosa*. *Cibicidoides wuellerstorfi* is present through the interval, having its lowermost occurrence in Section 208-1267A-10H-CC (104.0 mcd). In both mudline samples, the phytodetritus-consuming species *E. exigua* and *A. weddellensis* are common to abundant, indicating a strong influence of seasonal productivity. Through the uppermost 104 mcd, the relative abundance of phytodetritus-consuming species and *N. umbonifera* (abundant in Section 208-1267A-1H-CC; 3.1 mcd), an indicator of the presence of Antarctic Bottom Water, fluctuate strongly. At present, this species is common to abundant to the north of Walvis Ridge below depths of ~4200 m (Schmiedl et al., 1997). The fluctuations in relative abundances in this interval may indicate fluctuations in surface productivity and bottom water mass characteristics.

The in situ components in the assemblages between 108.6 and 139.5 mcd (Sections 208-1267B-11H-CC through 14H-CC) are thin walled and well preserved and consist of taxa common in abyssal Oligocene through lower–middle Miocene assemblages such as *N. umbonifera, E. exigua, G. subglobosa, Gyroidinoides* spp., *Pullenia* spp., and common *Siphonodosaria* spp., pleurostomellid, and unilocular taxa. *Nonion havanense* and *A. spissiformis* have their uppermost occurrences in this interval. Reworked components include *C. grimsdalei, C. eocaenus,* and *C. havanensis, S. pomuligera, V. spinosa,* and *S. spectabilis*.

Sections 208-1267A-14H-CC and 208-1267B-15H-CC (145.9–150.0 mcd) contain common *Nuttallides truempyi,* in addition to the taxa listed above as in situ components, with assemblages typical of upper to middle Eocene abyssal assemblages. Some of the *N. truempyi* specimens are large and abraded and thus probably reworked; other reworked components include *C. grimsdalei, C. eocaenus,* and *C. havanensis,* and *P. paucicostata* in Section 208-1267A-14H-CC (145.9 mcd). *Abyssamina poagi* and *Abyssamina quadrata* have their uppermost occurrence in Section 208-1267B-15H-CC (150.0 mcd).

Aragonia aragonensis has its uppermost appearance in Section 208-1267A-15H-CC (155.6 mcd). Assemblages between 155.6 and 231.5 mcd (Section 208-1267A-15H-CC through Sample 22H-7, 20–21 cm) contain the typical lower through lower middle Eocene assemblages occurring over a large depth range in the Atlantic Ocean (Clark and Wright, 1984; Müller-Merz and Oberhänsli, 1991; Thomas and Shackleton, 1996). These assemblages have been somewhat affected by dissolution, reworking, and downslope transport between 155.6 and 193.0 mcd (Section 208-1267A-15-H-CC through Sample 19H-3, 10–11 cm) (Table **T9**). The assemblages are characterized by the presence of *A. aragonensis, Alabamina dissonata,* and common to abundant small smooth-walled species of *Abyssamina, Quadrimorphina,* and *Clinapertina;* the occurrence of small smooth-walled buliminid species (e.g., *Bulimina kugleri* and *Bulimina simplex*); and small specimens of *N. truempyi, O. umbonatus, A. spissiformis,* and *N. havanense*. *Tappanina selmensis* and *Siphogenerinoides brevispinosa* vary strongly in relative abundance, and unilocular, siphonodosariid, laevidentalinid, and pleurostomellid taxa are present. Samples in relatively clay rich intervals at 193.0 mcd (Sam-

ple 208-1267A-19H-3, 10–11 cm) and 205.0 mcd (Sample 20H-3, 108–109 cm) contain assemblages with relatively low species richness, which are dominated by *Clinapertina complanata* and *A. poagi*.

In the lowermost part of this interval (231.2–231.5 mcd; Samples 208-1267A-22H-6, 148–149 cm, through 22H-7, 20–21 cm), species richness is extremely low and long-lived unilocular and laevidentalinid taxa are absent. Similar assemblages have been described from immediately after the P/E benthic foraminiferal extinction event (BEE) (Müller-Merz and Oberhänsli, 1991; Thomas and Shackleton, 1996) and occur at other Leg 208 sites. Minute specimens of *A. quadrata, B. kugleri, Clinapertina inflata, Quadrimorphina profunda,* and small specimens of *O. umbonatus* and *N. truempyi* are common to abundant. The latter two species dominate most samples, but the lowermost sample is dominated by *A. quadrata*.

The BEE, including the uppermost appearance of *Stensioeina beccariiformis,* occurs between Samples 208-1267A-22H-7, 28–29 cm, and 22H-7, 37–38 cm (231.53-231.62 mcd), and between Sections 208-1267B-22H-CC and 23H-CC (227.3–238.2 mcd). Sample 208-1267A-22H-7, 28–29 cm (231.53 mcd), immediately above the lithologic contact between clay-rich material and underlying carbonate-rich material, is barren.

Samples between 231.6 and 249.9 mcd (Sample 208-1267A-22H-7, 37–38 cm, through Section 208-1267B-24H-CC) contain a typical pre-extinction Paleocene species-rich abyssal assemblage with common *S. beccariiformis, Cibicidoides hyphalus, Pullenia coryelli, Bulimina thanetensis,* and *Aragonia velascoensis,* large agglutinant taxa such as *Clavulinoides amorpha, Clavulinoides trilatera,* and *Marssonella oxycona,* as well as large smooth-walled *Gyroidinoides* species such as *Gyroidinoides beisseli* and *Gyroidinoides globosus,* all of which became extinct during the BEE. *S. brevispinosa* and *Rectobulimina carpentierae* are present in most samples at highly variable relative abundances, as in coeval assemblages at Sites 1262 and 1266.

The assemblages change gradually in species composition between 249.9 and 286.5 mcd (Sections 208-1267B-24H-CC through 208-1267A-27X-CC), with *Abyssamina* and *Clinapertina* species and *B. thanetensis* becoming less common downhole, and *Nuttallinella florealis, Nuttallinella* sp., and various agglutinants such as *Rhizammina* spp. becoming more common. *Spiroplectammina dentata* has its local uppermost appearance in this interval, and *Tritaxia havanensis* and *B. thanetensis* have their lowermost occurrences. Benthic foraminiferal assemblages show a coeval, similar faunal change (including the B of *B. thanetensis*) at Site 1262 and at ODP Sites 689 and 690 at Maud Rise (Thomas, 1990), which may be the benthic foraminiferal expression of the mid-Paleocene biotic event, or it may have occurred slightly earlier. At Sites 1262 and 1267, the paleodepth changed in the middle Paleocene and the assemblages were affected by dissolution, reworking, and downslope transport (Fig. **F19**). These factors may have contributed to the faunal change at Sites 1262 and 1267, but widespread paleoceanographic changes may also have played a role.

The benthic foraminiferal assemblages between 296.6 mcd and the bottom of the hole at 368.0 mcd (Sections 208-1267A-28X-CC through 208-1267B-36X-CC) closely resemble assemblages in the Velasco Formation in Mexico, where many of the species present at Site 1267 were first described (Alegret and Thomas, 2001). Common to abundant species include some that range through the Paleocene, such as *S. beccariiformis, Clavulinoides* spp., *G. beisseli, G. globosus, Gyroidinoides quadratus, M. oxycona,* and *Gaudryina pyramidata,* and long-ranging species such *O.*

umbonatus and *N. truempyi*. Assemblages between 320.2 and 320.4 mcd (Samples 208-1267A-31X-3, 50–51 cm, through 74–75 cm), across the K/P boundary, document that benthic foraminifers at Site 1267 did not suffer significant extinction at that time, as observed at many other sites. As at Site 1262, the uppermost appearance of *Praebulimina reussi* occurs at the K/P boundary in the shipboard data, but it is not well documented whether the species disappeared globally.

PALEOMAGNETISM

Drilling and Core Orientation

Every other core at Site 1267 was recovered with a nonmagnetic core barrel until the first core barrel had to be drilled over (see "Operations," p. 2) (Table T1). As at other sites, no obvious difference was noticed in the magnetic data between sediments recovered with the nonmagnetic barrel and those recovered with a standard core barrel. All APC cores in Holes 1267A and 1267B were successfully oriented with the Tensor tool with the exception of Cores 208-1267A-1H, 2H, 8H, and 25H and 208-1267B-1H, 2H, 3H, and 21H (see "Operations," p. 2) (Table T1).

Archive-Half Measurements

The archive halves of 69 cores from Holes 1267A and 1267B were measured in the pass-through magnetometer. Natural remanent magnetization (NRM) was measured on all cores. Most cores were demagnetized at 10 and 15 mT. As at other sites, a strong vertical overprint is largely removed by demagnetization to 10 mT.

Remanent Magnetization Intensity

The initial NRM (prior to demagnetization) of the sediments exhibits weaker intensity in the upper 100 mcd (on the order of 10^{-3} to 10^{-2} A/m) and stronger intensity below 100 mcd (on the order of 10^{-2} to 10^{-1} A/m) (Fig. F21). After demagnetization to 15 mT, intensities are typically on the order of 10^{-4} to 10^{-2} A/m, with the notable exception being the interval between 73 and 83 mcd, where intensities are on the order of 10^{-5} A/m.

As discussed in the Site 1266 chapter, the upper 100 mcd at Site 1267 also exhibits low magnetic intensity (Fig. F21), low to negative susceptibility (Fig. F22), and elevated values of depositional remanent magnetization normalized by susceptibility (nDRM) (Fig. F23). This was observed at all Leg 208 sites and, if no change in the average geomagnetic field intensity is assumed, could be interpreted as diagenetic alteration of magnetite.

Magnetostratigraphy

The magnetostratigraphy of Site 1267 is similar to that of Site 1262 in that the mid- to upper Pliocene through the Pleistocene, as well as the Paleocene and uppermost Cretaceous, are well resolved (Fig. F24). Magnetostratigraphic age-depth tie points are given in Table T10. The placement of the top of Chron C2n (1.785 Ma) at ~17.5–18.0 mcd is confirmed by the shipboard cyclostratigraphy (see "Synthesis," p. 25,

F21. Intensities, 0- and 15-mT demagnetization, p. 48.

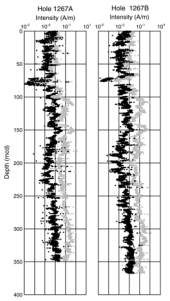

F22. Initial MS, p. 49.

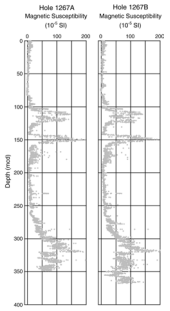

F23. $nDRM_{15\,mT}$, p. 50.

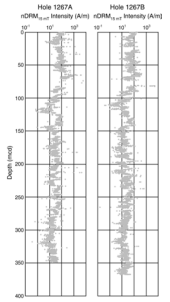

F24. Magnetostratigraphic interpretation, p. 51.

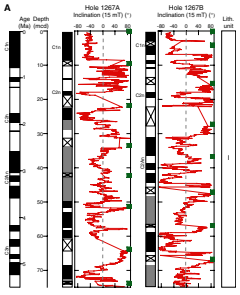

T10. Magnetostratigraphic age-depth tie points, p. 71.

in the "Leg 208 Summary" chapter) and agrees well with the bottom of nannofossil datum medium *Gephyrocapsa* spp. (1.69 Ma) at ~16.2–17.4 mcd (see Table T10; "Biostratigraphy," p. 9). The top of Chron C2An at ~31 mcd is also confirmed by the cyclostratigraphy.

Most of the Miocene and upper Oligocene are condensed or missing, but Chron C13n at the base of the Oligocene is well resolved (Fig. F24), as at all other sites. Chron C13n is constrained by the tops of nannofossil datums *E. formosa* and *D. saipanensis*. Most of the upper Eocene is lost in a hiatus, but we interpret the middle Eocene sequence from Chrons C20n through C22n. The lower Eocene is not well resolved, but the base of Chron C24n is tentatively identified in Hole 1267B at ~205 mcd. Confirmation of this awaits the analysis of discrete samples.

Below the P/E boundary, all of the polarity boundaries are identifiable in at least one of the two holes (Fig. F24). Whereas at other sites the inclination data from XCB cores are characterized by a high degree of scatter and are generally not interpretable, the data from Site 1267 XCB cores are excellent. This difference is attributed to the sediments at Site 1267 being relatively well lithified compared to those at the other sites. The lack of significant drilling-related deformation allows for the unambiguous determination of reversal boundaries for Chrons C26n through C31n.

GEOCHEMISTRY

Volatile Hydrocarbons

A total of 29 headspace samples from Site 1267 (all from Hole 1267A) were analyzed. The concentration of CH_4 (C_1) in most of the samples was at an atmospheric background level (range = 1.6–2.0 ppmv) and did not exceed 2.3 ppmv in any sample. No hydrocarbon gases higher than C_1 were detected.

Interstitial Water Chemistry

Interstitial waters from 23 samples were collected at Site 1267 from Hole 1267A (7.5–346.8 mcd). One sample (208-1267A-11H-5, 140–150 cm; 110.6 mcd) consisted of very fine grained clay-rich material, which when squeezed, passed through the filter paper into the syringe. At Site 1262 such sediments were also encountered, but no interstitial waters were recovered. However, by using three sheets of filter paper in the squeezer instead of the usual single sheet, ~3 mL of interstitial water was successfully squeezed from Sample 208-1267A-11H-5, 140–150 cm, before the sediments extruded from the press. This small sample provides insights into the influence of such clay-rich sediments on pore water chemistry. Chemical constituents were determined according to the procedures outlined in "Geochemistry," p. 23, in the "Explanatory Notes" chapter. Results of the chemical analyses are presented in Table T11.

T11. Results of interstitial water analyses, p. 72.

pH, Salinity, Alkalinity, Chloride, and Sodium

The pH of pore waters at Site 1267 ranges from 7.28 to 7.47 (average = 7.39 ± 0.05) (Table T11). All values are lower than the average seawater value of 8.1, and no distinct depth trend is recognizable. Salinity typically ranges from 34.0 to 35.5 g/kg (mean value = 34.9 ± 0.3 g/kg).

Alkalinity decreases with depth in Site 1267 pore waters from 3.34 mM at 7.5 mcd to a minimum of 1.17 mM at 334.8 mcd near the base of the section (Fig. F25A). At the transition from APC to XCB coring techniques (between 264.7 and 275.2 mcd), there is a marked increase in alkalinity probably related to increased seawater contamination in the XCB-recovered samples.

The chloride concentrations at Site 1267 are generally constant downhole, with values between 560 and 570 mM (Fig. F25B). Two anomalously low chloride values of 534 and 523 mM occur at depths of 29.2 and 71.2 mcd, respectively. The sodium profile does not exhibit any significant downhole trend, with concentrations varying between 459 and 481 mM (Fig. F25C).

Potassium, Calcium, Magnesium, Strontium, and Lithium

Site 1267 downhole trends in potassium, calcium, and magnesium are consistent with those resulting from exchange with basaltic basement at depth (Gieskes, 1981), with potassium and magnesium decreasing and calcium increasing with depth (Fig. F25D, F25E, F25F). Pore water potassium concentrations decrease with depth from 10.8 mM (7.5 mcd) to 6.9 mM (346.8 mcd) (Fig. F25D).

Interstitial water calcium values increase from 10.1 mM (7.5 mcd) to 26.6 mM (346.8 mcd) (Fig. F25E). The magnitude of the downhole increase in calcium concentrations (16.5 mM) is substantially larger than those observed at Sites 1262–1265 but is only slightly larger than the downhole increase in calcium measured for Site 1266 samples (15.4 mM).

The magnesium pore water profile (Fig. F25F) at Site 1267 is characterized by a general decrease with depth, from 52.4 mM in the shallowest sample (7.5 mcd) to 40.8 mM near the base of the section (334.8 mcd). The deepest sample (346.8 mcd) has an anomalously high magnesium concentration of 53.6 mM, which is close to the value of seawater (54 mM International Association of Physical Sciences of the Ocean certified value), suggesting seawater contamination of this sample. However, a similar seawater influence is not observed for other elements in this sample.

Strontium concentrations increase downhole from 143 µM in the shallowest sample (7.5 mcd) to peak at values between 386 and 412 µM from 49.7 to 110.6 mcd (Fig. F25G). Below 110.6 mcd, strontium concentrations decrease gradually downhole to 255 mM at the base of the section (346.8 mcd). The strontium pore water profile indicates a source of strontium to the interstitial waters between 49.7 and 110.6 mcd and diffusion of this strontium into the pore waters of the sediments above and below. The dissolution and recrystallization of carbonates is considered to be the major source of strontium to pore waters of carbonate-rich sediments (e.g., Baker et al., 1982), suggesting that a zone of carbonate recrystallization exists between 49.7 and 110.6 mcd at Site 1267.

Lithium concentrations generally increase downhole from 24.6 µM in the shallowest sample (7.5 mcd) to 40.4 µM at the base of the section (346.8 mcd) (Fig. F25H). Similar downhole increases in pore water lithium concentrations have been observed at all other sites with the exception of Site 1264, where the increase with depth starts below ~150 mcd as opposed to the top of the section. At all sites, there is a deep source of lithium from the sediments to the pore waters. However, the source of the pore water lithium remains elusive and could be present at depths greater than the recovered sections.

F25. Chemical constituents in interstitial waters, p. 56.

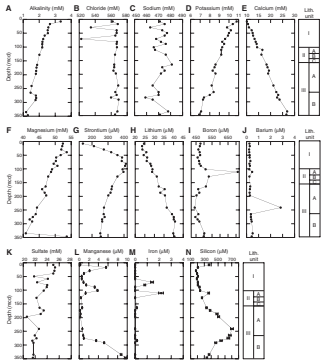

Boron and Barium

Pore water boron concentrations are relatively constant at values between 460 and 480 µM from 7.5 to 88.9 mcd, after which boron concentrations increase to values >500 µM to a depth of 164.2 mcd (Fig. F25I). Below 164.2 mcd, boron values drop to between 442 and 471 µM before increasing to values of ~500 µM at 334.8 and 346.8 mcd. At 110.6 mcd, there is a large spike (711 µM) in pore water boron concentrations occurring in the clay-rich sediments of lithostratigraphic Subunit IIA (see "Subunit IIA," p. 6, in "Unit II" in "Description of Lithostratigraphic Units" in "Lithostratigraphy"). A study of Leg 186 interstitial water samples (Deyhle and Kopf, 2002) concluded that the removal of boron from clays and volcanic ash was responsible for boron enrichment in the pore waters. Therefore, the pore water boron peak at 110.6 mcd suggests that boron is being leached from the clay-rich sediments of lithostratigraphic Subunit IIA.

Pore water barium values are consistently low and fluctuate downhole between 0.21 and 0.51 µM, with the only exception being a concentration of 2.83 µM that occurs at 240.7 mcd (Fig. F25J).

Sulfate, Manganese, and Iron

The sulfate pore water profile at Site 1267 displays a downhole decrease from 25.0 mM in the shallowest sample (7.5 mcd) to 21.6 mM at the base of the section (346.8 mcd) (Fig. F25K). The high sulfate concentrations at Site 1267 (average = 23.0 ± 1.4 mM) preclude significant sulfate reduction associated with the microbial decomposition of organic matter (e.g., Gieskes, 1981).

The Site 1267 manganese pore water profile (Fig. F25L) increases sharply from 0.21 µM at the top of the section (7.5 mcd) to 5.59 µM at 16.0 mcd before decreasing to values of ~0.50 µM at 49.7 and 58.7 mcd. Below this, manganese pore water concentrations rise to a second downhole peak of 3.81 µM at 101.6 mcd before dropping to values below 1 µM in the section spanning from 127.9 to 275.2 mcd. From 284.0 mcd, pore water manganese values increase sharply downhole to peak at 9.62 µM at the base of the section (346.8 mcd), which is the highest manganese value measured in all the pore water samples from Leg 208.

Pore water concentrations of dissolved iron are typically low and often below detection limits throughout the section (Table T12; Fig. F25M), but distinct peaks with iron concentrations of 1.40 and 2.15 µM are present at 71.2 and 110.6 mcd, respectively. The peak in dissolved iron at 71.2 mcd occurs in sediments containing iron oxide bands, which can be observed by a drop in chromaticity a* (see Fig. F12; "Lithostratigraphy," p. 4); the iron oxide bands provide a likely source for the dissolved iron in this interval. The pore water iron peak at 110.6 mcd occurs in the clay-rich sediments of lithostratigraphic Subunit IIA (see "Subunit IIA," p. 6, in "Unit II" in "Description of Lithostratigraphic Units" in "Lithostratigraphy") and is coincident with a large peak in pore water boron concentrations. This could indicate that, like with boron, these clays are a source of dissolved iron to the pore waters.

T12. Sedimentary calcium carbonate concentrations, p. 73.

Silicon

Dissolved silicon in pore waters from Site 1267 decreases slightly from 369 µM at a depth of 7.5 mcd to 179 µM at 29.2 mcd (Fig. F25N). Below this, the silicon concentrations generally increase downhole to

peak at values between 651 and 704 µM from 240.7 to 275.2 mcd before decreasing to 338 µM at the base of the section (346.8 mcd). Although this maximum dissolved silicon concentration of 704 µM at Site 1267 is greater than those observed at Sites 1262 (412 µM) and 1264 (340 µM), it is less than half the amount of dissolved silicon (>1400 µM) measured in the deepest samples from Sites 1263, 1265, and 1266 where cherts were recovered. Dispersed volcanic ash was observed below 148.1 mcd at Site 1267, and the weathering of this silicate material is a likely source of the dissolved silicon in the pore waters.

Summary of Interstitial Water Chemistry

Although the calcium, potassium, and magnesium interstitial water profiles at Site 1267 suggest that a simple diffusion profile between seawater and basement basalt is responsible for the chemistry of the pore waters, other elements including strontium, lithium, manganese, iron, and silicon indicate that diagenetic processes occurring in the sediments also have a strong impact on the interstitial water chemistry. The pore water profile of strontium from Site 1267 is very similar to that of Site 1262, with both indicating a relatively shallow zone of maximum carbonate recrystallization in the sediments.

Sediment Geochemistry

Carbonate determinations by coulometry were made for a total of 157 samples from Site 1267 (Table **T12;** Fig. **F26**). The carbonate values in Unit I average 92.6 wt%. In clay-rich Subunit IIA, carbonate content drops dramatically (average = 48.0 wt%) before increasing again in Subunit IIB, where the average carbonate value is 83.5 wt%. In Subunit IIC, the average carbonate content is 54.6 wt%. Excluding the high-resolution P/E boundary samples, the average carbonate content in Subunit IIIA is 90.5 wt%, and in Subunit IIIB, carbonate content decreases downhole, giving an average value of 80.3 wt%.

Closely spaced (every 2 to 10 cm) samples were analyzed for carbonate content across the P/E boundary section from Holes 1267A and 1267B (Fig. **F26B**). Although a small offset in the occurrence of the carbonate minimum interval exists between the Hole 1267A and 1267B records, there are remarkable similarities in the fine structure (e.g., the small dip in carbonate content between 231.6 and 231.7 mcd and the slowing in the rate of recovery of carbonate preservation after the P/E minimum at ~231.3 mcd). At the P/E boundary above 231.6 mcd, carbonate drops from ~80 to <1 wt% within <10 cm of sediment. The carbonate minimum spans over 10 cm, and above 231.5 mcd, the carbonate values increase uphole to ~90 wt% over ~30 cm.

F26. Sedimentary carbonate content vs. composite depth, p. 57.

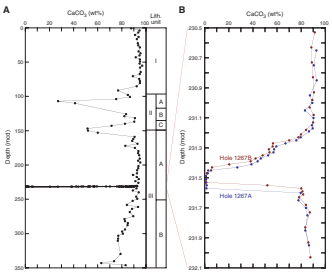

Extractable Hydrocarbons

Extraction of organic matter (24-hr duration) was performed on four samples (Samples 208-1267A-1H-5, 140–150 cm, at 7.5 mcd; 16H-4, 140–150 cm, at 164.2 mcd, and 32X-4, 140–150 cm, at 334.8 mcd after squeezing interstitial water, and Sample 15H-7, 23–29 cm, at 155.3 mcd).

Mass chromatograms (*m*/*z* 85) of all samples analyzed showed *n*-C_{14} through *n*-C_{18} alkanes (Fig. **F27**). Branched isoprenoids were minor components except for pristane and phytane in the aliphatic hydrocarbon fraction of each sample. This feature is generally observed in the

F27. Mass chromatograms of aliphatic hydrocarbon, p. 58.

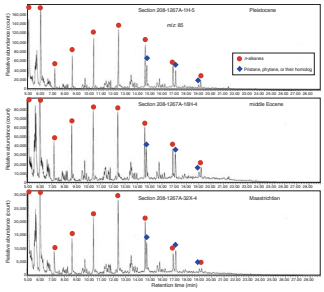

sediments of Oligocene age and also in younger sediments from the other Leg 208 sites. The results from Sections 208-1267A-15H-7, 16H-4, and 32X-4 (Fig. F27) indicate that this character of aliphatic hydrocarbons occurs down to the upper Maastrichtian. On the other hand, Paleocene and Eocene samples from Sites 1262 and 1263 showed a predominance of anteiso-alkanes or 3-methyl-hosted branched isoprenoids, some of which are also found as minor components in the samples analyzed.

Pristane and phytane were also abundant in the aliphatic hydrocarbon fraction of all samples, exhibiting clear peaks in the mass chromatograms (Fig. F27).

AGE MODEL AND MASS ACCUMULATION RATES

A 368.0-mcd-thick (329.3 mbsf) Maastrichtian (~68 Ma) to Pleistocene pelagic sediment sequence was recovered at Site 1267. A total of 116 biostratigraphic datums and 29 magnetostratigraphic age-depth tie points (Table T13) were used to construct an age-depth model for this site (Table T14; Fig. F28). Linear sedimentation rates (LSRs), total mass accumulation rates (MARs), and carbonate MARs were calculated at 1-m.y. intervals (see "Age Model and Mass Accumulation Rates," p. 33, in the "Explanatory Notes" chapter).

T13. Datum levels, p. 74.

T14. Age-depth model, LSRs, and MARs, p. 77.

F28. Age-depth model, p. 59.

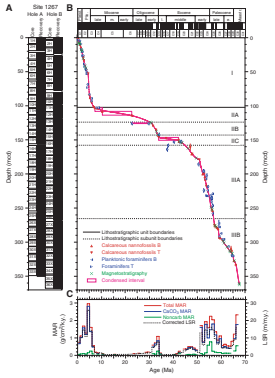

Age-Depth Model

The main objective of Site 1267 was to recover a complete and well-resolved Maastrichtian to lower Eocene section, and the site was chosen to yield this critical stratigraphic interval at a relatively shallow burial depth. The sediment section at Site 1267 is therefore characterized by significant condensed intervals and unconformities throughout the middle Eocene to upper Miocene section, with unconformities identified at 42–34 Ma (151–146 mcd), 30–23 Ma (126–125 mcd), ~22.8–10.5 Ma (113–108 mcd), and 10.5–7.4 Ma (108–113 mcd). The age-depth model relies primarily on paleomagnetic and nannofossil data. Planktonic foraminiferal data generally agree with the calcareous nannofossil data but show considerably more scatter in some intervals, particularly the upper Paleocene to lower Eocene. Discrepancies in the interval between ~100 and 150 mcd result from massive reworking and severe dissolution, resulting in a condensed section interrupted by unconformities. Discrepancies in the upper Paleocene–lower Eocene probably result from the low resolution of shipboard studies and lack of intercalibration.

Linear Sedimentation and Mass Accumulation Rates

LSRs range between <1 and 26 m/m.y., and total MARs range from <0.1 to 3.0 g/cm²/k.y. Both LSR and MAR show high values in the Maastrichtian (67–65 Ma), low to moderate values in the lower Paleocene (65–60 Ma), and a broad peak from 60 to 50 Ma. Two minor peaks in the middle Eocene (50–42 Ma) and in the lower Oligocene (43–31 Ma) are separated by an interval of very low LSR and MAR that comprise a middle and late Eocene condensed interval/unconformity. The upper Oligocene to upper Miocene interval (31–7 Ma) is condensed and comprises two major unconformities. The Pliocene–Pleistocene interval has moderately high LSRs and MARs, apparently peaking at 5–4 Ma.

Noncarbonate MARs averaged over 1-m.y. intervals are generally low (<0.3 g/cm²/k.y.) throughout the section, and total MAR fluctuations essentially represent variations in carbonate MAR. The moderately high noncarbonate MAR values in the P/E boundary interval (56–54 Ma) are an exception. They result from carbonate-poor intervals a few centimeters to several decimeters thick (see "Lithostratigraphy," p. 4, and "Geochemistry," p. 21). These short-term carbonate dissolution events are smoothed out in the MAR record as a result of our 1-m.y. sampling of the age-depth model, dictated by the limited resolution of the shipboard age-depth control points and density and carbonate data.

REFERENCES

Alegret, L., and Thomas, E., 2001. Upper Cretaceous and lower Paleogene benthic foraminifera from northeastern Mexico. *Micropaleontology,* 47:269–316.

Baker, P.A., Gieskes, J.M., and Elderfield, H., 1982. Diagenesis of carbonates in deep-sea sediments—evidence from Sr^{2+}/Ca^{2+} ratios and interstitial dissolved Sr^{2+} data. *J. Sediment. Petrol.,* 52:71–82.

Boersma, A., 1984. Cretaceous–Tertiary planktonic foraminifers from the southeastern Atlantic, Walvis Ridge area, Deep Sea Drilling Project Leg 74. *In* Moore, T.C., Jr., Rabinowitz, P.D., et al., *Init. Repts. DSDP,* 74: Washington (U.S. Govt. Printing Office), 501–523.

Cande, S.C., and Kent, D.V., 1995. Revised calibration of the geomagnetic polarity timescale for the Late Cretaceous and Cenozoic. *J. Geophys. Res.,* 100:6093–6095.

Clark, M.W., and Wright, R.C., 1984. Paleogene abyssal foraminifers from the Cape and Angola basins, South Atlantic Ocean: DSDP 73. *In* Hsü, K.J., LaBrecque, J.L., et al., *Init. Repts. DSDP,* 73: Washington (U.S. Govt. Printing Office), 459–480.

Deyhle, A., and Kopf, A., 2002. Strong B-enrichment and anomalous boron isotope geochemistry in the Japan forearc. *Mar. Geol.,* 183:1–15.

Gieskes, J.M., 1981. Deep-sea drilling interstitial water studies: implications for chemical alteration of the oceanic crust, layers I and II. *In* Warme, J.E., Douglas, R.G., and Winterer, E.L. (Eds.), *The Deep Sea Drilling Project: A Decade of Progress*. Spec. Publ.—Soc. Econ. Paleontol. Mineral., 32:149–167.

Kelly, D.C., Bralower, T.J., Zachos, J.C., Premoli Silva, I., and Thomas, E., 1996. Rapid diversification of planktonic foraminifera in the tropical Pacific (ODP Site 865) during the late Paleocene Thermal Maximum. *Geology,* 24:423–426.

Lourens, L.J., Hilgen, F.J., Laskar, J., Shackleton, N.J., and Wilson, D., in press. The Neogene period. *In* Gradstein, F.M., Ogg, J., and Smith, A.G. (Eds.), *A Geological Time Scale 2004:* Cambridge (Cambridge Univ. Press).

Moore, T.C., Jr., Rabinowitz, P.D., et al., 1984. *Init. Repts. DSDP,* 74: Washington (U.S. Govt. Printing Office).

Müller-Merz, E., and Oberhänsli, H., 1991. Eocene bathyal and abyssal benthic foraminifera from a South Atlantic transect at 20–30°S. *Palaeogeogr., Palaeoclimatol., Palaeoecol.,* 83:117–171.

Raffi, I., Backman, J., and Rio, D., 1998. Evolutionary trends of calcareous nannofossils in the late Neogene. *Mar. Micropaleontol.,* 35:17–41.

Schmiedl, G., Mackensen, A., and Müller, P.J., 1997. Recent benthic foraminifera from the eastern South Atlantic Ocean: dependence on food supply and water masses. *Mar. Micropaleontol.,* 32:249–287.

Thomas, D.J., Bralower, T.J., and Zachos, J.C., 1999. New evidence for subtropical warming during the late Paleocene Thermal Maximum: stable isotopes from Deep Sea Drilling Project Site 527, Walvis Ridge. *Paleoceanography,* 14:561–570.

Thomas, E., 1990. Late Cretaceous through Neogene deep-sea benthic foraminifers (Maud Rise, Weddell Sea, Antarctica). *In* Barker, P.F., Kennett, J.P., et al., *Proc. ODP, Sci. Results,* 113: College Station, TX (Ocean Drilling Program), 571–594.

Thomas, E., and Shackleton, N., 1996. The Palaeocene–Eocene benthic foraminiferal extinction and stable isotope anomalies. *In* Knox, R.W.O'B., Corfield, R.M., and Dunay, R.E. (Eds.), *Correlation of the Early Paleogene in Northwest Europe*. Geol. Soc. Spec. Publ., 101:401–441.

Figure F1. *Meteor* Cruise M49/1 track chart showing the locations of Site 1267 (proposed Site WALV-11B) and alternate Site WALV-11A (DSDP Site 527) along line GeoB 01-039.

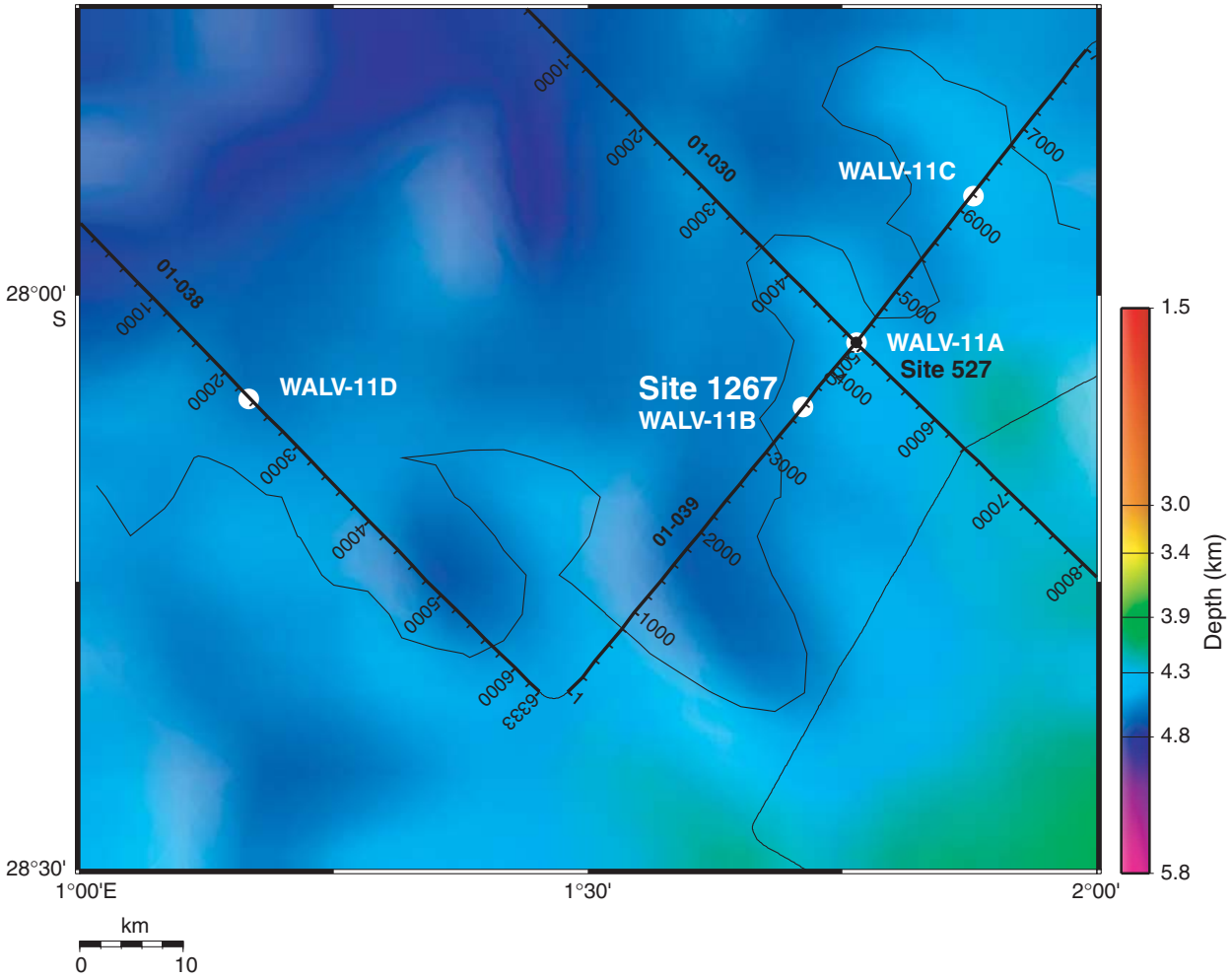

Figure F2. Locations of Site 1267 and DSDP Site 527 along Line GeoB 01-039. R_1 is a regional reflector that marks an unconformity or condensed interval. Although time transgressive, sediments below the reflector tend to be Paleogene in age and those above the reflector tend to be Neogene. The Paleocene/Eocene boundary reflector ($R_{P/E}$) is estimated to be at 216 mbsf, and the Cretaceous/Paleogene boundary ($R_{K/P}$) is estimated to be at 279 mbsf. Both reflectors can be traced over most of the ridge. CDP = common depth point.

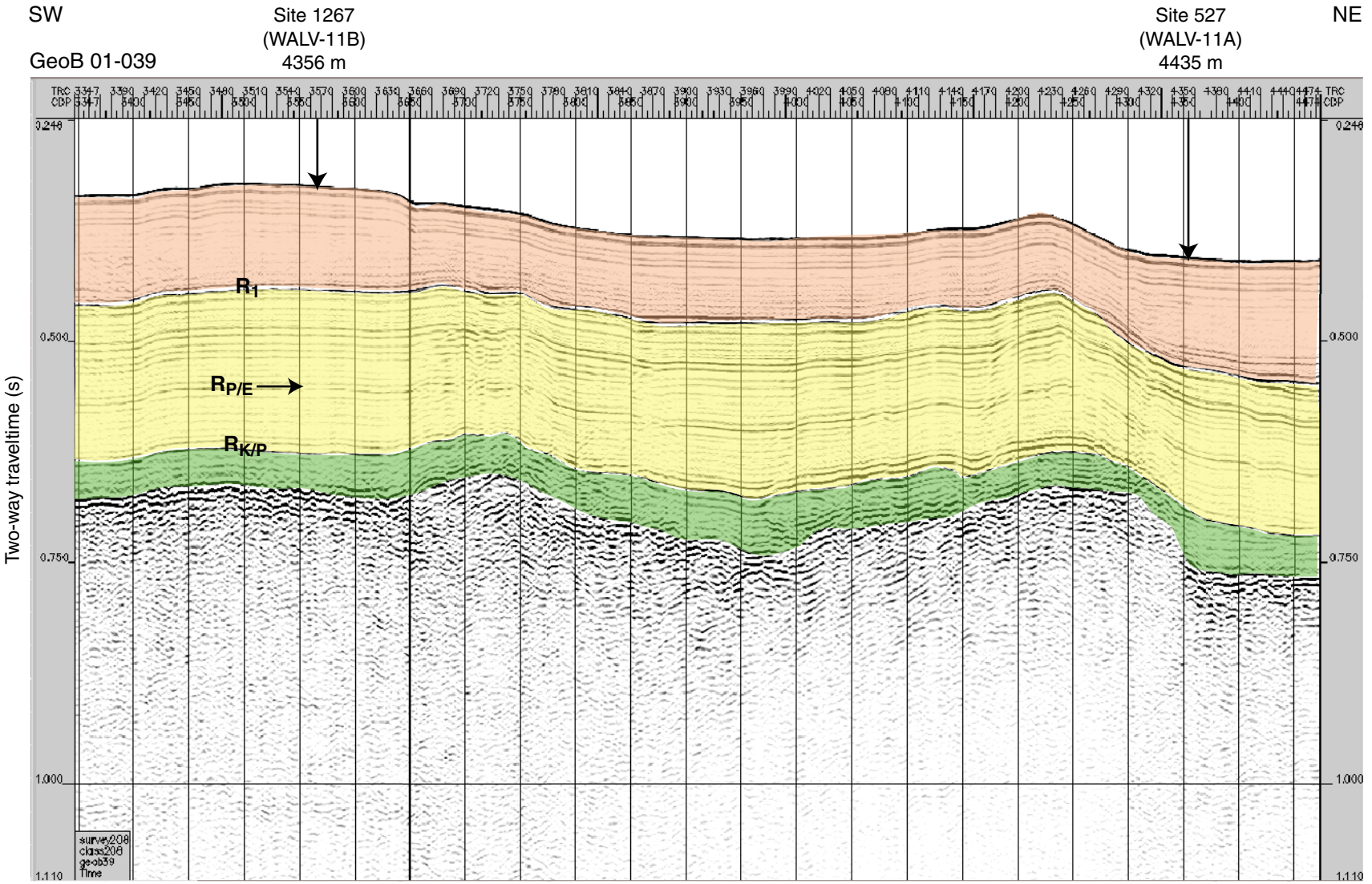

Figure F3. Magnetic susceptibility data from 0 to 367.5 mcd of Site 1267. Data from Holes 1267A and 1267B are offset from the spliced record by 10 and 100 times their values, respectively. Magnetic susceptibility values less than –1 instrument units were cut off at –1, and all values lower than 2 were multiplied by 0.5 and incremented by 1. Numbers near the tops of the individual core records refer to the core numbers. * = data from the top of the core is missing or was removed because of coring disturbance. O = Oligocene, E = Eocene.

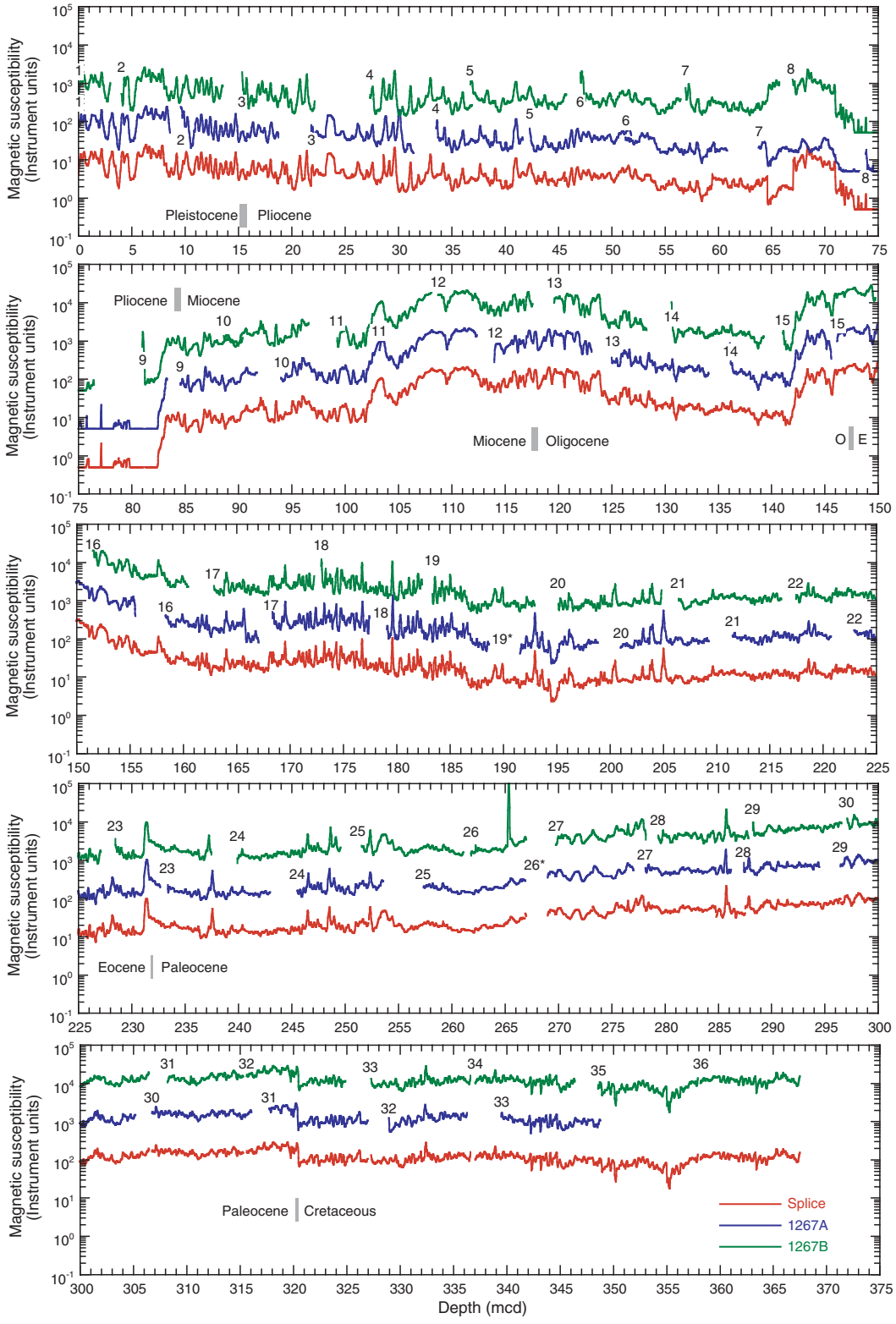

Figure F4. Orange (600 nm) to blue (450 nm) ratio from 0 to 367.5 mcd of Site 1267. Data from Holes 1267A and 1267B are offset from the spliced record by 1.5 and 3.0, respectively. Numbers near the tops of the individual core records refer to the core numbers. * = data from the top of the core is missing or was removed because of coring disturbance. O = Oligocene, E = Eocene.

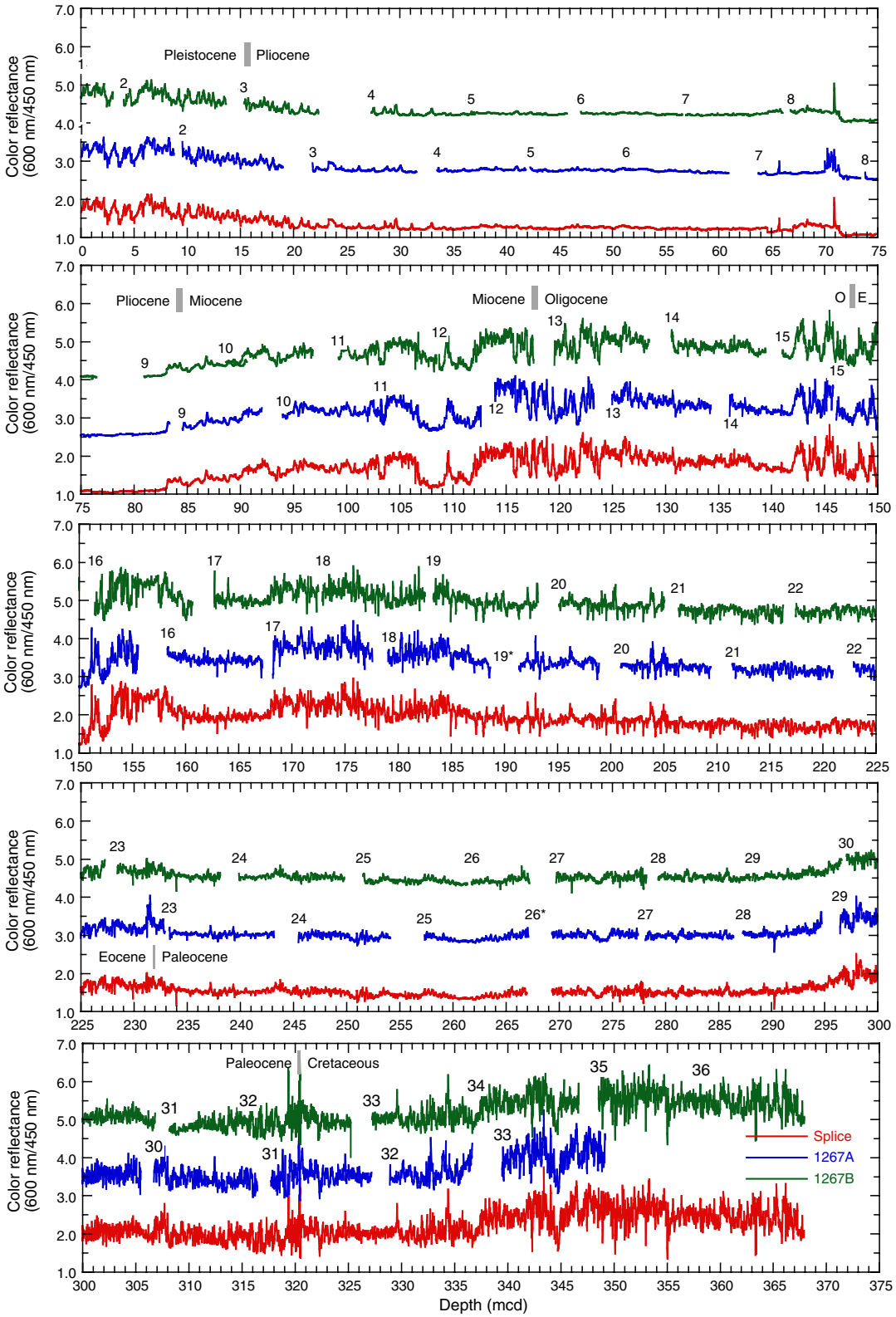

Figure F5. Mbsf vs. mcd growth rates for Holes 1267A and 1267B.

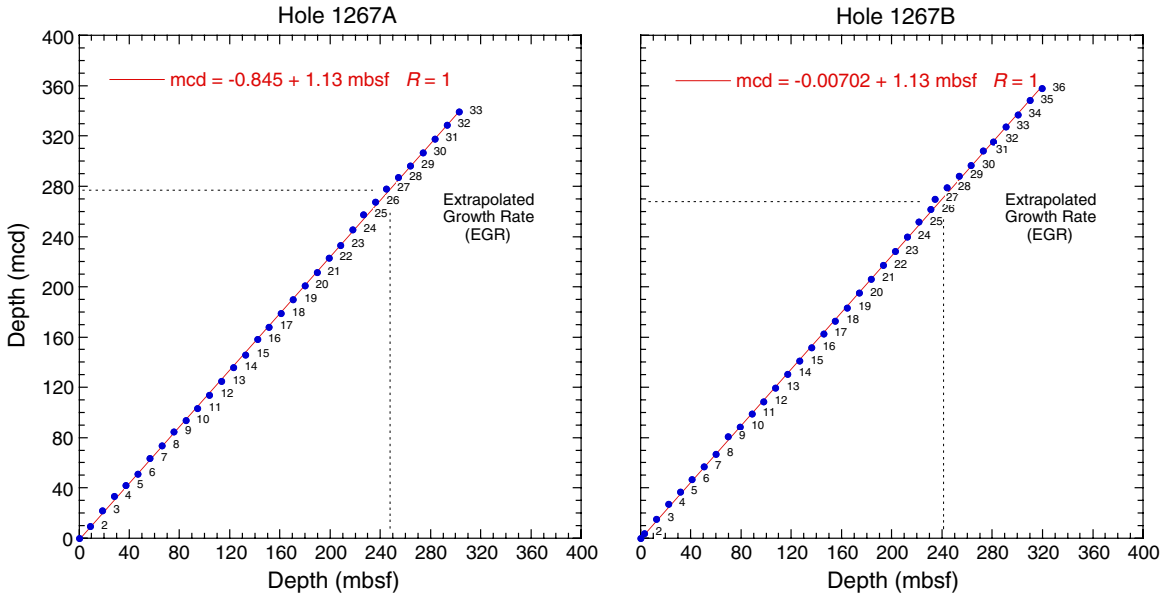

Figure F6. Site 1267 lithostratigraphic composite illustrating downhole variation in magnetic susceptibility (MS), natural gamma radiation (NGR), carbonate concentration, and sediment lightness (L*). Major lithostratigraphic unit boundaries coincide with step changes in these parameters. MS and NGR variations largely correlate with clay and ash content.

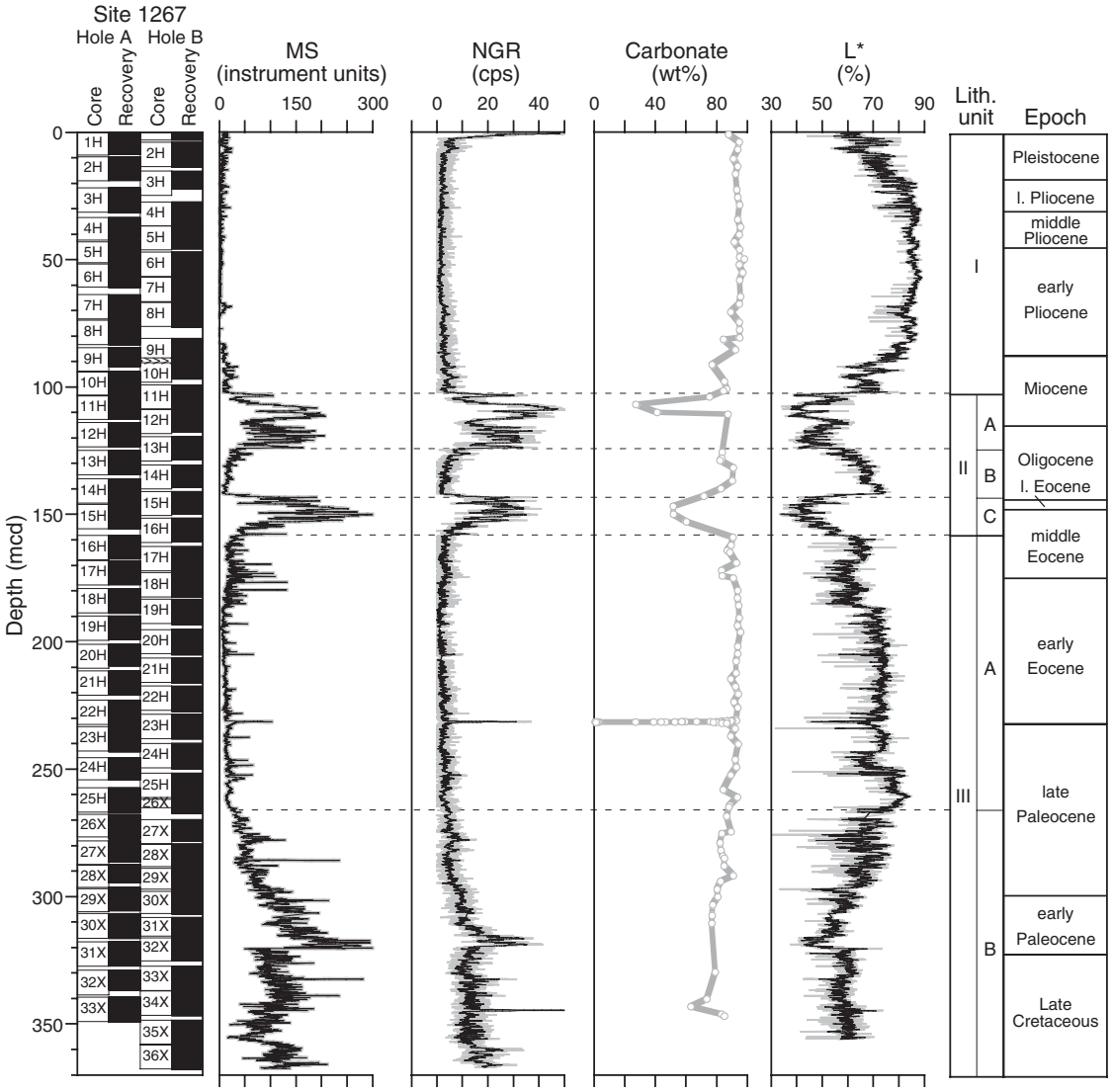

Figure F7. Site 1267 lithostratigraphic composite illustrating stratigraphic variation in whole-core multisensor track measurements of magnetic susceptibility (MS), natural gamma radiation (NGR), and gamma ray attenuation (GRA) bulk density. NGR data are smoothed with a 10-point moving average; all other data are smoothed with a 5-point moving average.

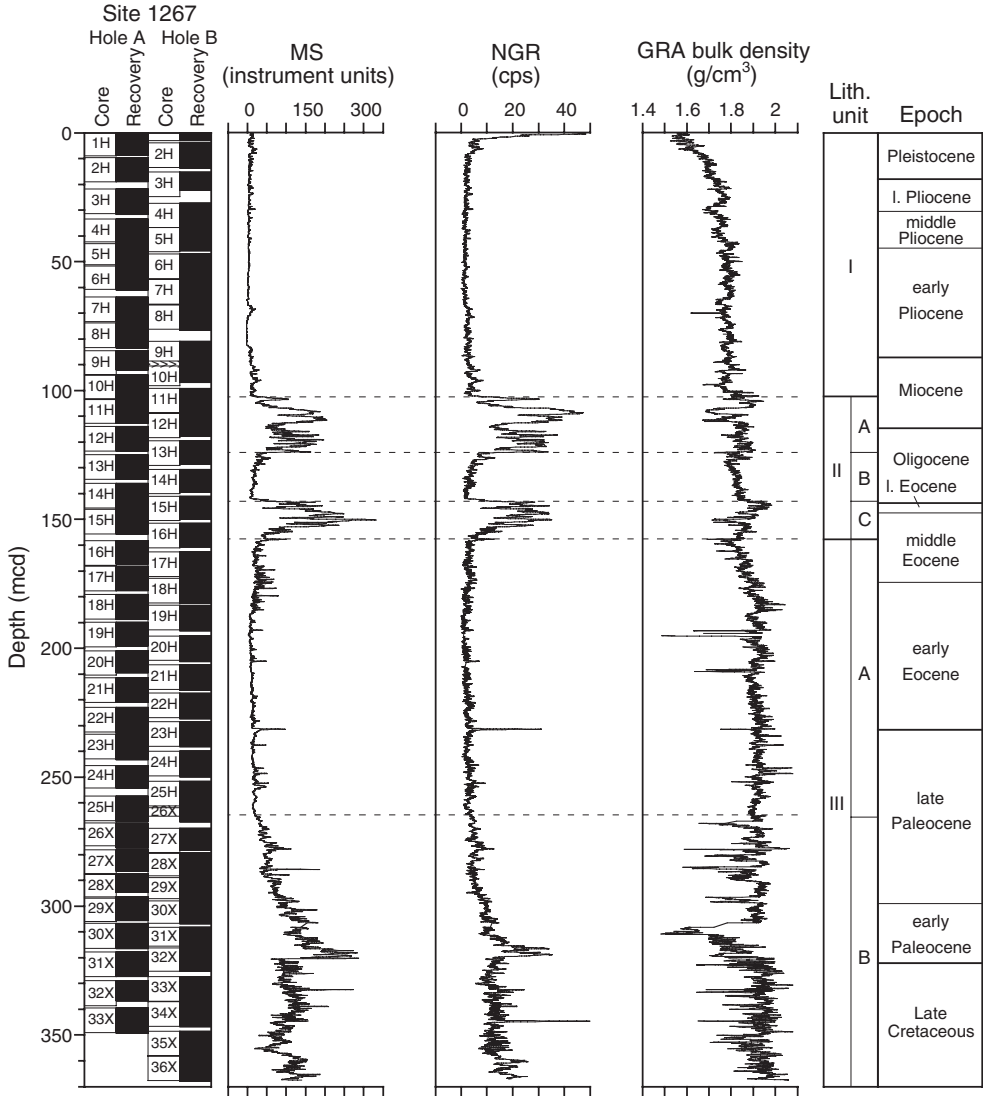

Figure F8. Site 1267 lithostratigraphic composite illustrating stratigraphic variation in lightness (L*), carbonate content, and chromaticity (a* and b*).

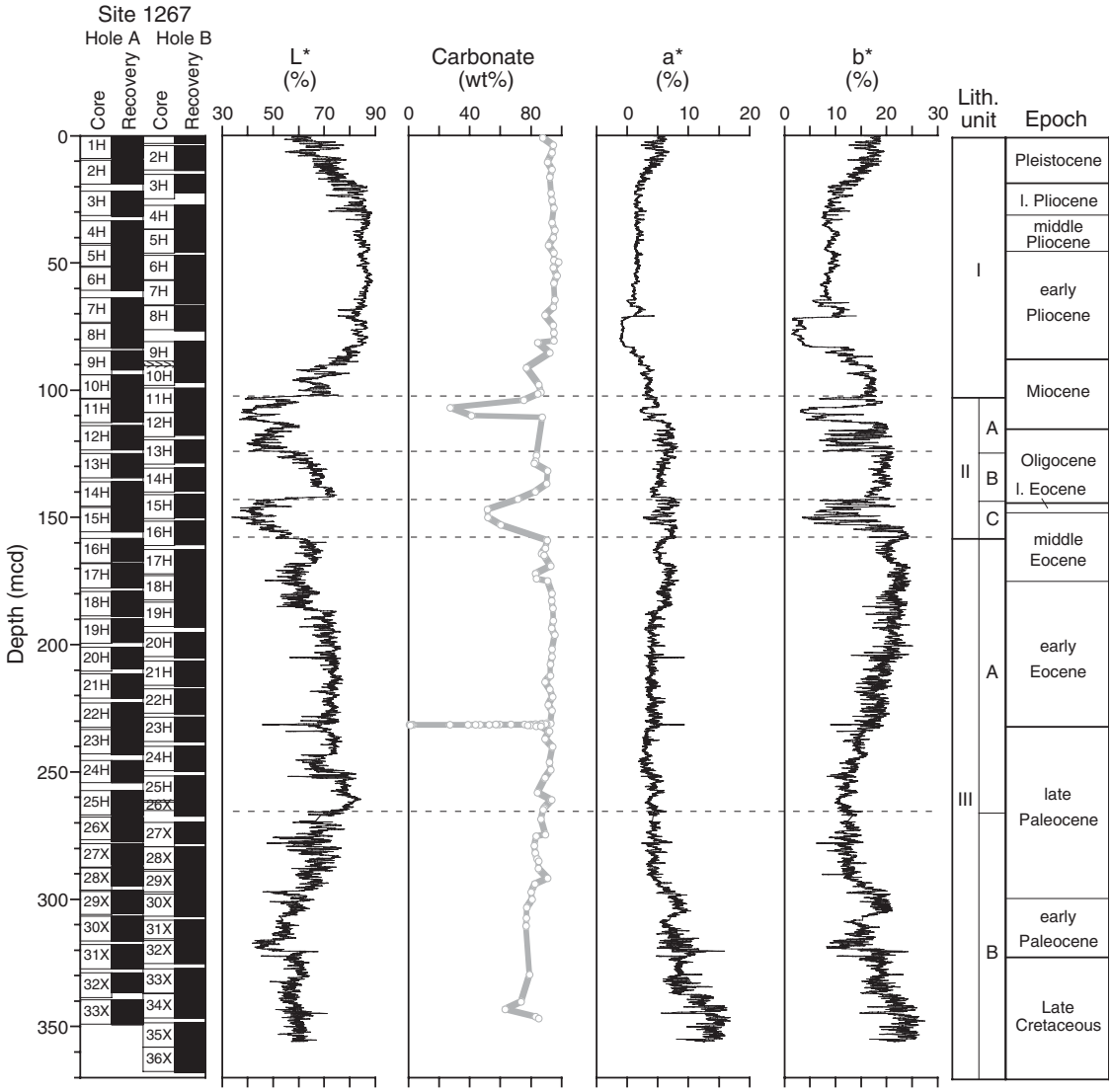

Figure F9. Site 1263 (single points) lithostratigraphic composite illustrating stratigraphic variation in predominant and accessory smear slide components.

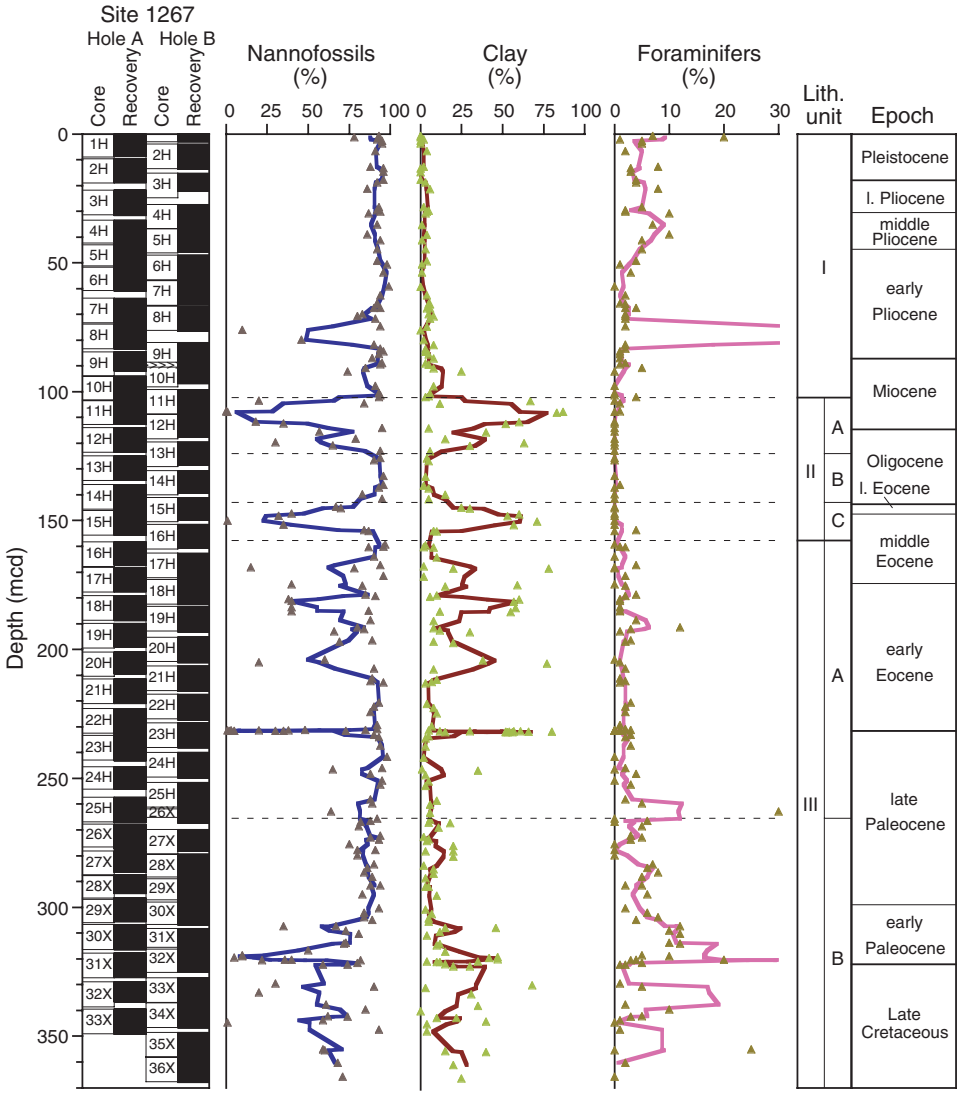

Figure F10. Site 1267 lithostratigraphic composite illustrating stratigraphic variation in physical properties of grain density (GD), bulk density (BD; MAD method), porosity, and *P*-wave velocity.

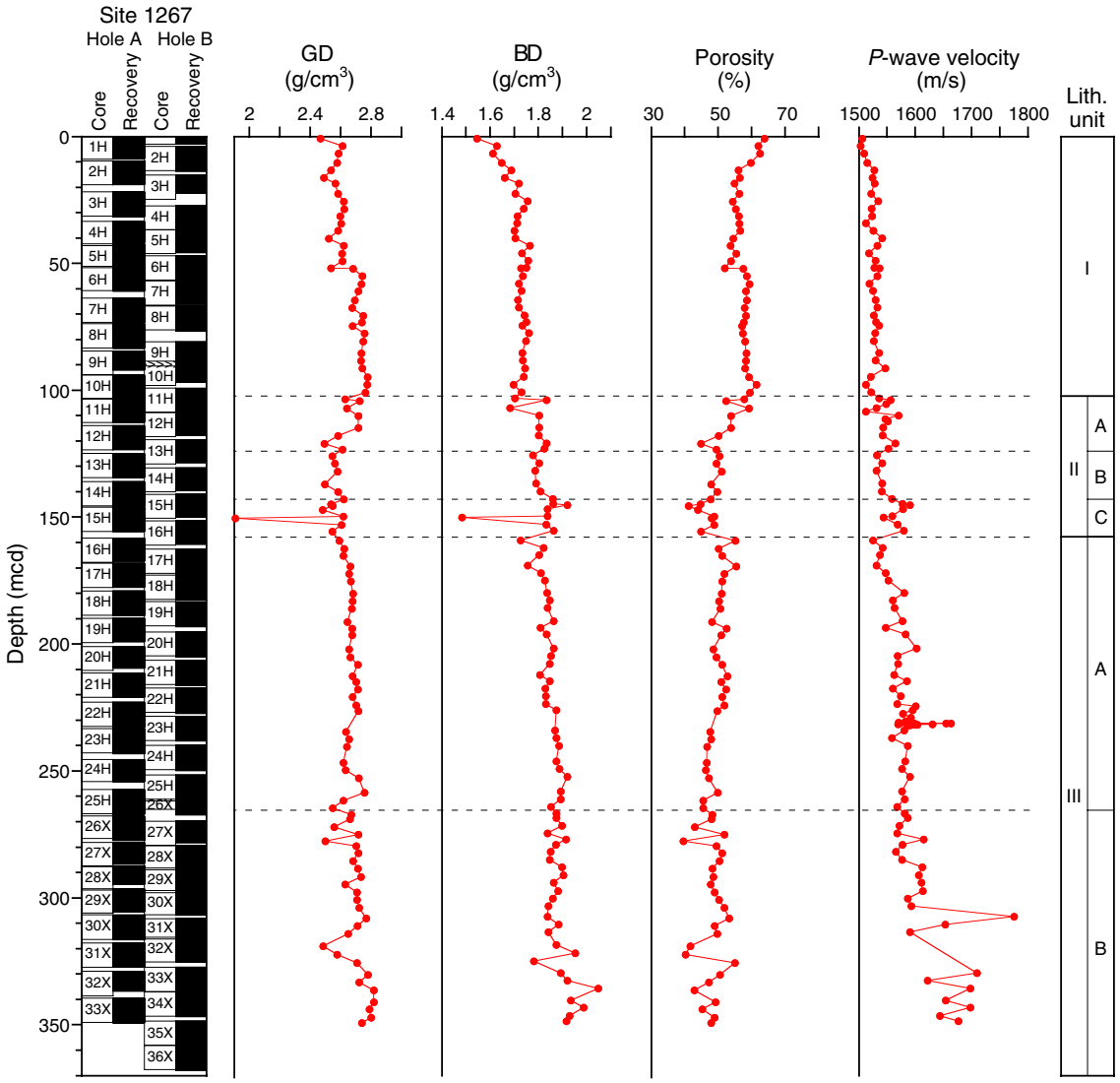

Figure F11. A, B. Comparison between bulk density (BD) measured with MAD (circles) and gamma ray attenuation (GRA) methods (light line = original MST data, dark line = 10-point average). **C.** Comparison between BD (MAD method) and grain density (GD). **D.** Comparison between BD (MAD method) and porosity. **E.** Comparison between BD (MAD method) and sound velocity measured with the *P*-wave velocity sensor number 3 (PWS3).

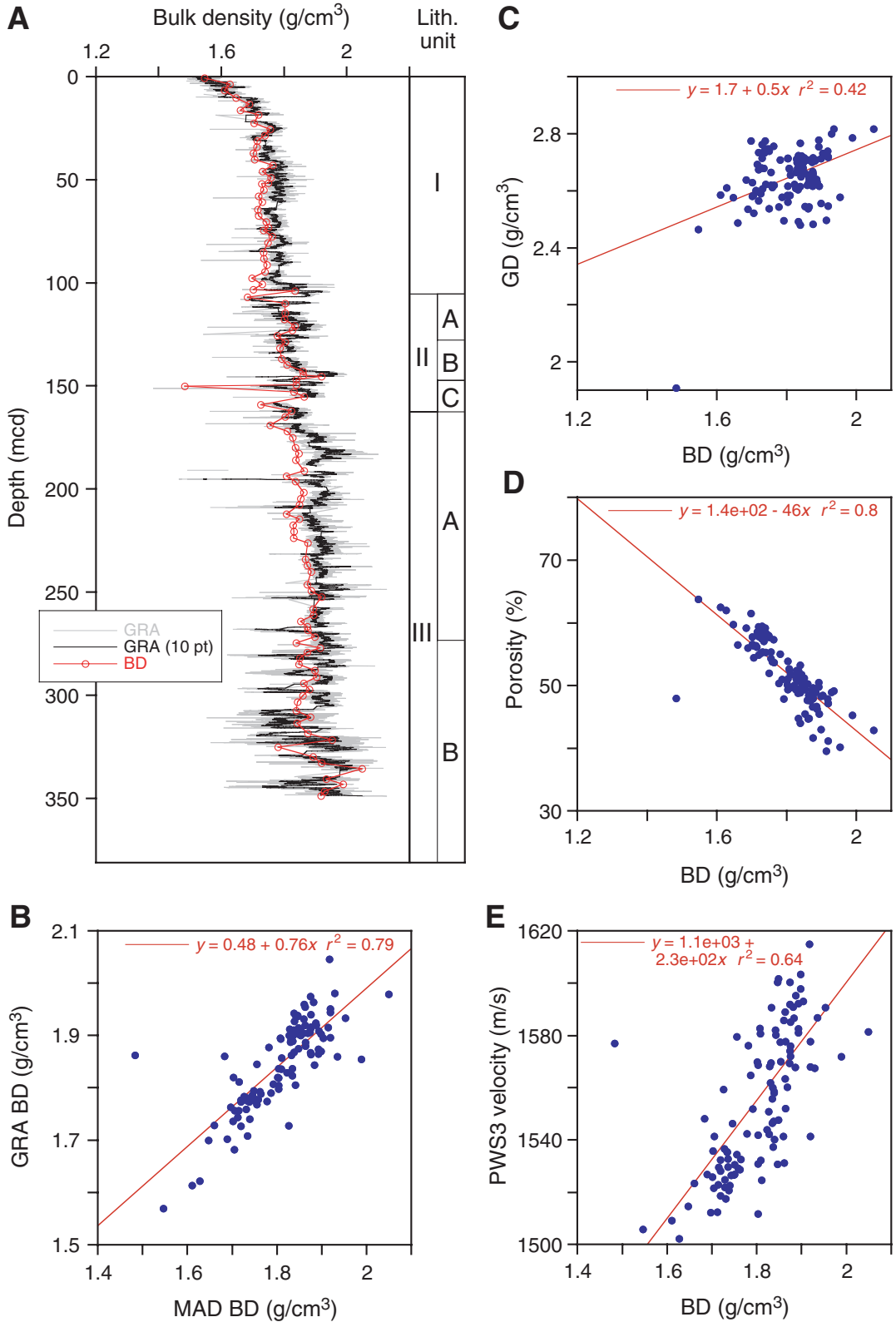

Figure F12. Site 1267 lithostratigraphic composite illustrating chromaticity (a*), manganese and iron concentrations in the interstitial waters, and grain density in lithostratigraphic units in Hole 1267A.

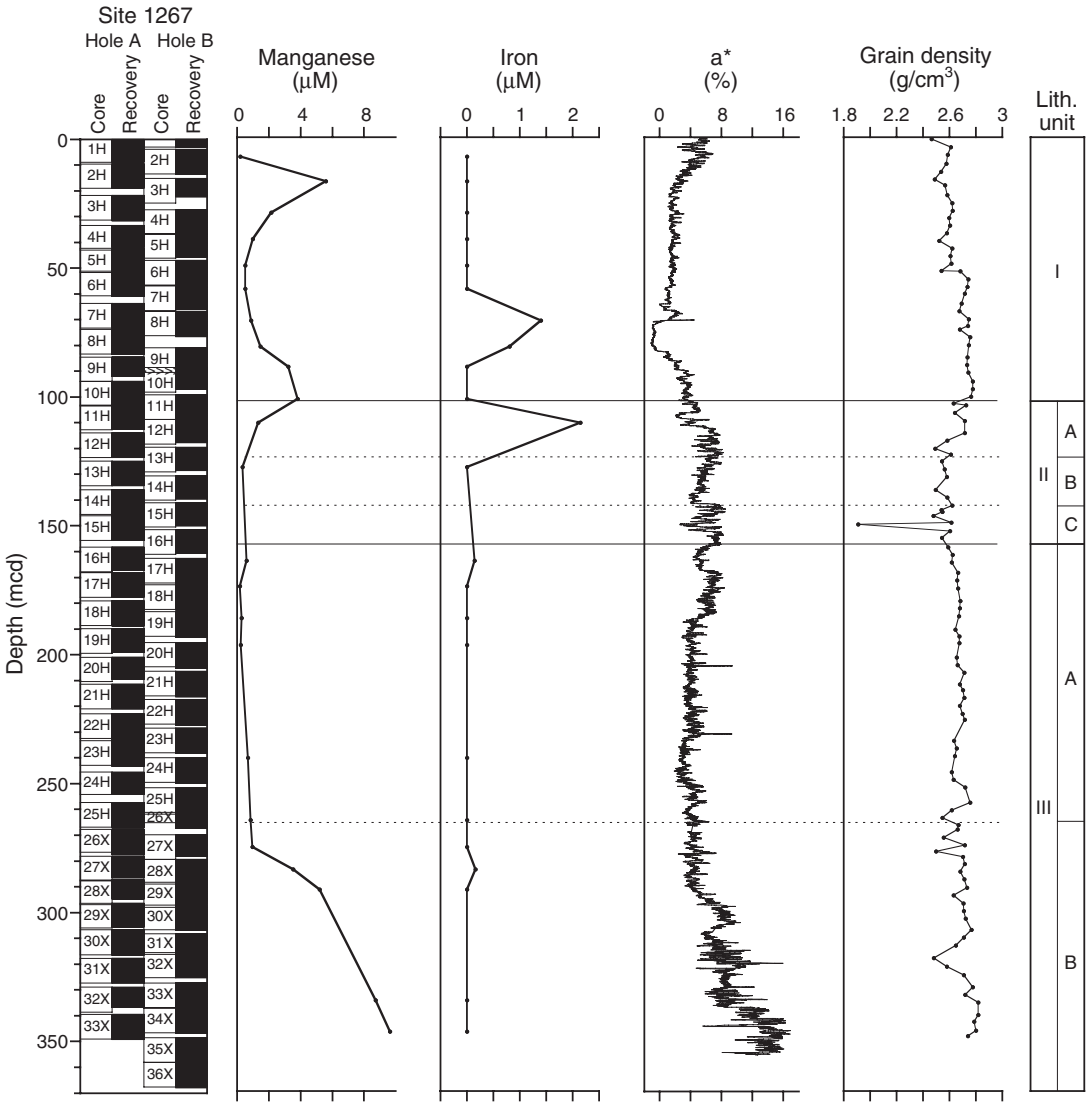

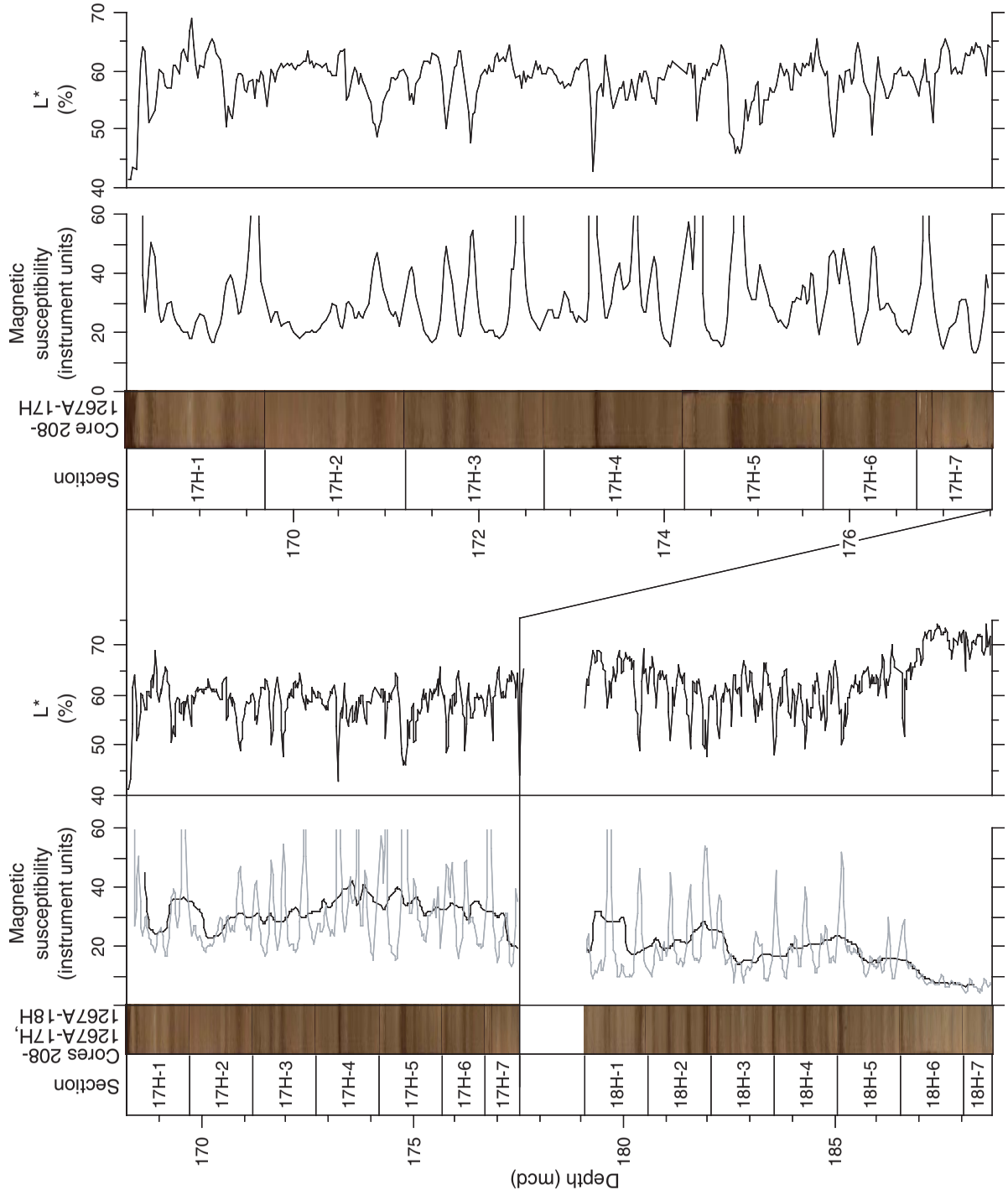

Figure F13. Composite digital images and cyclic patterns of sedimentation recorded in magnetic susceptibility and sediment lightness (L*) in Subunit IIIA.

Figure F14. Composite digital image, magnetic susceptibility, natural gamma radiation, sediment lightness (L*), and gamma ray attenuation (GRA) bulk density across the E/O boundary interval (153.1–133.2 mcd). The boundary is present in an upward lithologic transition from brown clay to light brown nannofossil ooze and is reflected in an increase in sediment L* and a decrease in magnetic susceptibility, natural gamma radiation, and GRA bulk density.

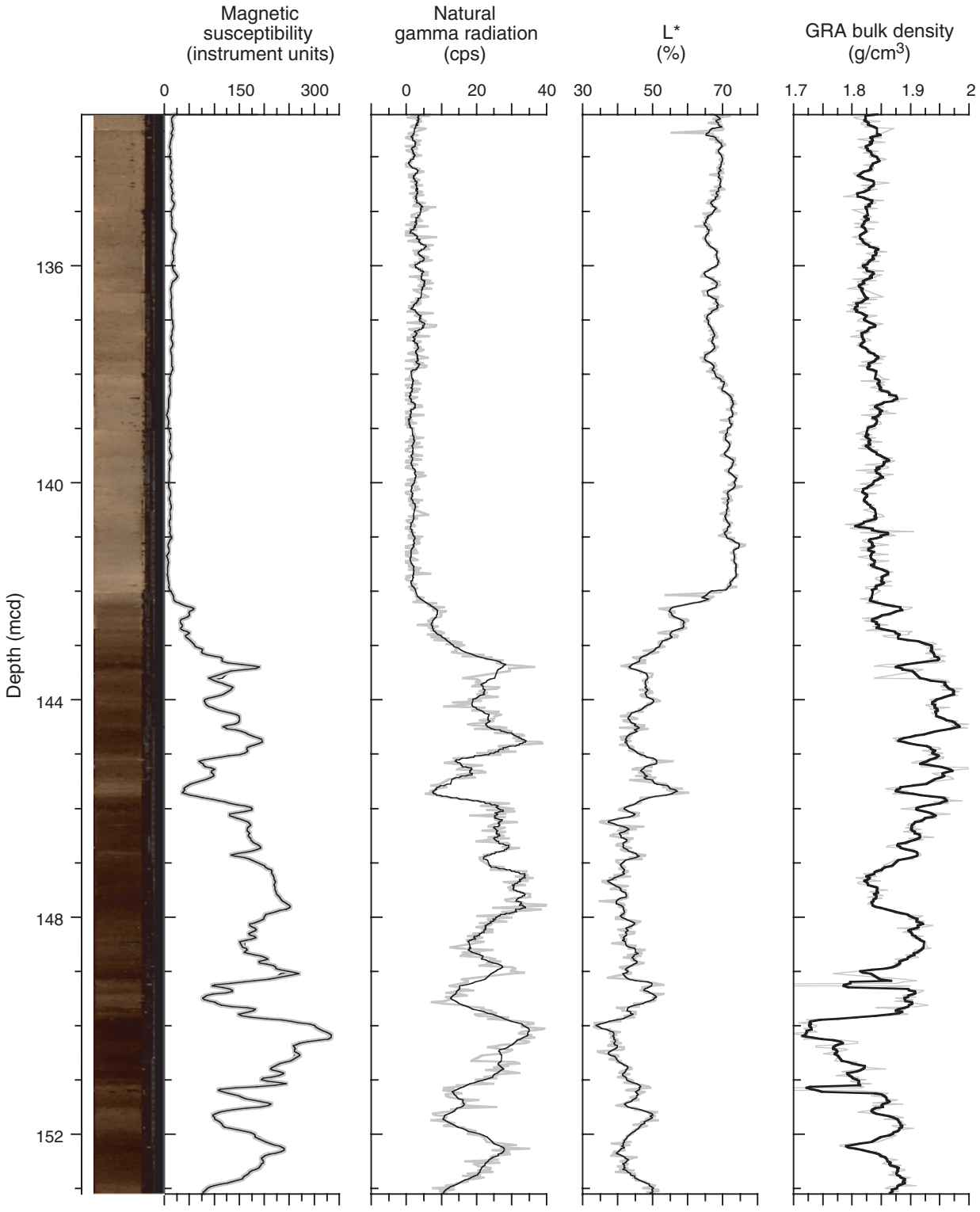

Figure F15. Composite digital images, magnetic susceptibility (black), carbonate content (blue), and chromaticity a* (red) across the P/E boundary in Cores 208-1267A-22H and 208-1267B-23H.

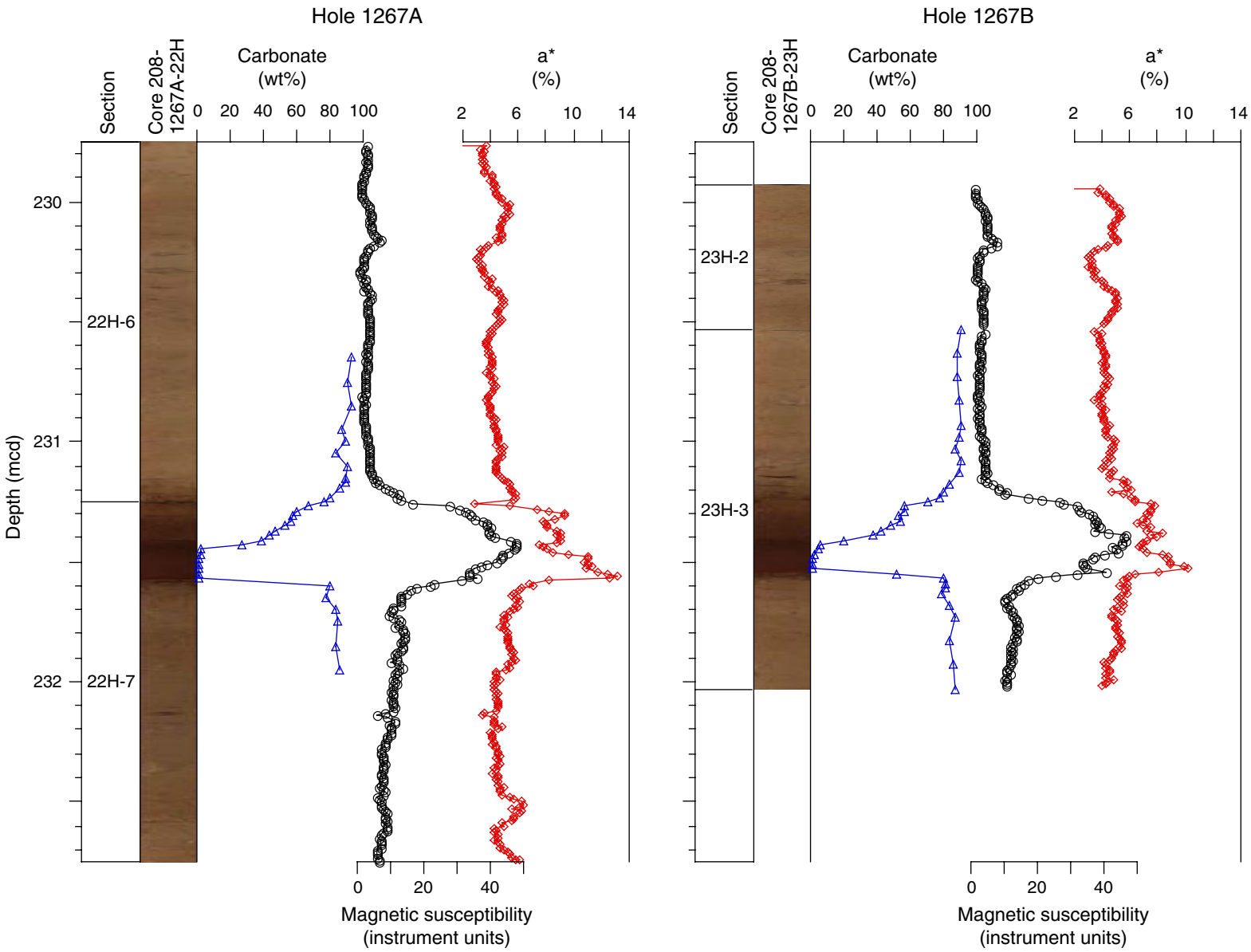

Figure F16. *P*-wave velocity measured on the *P*-wave sensor 3 (PWS3) at the Paleocene (P)/Eocene (E) boundary of (**A**) Hole 1267A and (**B**) Hole 1267B.

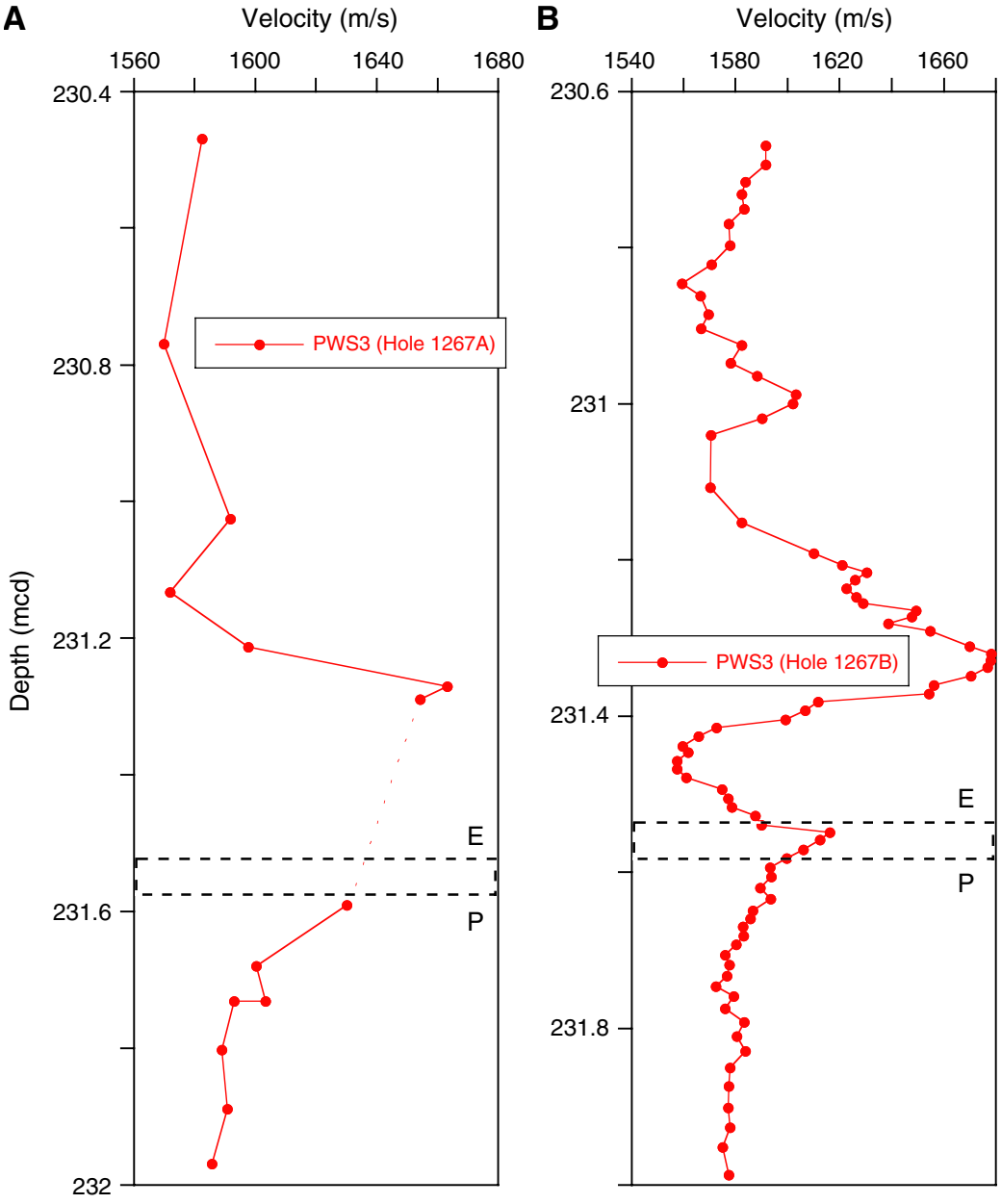

Figure F17. Composite digital images, magnetic susceptibility (black), and green-red chromaticity (a*; red) for sections spanning the red clay layer, ~25 mcd above the P/E boundary.

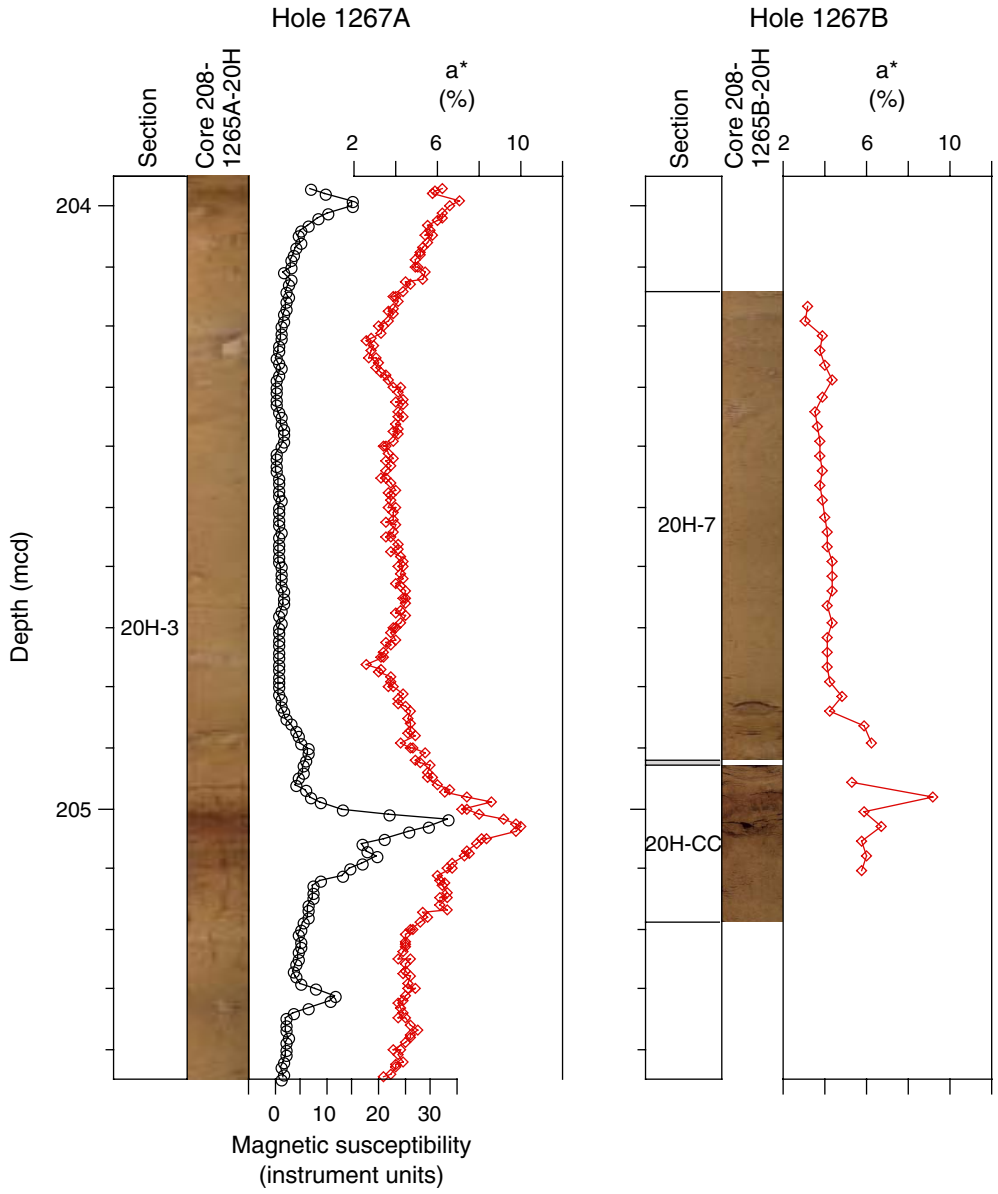

Figure F18. Composite digital images, magnetic susceptibility, and sediment lightness (L*) of the K/P boundary interval.

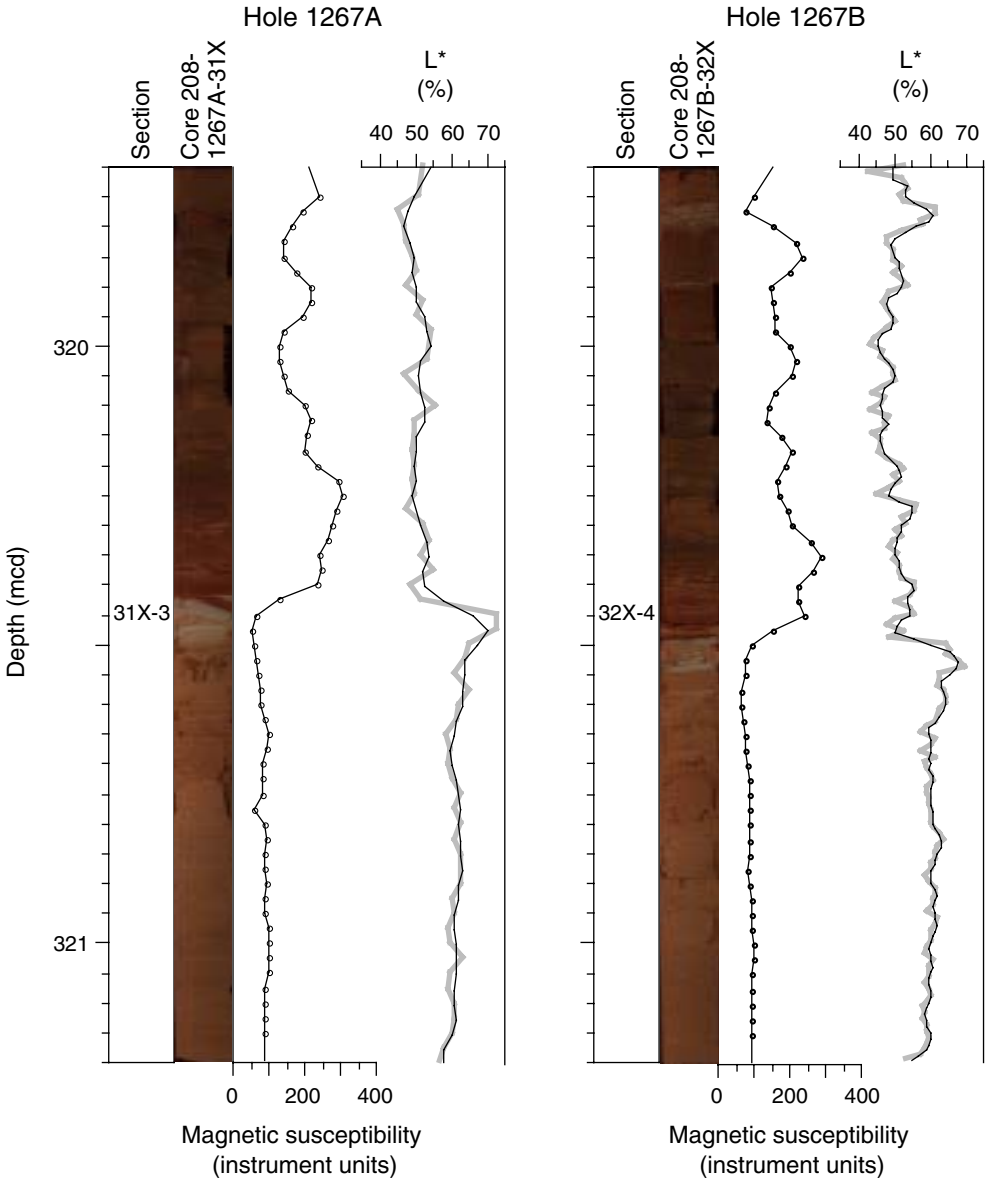

Figure F19. Summary of composite planktonic foraminiferal and calcareous nannofossil biozonations constructed for Site 1267. The paleobathymetric history of Site 1267 is inferred from benthic foraminifers shown on the right. Light shading = intervals of downslope transport and/or extensive reworking, dark shading = intervals of intense dissolution. Nanno = nannofossils. B = bottom. P/E = Paleocene/Eocene.

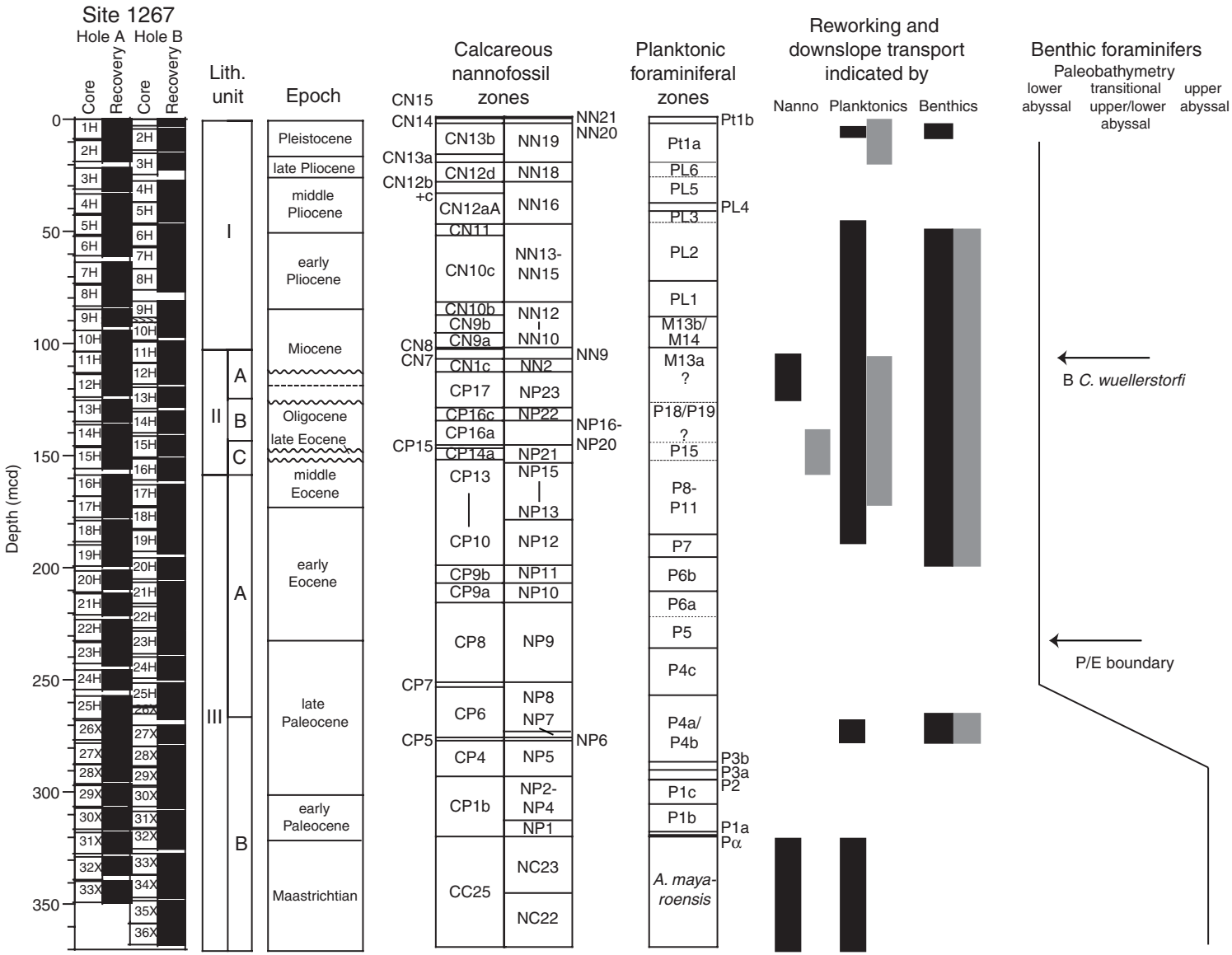

Figure F20. Summary of sedimentation rates at Site 1267 as delineated by a composite age/depth curve constructed using calcareous nannofossils and planktonic and benthic foraminifers. The outlying data points between 150 and 156 mcd reflect the severe dissolution and reworking in this interval.

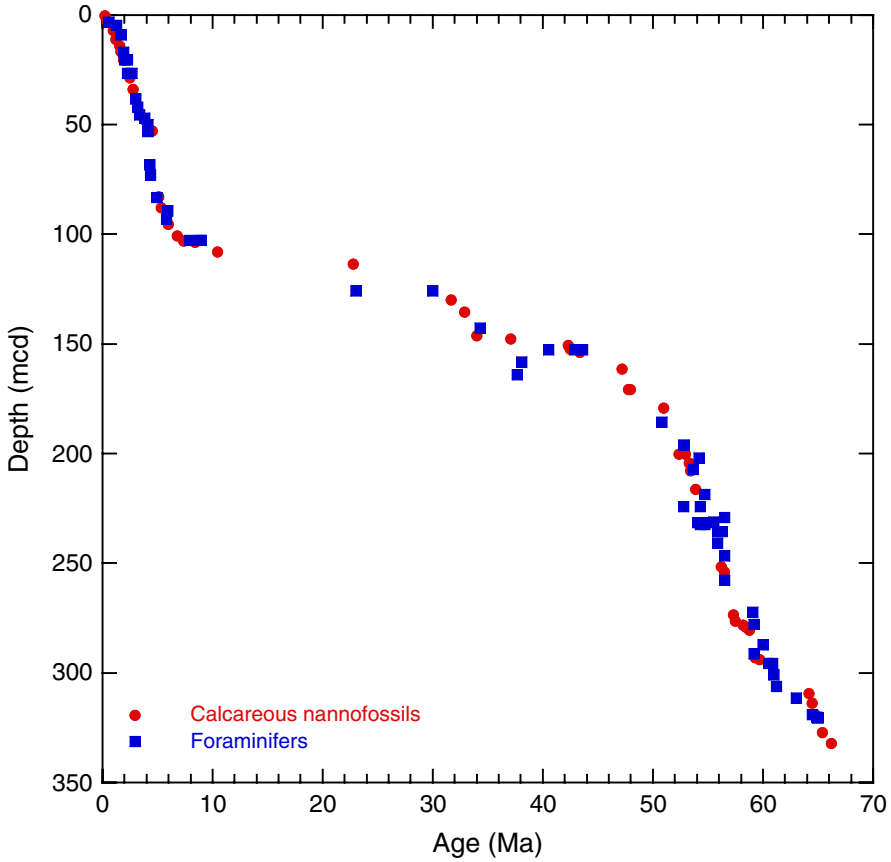

Figure F21. Downhole variation in intensities of remanent magnetization before (gray) and after (black) demagnetization to 15 mT at Holes 1267A and 1267B.

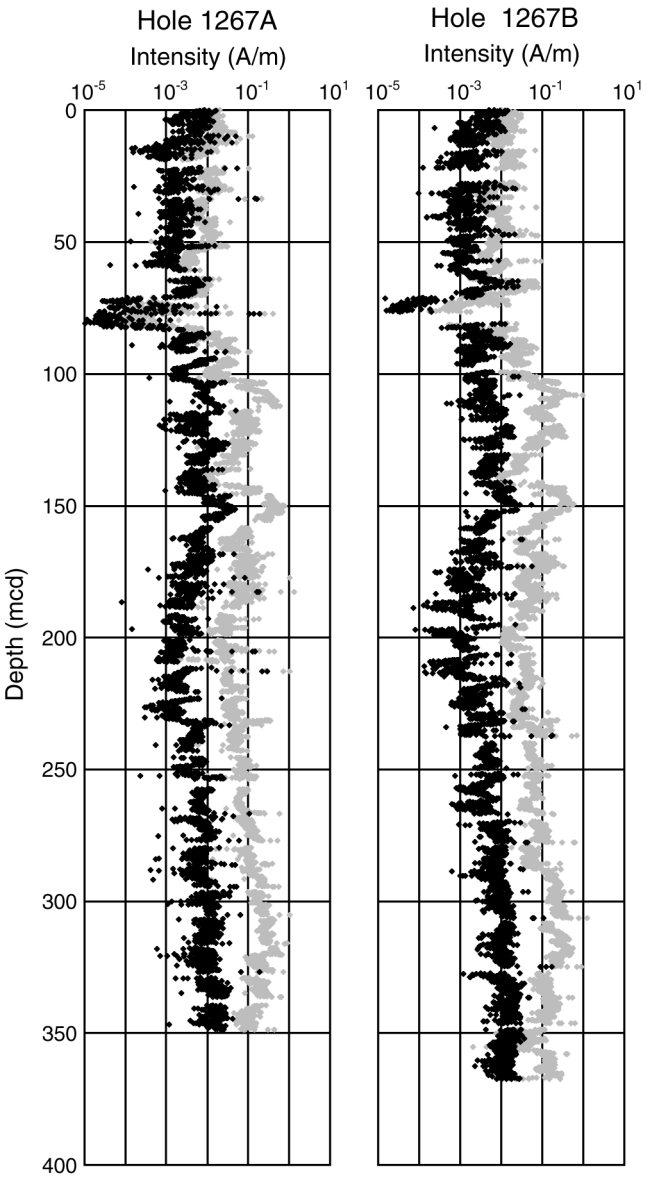

Figure F22. Downhole variation in initial magnetic susceptibility in Holes 1267A and 1267B.

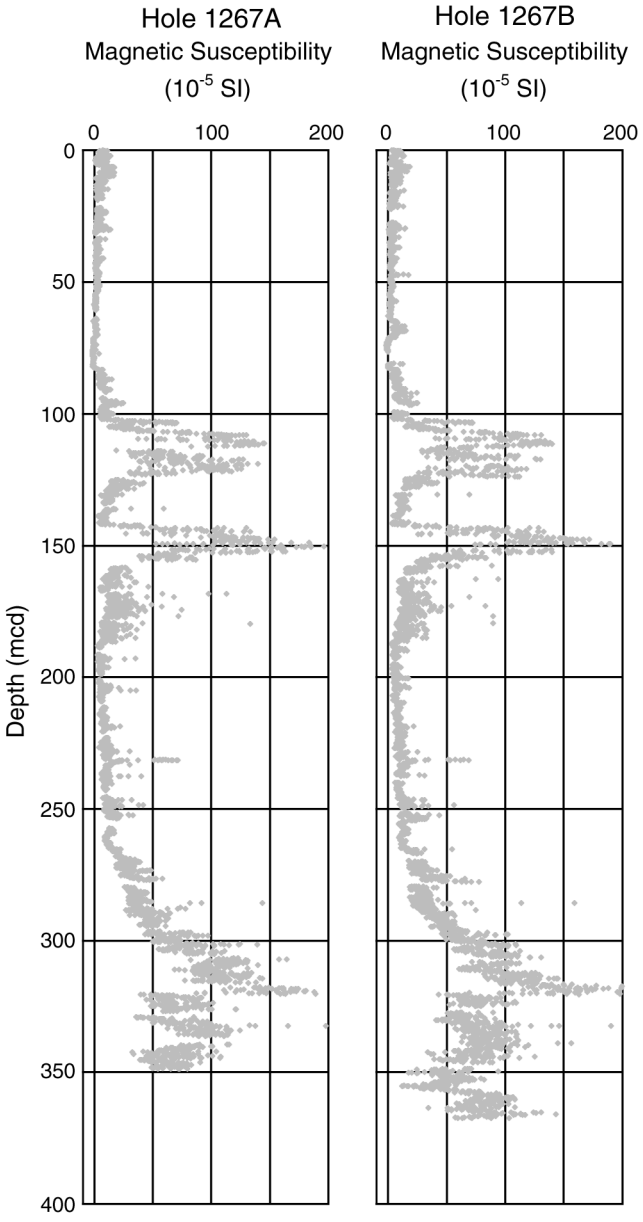

Figure F23. Downhole variation in depositional remanent magnetization after demagnetization to 15 mT and normalized by magnetic susceptibility ($nDRM_{15\ mT}$) in Holes 1267A and 1267B.

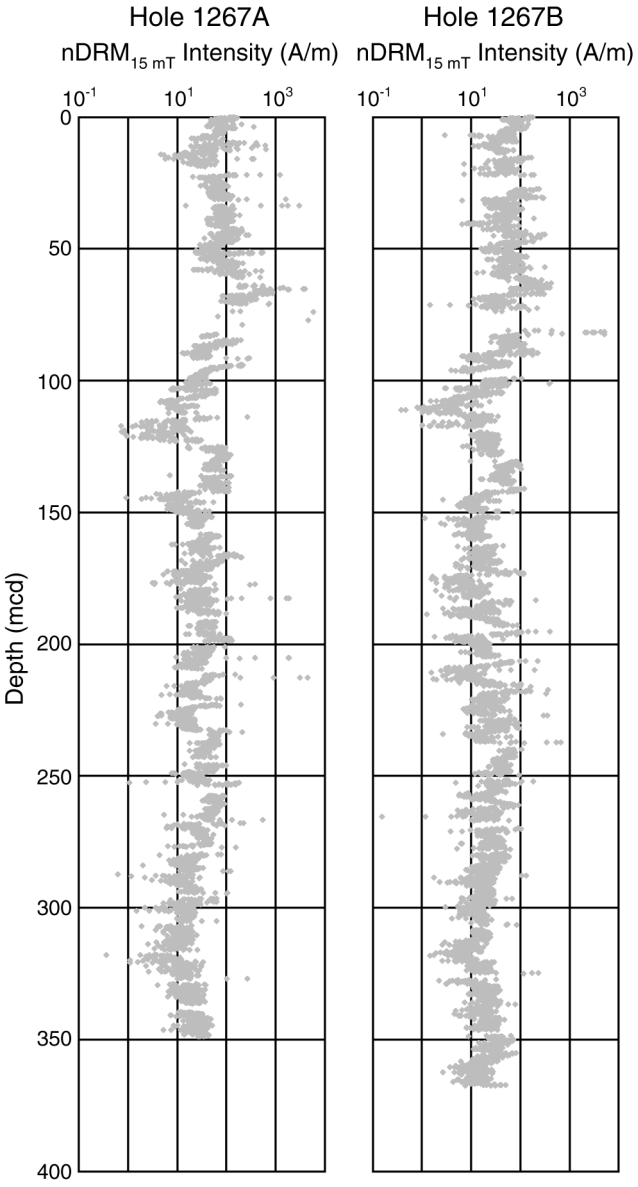

Figure F24. Preliminary magnetostratigraphic interpretation. Inclination data after demagnetization to 15 mT is shown for Holes 1267A and 1267B. Data within 50 cm of a core top and 5 cm of section ends are not shown. Core breaks are denoted by green squares. Black rectangles = normal polarity, white = reversed polarity, shaded = uncertain polarity. X = intervals with no core recovery. **A.** 0–75 mcd. (Continued on next four pages.)

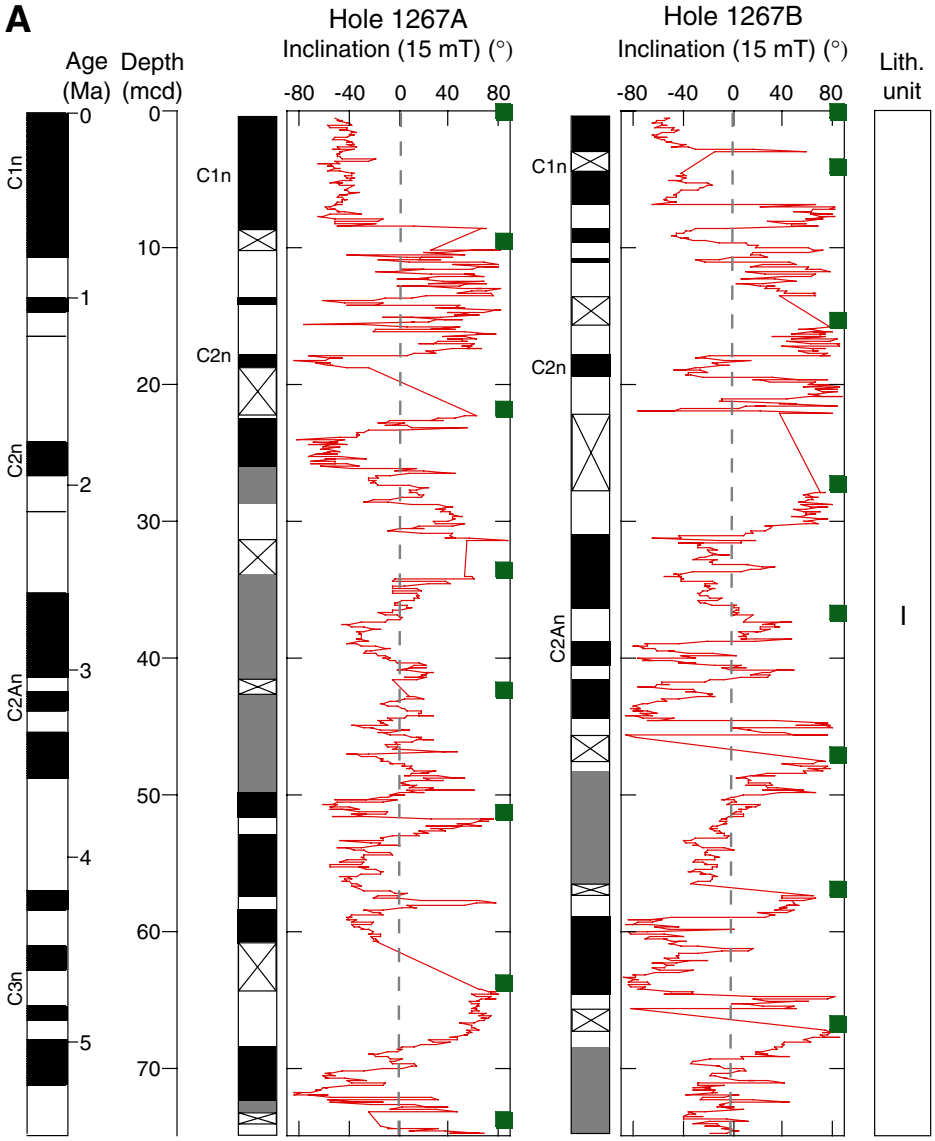

Figure F24 (continued). B. 65–150 mcd.

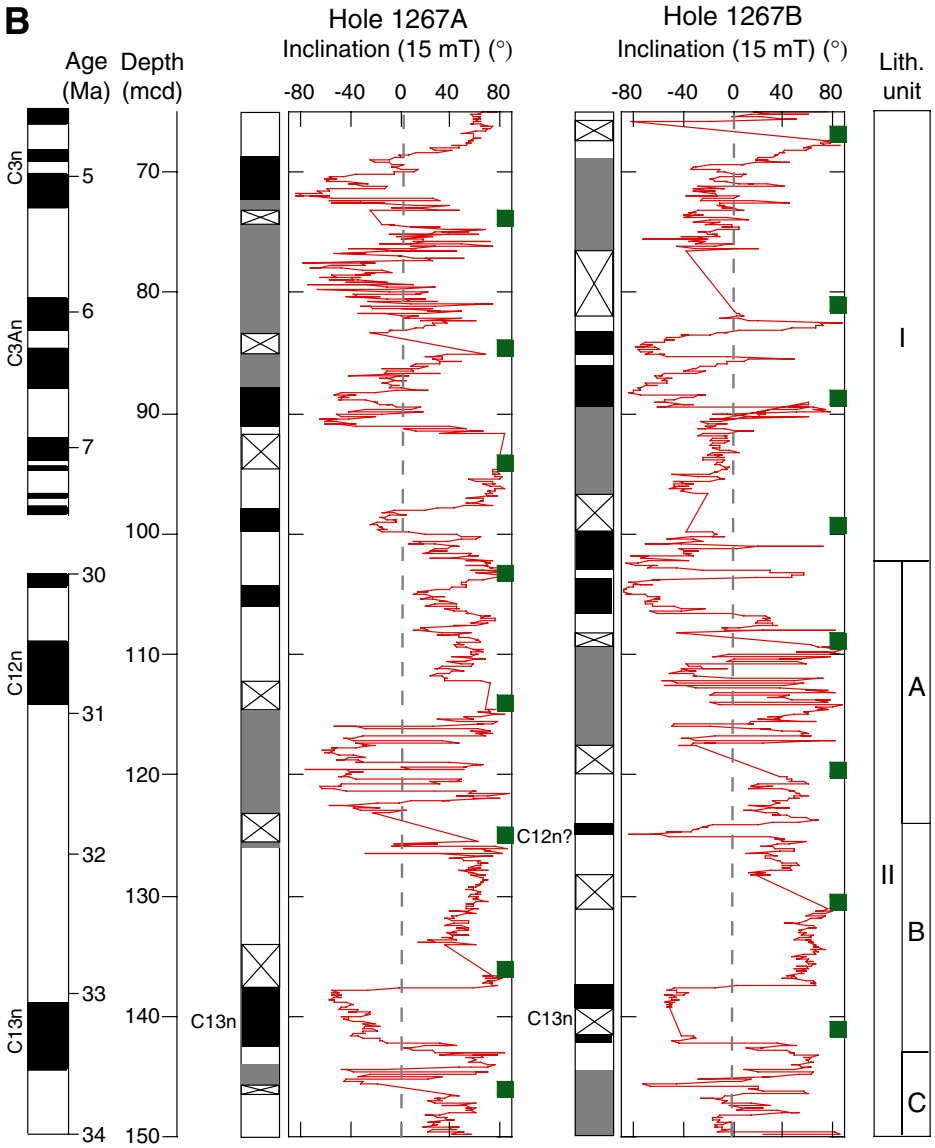

Figure F24 (continued). C. 140–225 mcd.

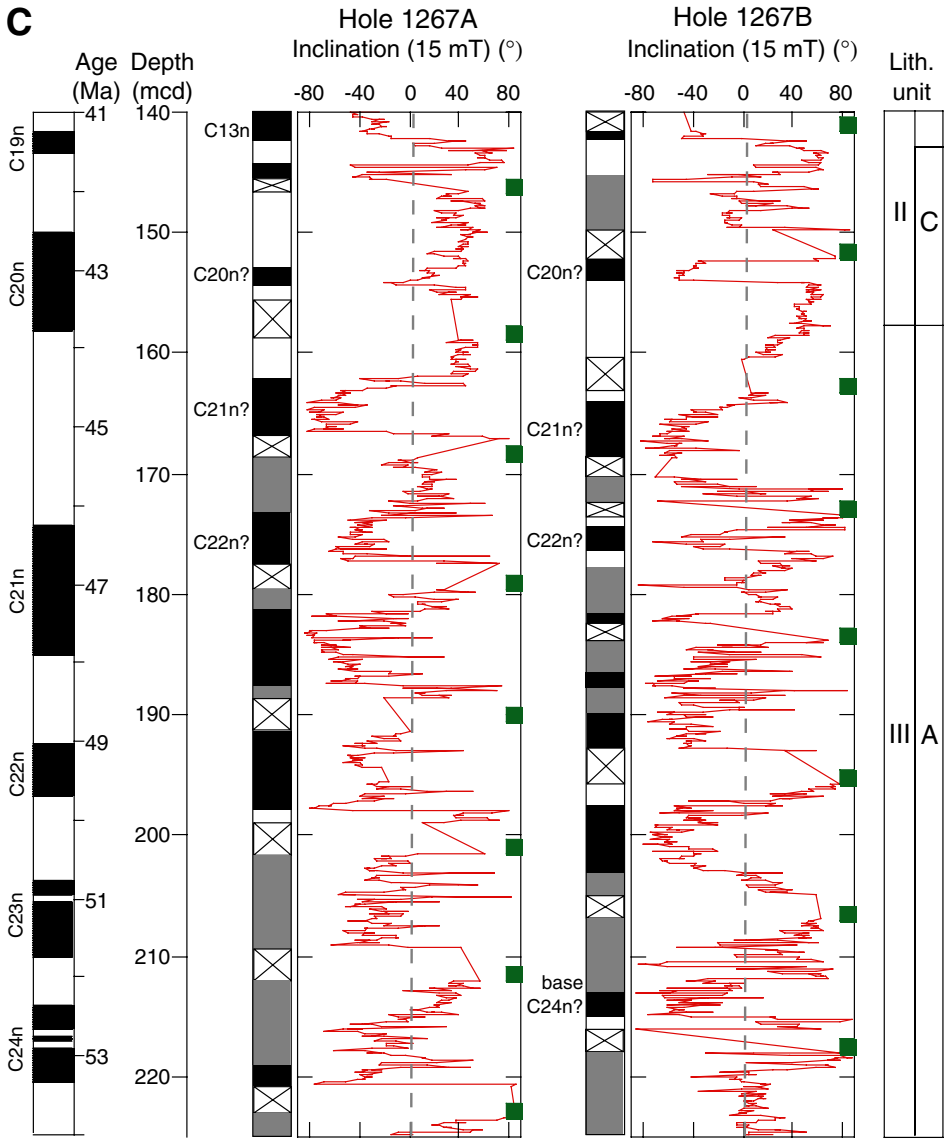

Figure F24 (continued). D. 215–300 mcd.

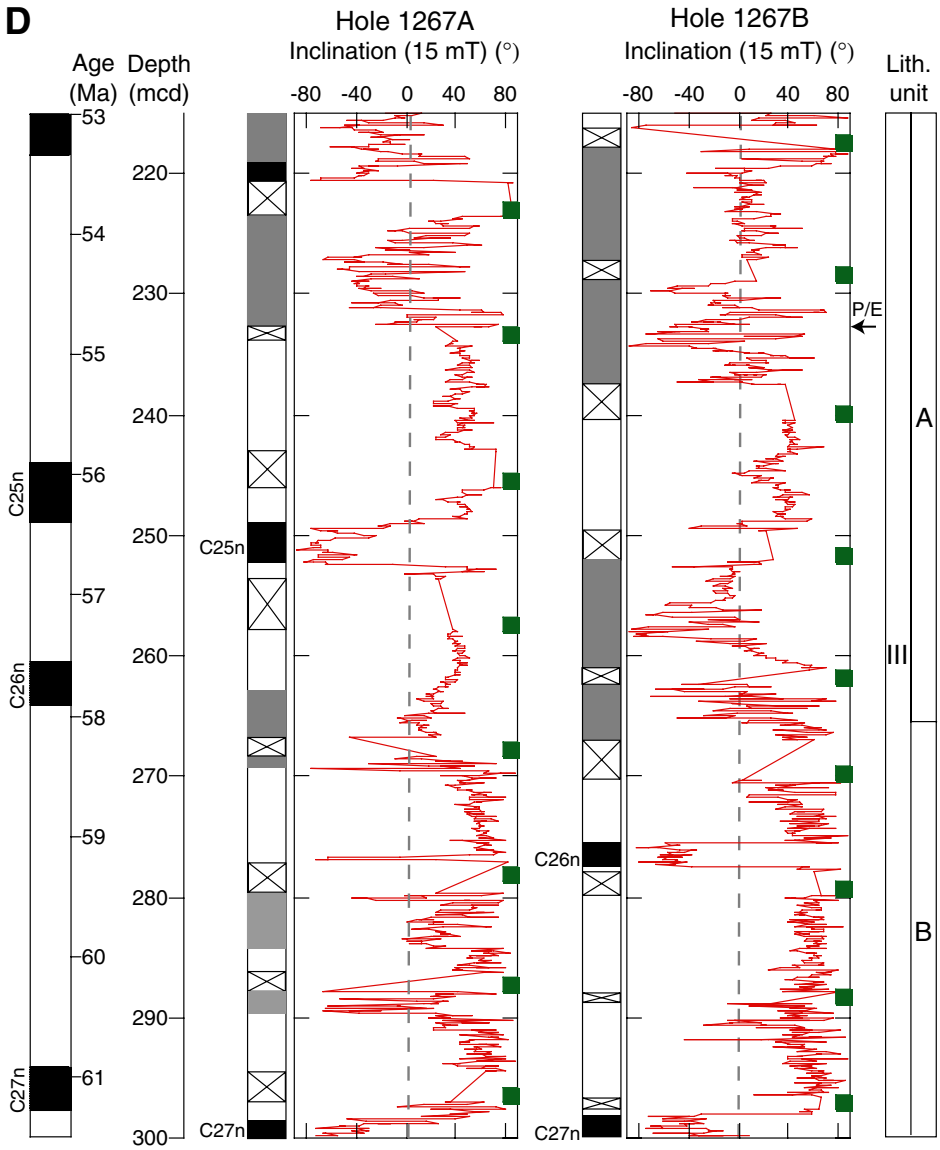

Figure F24 (continued). E. 290–375 mcd.

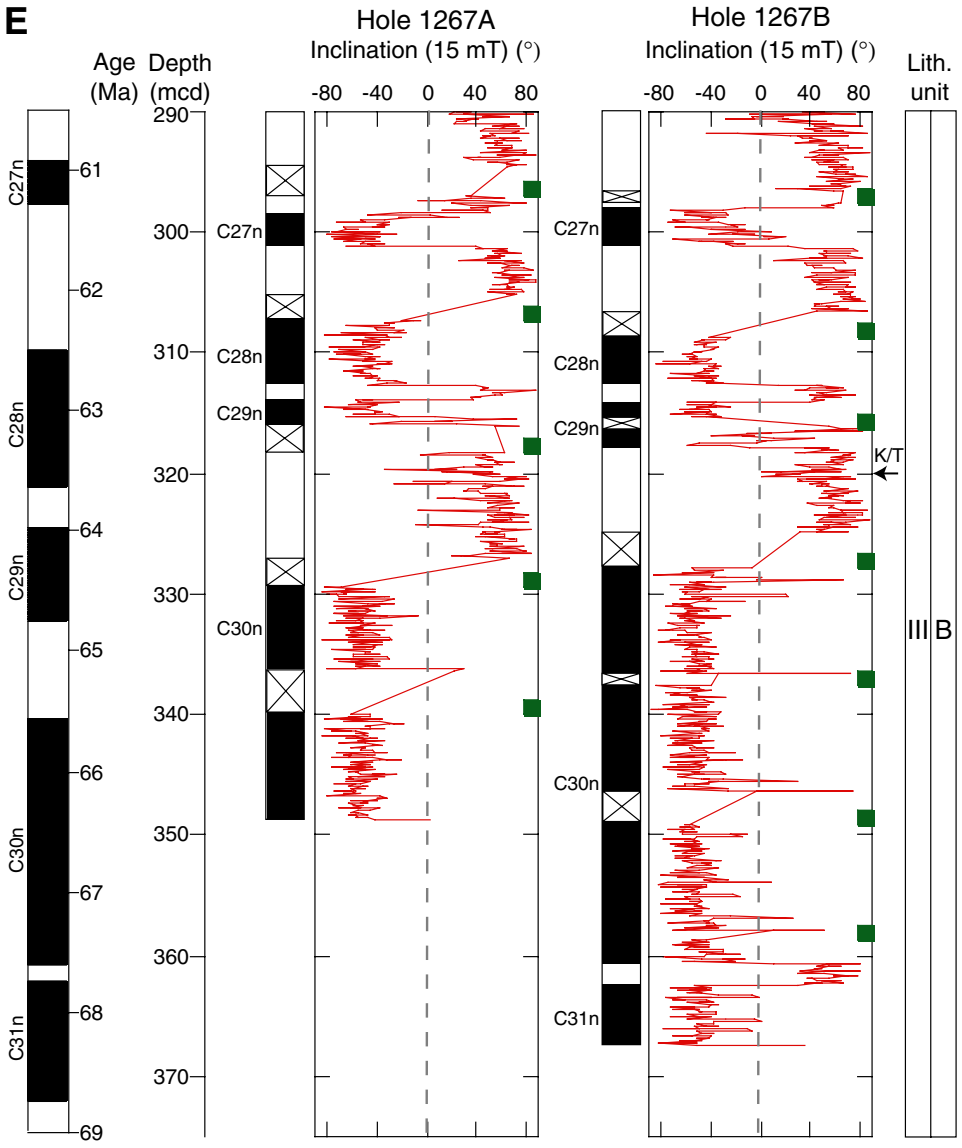

Figure F25. Profiles of chemical constituents in interstitial waters. Error bars (1 σ relative standard deviation percentage) are plotted where they are larger than the plot symbols. **A.** Alkalinity. **B.** Chloride. **C.** Sodium. **D.** Potassium. **E.** Calcium. **F.** Magnesium. **G.** Strontium. **H.** Lithium. **I.** Boron. **J.** Barium. **K.** Sulfate. **L.** Manganese. **M.** Iron. **N.** Silicon.

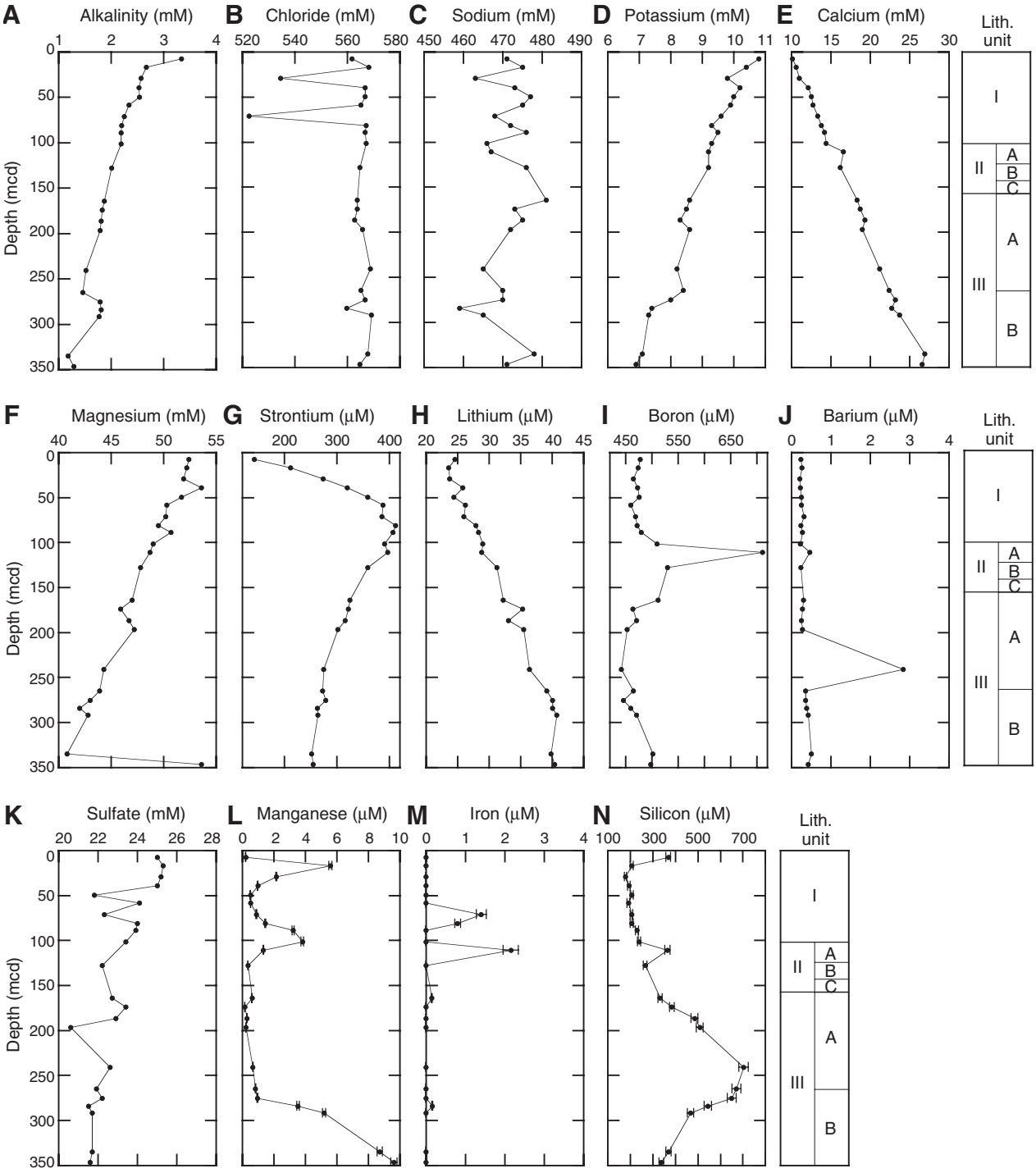

Figure F26. Sedimentary carbonate contents vs. composite depth for (**A**) the entire section and (**B**) the P/E boundary interval at high resolution.

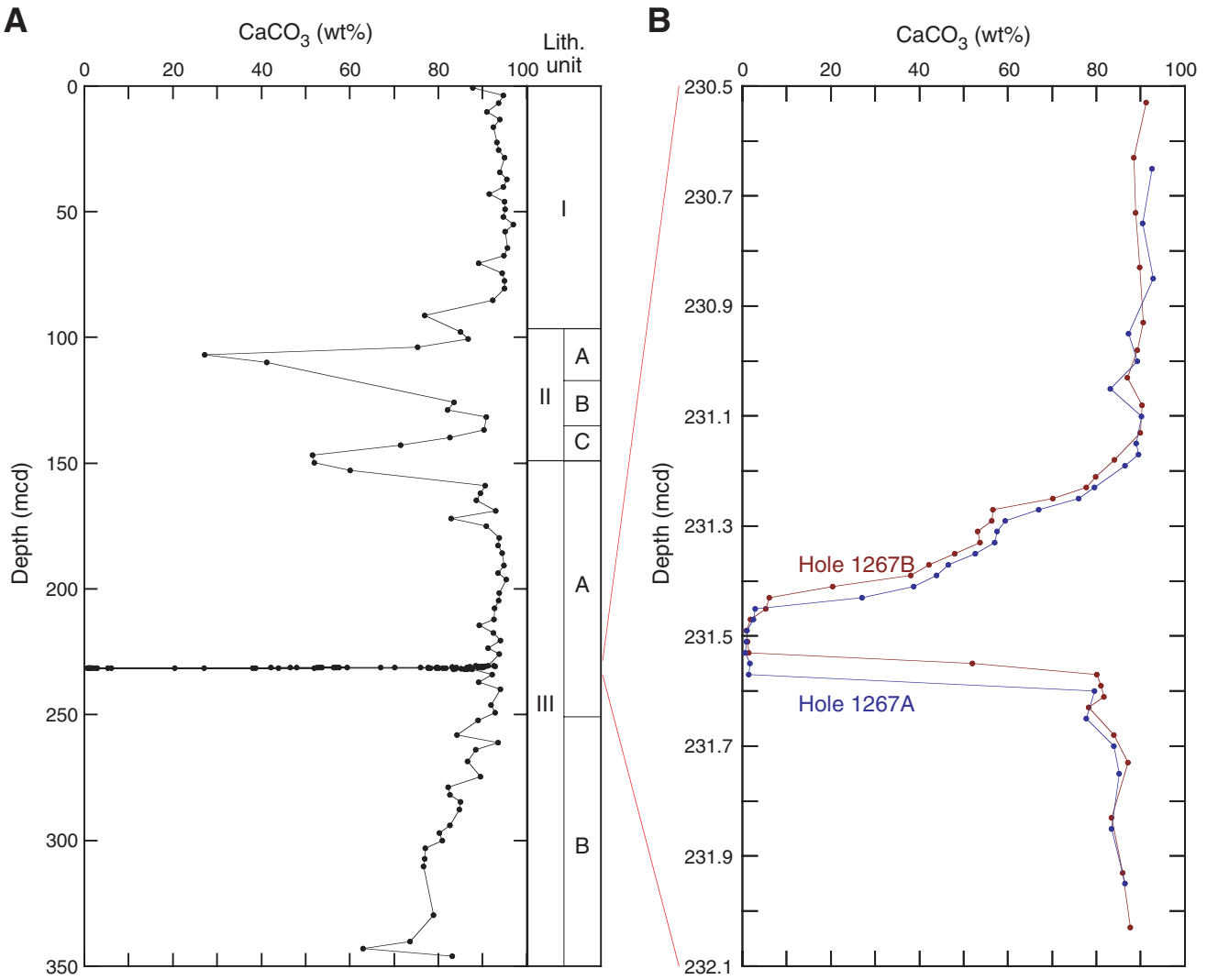

Figure F27. Mass chromatograms (*m*/*z* 85) of aliphatic hydrocarbons extracted from Sections 208-1267A-1H-5, 16H-4, and 32X-4.

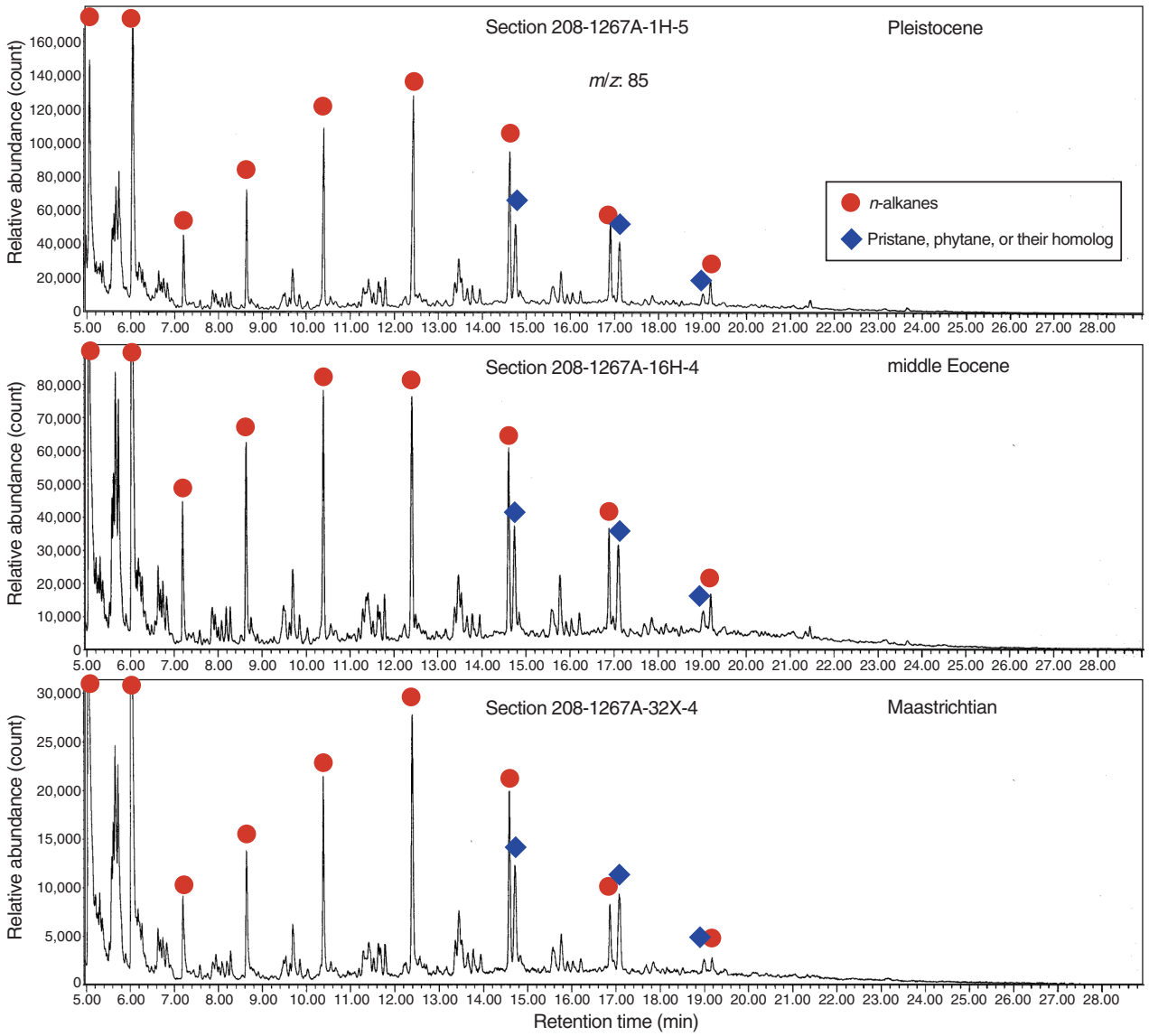

Figure F28. **A.** Core recovery plot. **B.** Shipboard biostratigraphic and magnetostratigraphic datums and the interpreted age-depth model. **C.** Corrected linear sedimentation rate (LSR), total, carbonate, and noncarbonate mass accumulation rates (MARs), calculated from the age model sampled at 1-m.y. intervals, and dry density and calcium carbonate concentrations averaged over the same 1-m.y. intervals. B = bottom, T = top.

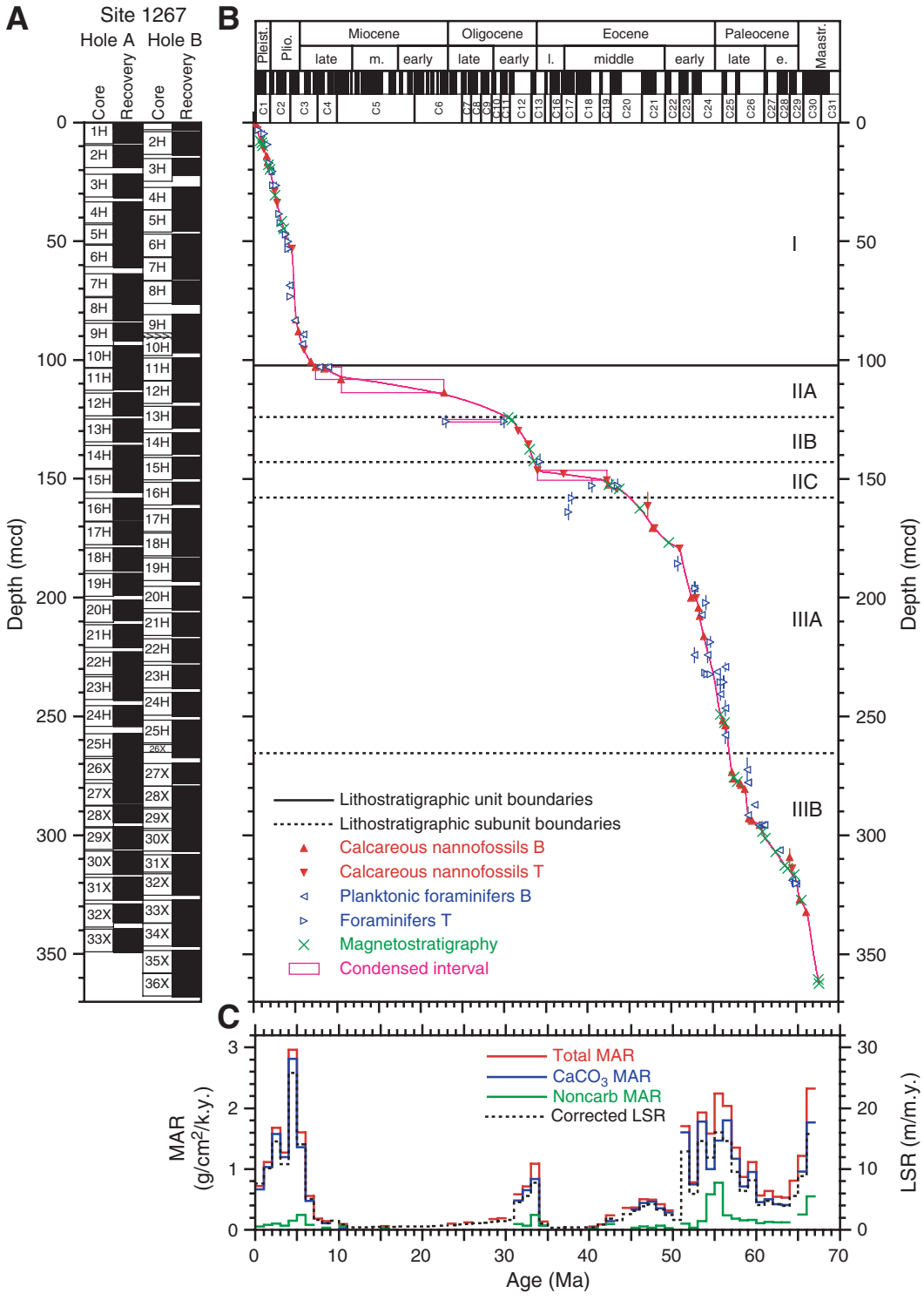

Table T1. Coring summary, Site 1267. (See table notes. Continued on next page.)

Core	Date (Apr 2003)	Local time (hr)	Depth (mbsf) Top	Depth (mbsf) Bottom	Length (m) Cored	Length (m) Recovered	Recovery (%)	Tool deployment
208-1267A-								
1H	21	1925	0.0	8.9	8.9	8.90	100.0	
2H	21	2030	8.9	18.4	9.5	9.51	100.1	NMCB
3H	21	2135	18.4	27.9	9.5	9.96	104.8	Tensor
4H	21	2300	27.9	37.4	9.5	8.44	88.8	APCT, Tensor
5H	22	25	37.4	46.9	9.5	9.79	103.1	Tensor
6H	22	145	46.9	56.4	9.5	9.83	103.5	Tensor, NMCB
7H	22	300	56.4	65.9	9.5	9.72	102.3	APCT, Tensor
8H	22	405	65.9	75.4	9.5	9.77	102.8	Tensor, NMCB
9H	22	505	75.4	84.9	9.5	7.59	79.9	Tensor
10H	22	630	84.9	94.4	9.5	10.10	106.3	APCT, Tensor
11H	22	740	94.4	103.9	9.5	9.52	100.2	Tensor
12H	22	845	103.9	113.4	9.5	9.50	100.0	Tensor, NMCB
13H	22	1025	113.4	122.9	9.5	9.50	100.0	DO, APCT, Tensor
14H	22	1145	122.9	132.4	9.5	9.85	103.7	DO, APCT, Tensor
15H	22	1410	132.4	141.9	9.5	9.64	101.5	Tensor
16H	22	1520	141.9	151.4	9.5	9.07	95.5	Tensor
17H	22	1655	151.4	160.9	9.5	9.50	100.0	DO, Tensor
18H	22	1810	160.9	170.4	9.5	9.84	103.6	Tensor
19H	22	1920	170.4	179.9	9.5	9.28	97.7	Tensor
20H	22	2030	179.9	189.4	9.5	8.61	90.6	Tensor
21H	22	2210	189.4	198.9	9.5	9.61	101.2	DO, Tensor
22H	22	2315	198.9	208.4	9.5	10.11	106.4	Tensor
23H	23	45	208.4	217.9	9.5	9.98	105.1	DO, Tensor
24H	23	345	217.9	226.6	8.7	8.77	100.8	DO, Tensor
25H	23	700	226.6	236.1	9.5	9.89	104.1	DO, Tensor
26X	23	830	236.1	244.9	8.8	9.70	110.2	
27X	23	945	244.9	254.5	9.6	8.40	87.5	
28X	23	1100	254.5	264.1	9.6	7.52	78.3	
29X	23	1220	264.1	273.7	9.6	9.17	95.5	
30X	23	1345	273.7	283.3	9.6	9.85	102.6	
31X	23	1500	283.3	292.9	9.6	9.61	100.1	
32X	23	1625	292.9	302.5	9.6	7.90	82.3	
33X	23	1745	302.5	312.1	9.6	9.85	102.6	
			Cored totals:		312.1	308.28	98.8	
208-1267B-								
1H	24	120	0.0	3.1	3.1	3.18	102.6	APCT
2H	24	225	3.1	12.6	9.5	9.75	102.6	NMCB
3H	24	320	12.6	22.1	9.5	7.12	75.0	
4H	24	450	22.1	31.6	9.5	9.89	104.1	APCT, Tensor
5H	24	555	31.6	41.1	9.5	9.20	96.8	Tensor
6H	24	655	41.1	50.6	9.5	9.66	101.7	Tensor, NMCB
7H	24	755	50.6	60.1	9.5	9.22	97.1	Tensor
8H	24	900	60.1	69.6	9.5	9.85	103.7	Tensor, NMCB
9H	24	1005	69.6	79.1	9.5	9.8	103.2	Tensor
10H	24	1135	79.1	88.6	9.5	8.33	87.7	Tensor, NMCB
11H	24	1240	88.6	98.1	9.5	9.37	98.6	Tensor
12H	24	1405	98.1	107.6	9.5	9.05	95.3	Tensor, NMCB
13H	24	1505	107.6	117.1	9.5	9.01	94.8	Tensor
14H	24	1615	117.1	126.6	9.5	9.01	94.8	Tensor, NMCB
15H	24	1730	126.6	136.1	9.5	9.07	95.5	Tensor
16H	24	1835	136.1	145.6	9.5	9.28	97.7	Tensor, NMCB
17H	24	1935	145.6	155.1	9.5	9.92	104.4	Tensor
18H	24	2040	155.1	164.6	9.5	9.76	102.7	Tensor, NMCB
19H	24	2145	164.6	174.1	9.5	9.98	105.1	Tensor
20H	24	2355	174.1	183.6	9.5	10.05	105.8	Tensor, NMCB
21H	25	105	183.6	193.1	9.5	9.95	104.7	Tensor
22H	25	210	193.1	202.6	9.5	9.96	104.8	Tensor
23H	25	315	202.6	212.1	9.5	9.78	103.0	Tensor
24H	25	630	212.1	221.6	9.5	10.05	105.8	DO, Tensor
25H	25	1130	221.6	231.1	9.5	9.92	104.4	DO, Tensor
26X	25	1230	231.1	234.4	3.3	5.55	168.2	
27X	25	1345	234.4	244.0	9.6	8.57	89.3	
28X	25	1505	244.0	253.6	9.6	8.80	91.7	
29X	25	1620	253.6	263.3	9.7	8.53	87.9	
30X	25	1805	263.3	272.9	9.6	9.87	102.8	
31X	25	1920	272.9	281.0	8.1	7.75	95.7	

Table T1 (continued).

Core	Date (Apr 2003)	Local time (hr)	Depth (mbsf) Top	Depth (mbsf) Bottom	Length (m) Cored	Length (m) Recovered	Recovery (%)	Tool deployment
32X	25	2050	281.0	290.6	9.6	9.73	101.4	
33X	25	2305	290.6	300.2	9.6	9.88	102.9	
34X	26	30	300.2	309.8	9.6	9.80	102.1	
35X	26	205	309.8	319.4	9.6	9.84	102.5	
36X	26	330	319.4	329.0	9.6	9.87	102.8	
				Cored totals:	329.0	328.35	99.8	
				Total:	641.1	636.6	99.3	

Notes: NMCB = nonmagnetic core barrel, including cutting shoe (made from Monel). Tensor = brand name for core barrel orientation tool. APCT = Advanced Piston Corer Temperature tool (stainless steel housing is cutting shoe). DO = drillover. See Table **T1,** p. 106, in the "Leg 208 Summary" chapter.

Table T2. Composite depth scale, Site 1267.

Core	Offset (m)	Depth (mbsf)	Depth (mcd)
208-1267A-			
1H	0.00	0.00	0.00
2H	0.70	8.90	9.60
3H	3.40	18.40	21.80
4H	5.60	27.90	33.50
5H	4.90	37.40	42.30
6H	4.40	46.90	51.30
7H	7.40	56.40	63.80
8H	7.90	65.90	73.80
9H	9.10	75.40	84.50
10H	9.10	84.90	94.00
11H	8.80	94.40	103.20
12H	10.10	103.90	114.00
13H	11.60	113.40	125.00
14H	13.20	122.90	136.10
15H	13.70	132.40	146.10
16H	16.40	141.90	158.30
17H	16.80	151.40	168.20
18H	18.20	160.90	179.10
19H	19.50	170.40	189.90
20H	21.10	179.90	201.00
21H	22.10	189.40	211.50
22H	24.00	198.90	222.90
23H	24.90	208.40	233.30
24H	27.60	217.90	245.50
25H	30.70	226.60	257.30
26X	31.70	236.10	267.80
27X	33.20	244.90	278.10
28X	32.80	254.50	287.30
29X	32.30	264.10	296.40
30X	33.00	273.70	306.70
31X	34.40	283.30	317.70
32X	36.00	292.90	328.90
33X	37.00	302.50	339.50
208-1267B-			
1H	0.00	0.00	0.00
2H	0.90	3.10	4.00
3H	2.70	12.60	15.30
4H	5.20	22.10	27.30
5H	5.10	31.60	36.70
6H	5.90	41.10	47.00
7H	6.30	50.60	56.90
8H	6.70	60.10	66.80
9H	11.40	69.60	81.00
10H	9.50	79.10	88.60
11H	10.60	88.60	99.20
12H	10.60	98.10	108.70
13H	12.00	107.60	119.60
14H	13.50	117.10	130.60
15H	14.40	126.60	141.00
16H	15.40	136.10	151.50
17H	17.10	145.60	162.70
18H	17.80	155.10	172.90
19H	18.70	164.60	183.30
20H	21.00	174.10	195.10
21H	22.80	183.60	206.40
22H	24.30	193.10	217.40
23H	25.80	202.60	228.40
24H	27.80	212.10	239.90
25H	30.00	221.60	251.60
26X	30.70	231.10	261.80
27X	35.40	234.40	269.80
28X	35.30	244.00	279.30
29X	34.60	253.60	288.20
30X	33.70	263.30	297.00
31X	35.30	272.90	308.20
32X	34.60	281.00	315.60
33X	36.60	290.60	327.20
34X	36.80	300.20	337.00
35X	38.80	309.80	348.60
36X	38.80	319.40	358.20

Table T3. Splice tie points, Site 1267.

Hole, core, section, interval (cm)	Depth (mbsf)	Depth (mcd)		Hole, core, section, interval (cm)	Depth (mbsf)	Depth (mcd)
208-				208-		
1267B-1H-2, 72.5	2.22	2.22	Tie to	1267A-1H-2, 68.5	2.19	2.22
1267A-1H-5, 42.5	6.42	6.45	Tie to	1267B-2H-2, 92.5	5.52	6.45
1267B-2H-5, 97.5	10.08	11.01	Tie to	1267A-2H-1, 144	10.34	11.01
1267A-2H-6, 47.5	16.88	17.55	Tie to	1267B-3H-2, 71	14.81	17.55
1267B-3H-5, 52.5	19.12	21.86	Tie to	1267A-3H-1, 6	18.47	21.86
1267A-3H-5, 82.5	25.22	28.61	Tie to	1267B-4H-1, 130	23.40	28.61
1267B-4H-6, 137.5	30.98	36.19	Tie to	1267A-4H-2, 126	30.57	36.19
1267A-4H-5, 137.5	35.18	40.80	Tie to	1267B-5H-3, 104.5	35.66	40.80
1267B-5H-7, 37.5	40.48	45.62	Tie to	1267A-5H-3, 32	40.73	45.62
1267A-5H-7, 32.5	46.72	51.61	Tie to	1267B-6H-4, 6	45.67	51.61
1267B-6H-6, 145	50.05	55.99	Tie to	1267A-6H-4, 22	51.63	55.99
1267A-6H-6, 67.5	55.08	59.44	Tie to	1267B-7H-2, 102	53.13	59.44
1267B-7H-6, 20	58.30	64.61	Tie to	1267A-7H-1, 85	57.25	64.61
1267A-7H-3, 27.5	59.68	67.04	Tie to	1267B-8H-1, 24.5	60.36	67.04
1267B-8H-7, 22.5	69.32	76.00	Tie to	1267A-8H-2, 70	68.10	76.00
1267A-8H-7, 45	75.35	83.25	Tie to	1267B-9H-2, 80	71.90	83.25
1267B-9H-5, 62.5	76.22	87.57	Tie to	1267A-9H-3, 2	78.43	87.57
1267A-9H-5, 35	81.75	90.89	Tie to	1267B-10H-2, 76	81.37	90.89
1267B-10H-5, 120	86.30	95.82	Tie to	1267A-10H-2, 33.5	86.74	95.82
1267A-10H-6, 37.5	92.78	101.86	Tie to	1267B-11H-2, 112	91.23	101.86
1267B-11H-5, 127.5	95.88	106.51	Tie to	1267A-11H-3, 30	97.70	106.51
1267A-11H-5, 32.5	100.72	109.53	Tie to	1267B-12H-1, 82.5	98.92	109.53
1267B-12H-6, 67.5	106.28	116.89	Tie to	1267A-12H-2, 142	106.83	116.89
1267A-12H-6, 5	111.45	121.51	Tie to	1267B-13H-2, 43.5	109.54	121.51
1267B-13H-5, 130	114.85	126.82	Tie to	1267A-13H-2, 35	115.25	126.82
1267A-13H-6, 75	121.65	133.22	Tie to	1267B-14H-2, 118.5	119.75	133.22
1267B-14H-6, 97.5	125.54	139.01	Tie to	1267A-14H-2, 146	125.86	139.01
1267A-14H-6, 97.5	131.38	144.53	Tie to	1267B-15H-3, 52.5	130.12	144.53
1267B-15H-6, 12.5	134.22	148.63	Tie to	1267A-15H-2, 102	134.93	148.63
1267A-15H-5, 100	139.40	153.10	Tie to	1267B-16H-2, 12.5	137.72	153.10
1267B-16H-6, 95	144.55	159.93	Tie to	1267A-16H-2, 12	143.53	159.93
1267A-16H-5, 120	149.10	165.50	Tie to	1267B-17H-2, 132.5	148.42	165.50
1267B-17H-7, 32.5	154.92	172.00	Tie to	1267A-17H-3, 78.5	155.19	172.00
1267A-17H-6, 85	159.75	176.56	Tie to	1267B-18H-3, 67.5	158.78	176.56
1267B-18H-7, 5	164.15	181.93	Tie to	1267A-18H-2, 134.5	163.76	181.93
1267A-18H-4, 140	166.80	184.97	Tie to	1267B-19H-2, 15	166.25	184.97
1267B-19H-7, 35	173.95	192.67	Tie to	1267A-19H-2, 130	173.20	192.67
1267A-19H-7, 32.5	179.28	198.75	Tie to	1267B-20H-3, 61	177.71	198.75
1267B-20H-6, 142.5	183.02	204.06	Tie to	1267A-20H-3, 11	183.01	204.06
1267A-20H-6, 115	188.15	209.20	Tie to	1267B-21H-2, 127.5	186.38	209.20
1267B-21H-7, 32.5	192.92	215.74	Tie to	1267A-21H-4, 48.5	193.69	215.74
1267A-21H-6, 117.5	197.38	219.43	Tie to	1267B-22H-2, 50.5	195.12	219.43
1267B-22H-6, 120	201.80	226.11	Tie to	1267A-22H-3, 86	202.13	226.11
1267A-22H-5, 142.5	205.70	229.68	Tie to	1267B-23H-1, 125	203.85	229.68
1267B-23H-6, 132.5	210.52	236.35	Tie to	1267A-23H-3, 2	211.43	236.35
1267A-23H-6, 125	217.15	242.07	Tie to	1267B-24H-2, 70	214.30	242.07
1267B-24H-6, 87.5	220.48	248.25	Tie to	1267A-24H-2, 124.5	220.66	248.25
1267A-24H-5, 75	224.65	252.24	Tie to	1267B-25H-1, 68.5	222.29	252.24
1267B-25H-6, 15	229.25	259.20	Tie to	1267A-25H-2, 36	228.47	259.20
1267A-25H-7, 55	236.15	266.88	Tie to	1267B-26X-4, 61	236.21	266.88
1267B-26X-4, 75	236.35	267.02	Append to	1267A-26X-1, 0	236.10	267.83
1267A-26X-4, 87.5	241.48	273.21	Tie to	1267B-27X-3, 44.5	237.86	273.21
1267B-27X-7, 27.5	242.86	278.21	Tie to	1267A-27X-1, 7.5	244.98	278.21
1267A-27X-5, 70	251.60	284.83	Tie to	1267B-28X-4, 98.5	249.49	284.83
1267B-28X-6, 70	252.20	287.54	Tie to	1267A-28X-1, 23.5	254.74	287.54
1267A-28X-4, 47.5	259.48	292.28	Tie to	1267B-29X-3, 106	257.67	292.28
1267B-29X-6, 82.5	261.92	296.53	Tie to	1267A-29X-1, 8.5	264.19	296.53
1267A-29X-5, 135	271.45	303.79	Tie to	1267B-30X-5, 73	270.05	303.79
1267B-30X-C, 30	273.11	306.85	Append to	1267A-30X-1, 0	273.70	306.71
1267A-30X-4, 5	278.25	311.26	Tie to	1267B-31X-3, 11	276.01	311.26
1267B-31X-C, 40	280.55	315.80	Append to	1267B-32X-1, 0	281.00	315.60
1267B-32X-4, 115	286.25	320.85	Tie to	1267A-31X-3, 115	286.45	320.85
1267A-31X-C, 17.5	292.82	327.21	Append to	1267B-33X-1, 0	290.60	327.24
1267B-33X-C, 30	300.36	337.00	Append to	1267B-34X-1, 0	300.20	337.02
1267B-34X-5, 37.5	306.58	343.40	Tie to	1267A-33X-3, 95	306.45	343.40
1267A-33X-7, 75	311.75	348.70	Tie to	1267B-35X-1, 15	309.95	348.70
1267B-35X-C, 27.5	319.57	358.32	Append to	1267B-36X-1, 0	319.40	358.15
1267B-36X-C, 37.5	329.20	367.95				

Note: This table is also available in **ASCII.**

Table T4. Lithostratigraphic subdivisions, Site 1267.

Unit/ subunit	Unit boundary depth (mcd)	Hole 1267A						Hole 1267B					
		Core, section, interval (cm)		Depth (mbsf)		Depth (mcd)		Core, section, interval (cm)		Depth (mbsf)		Depth (mcd)	
		Top	Base	Top	Base	Top	Base	Top	Base	Top	Base	Top	Base
I	102.3	1H-1	**10H-7, 0**	0.0	**93.4**	0.0	**102.5**	**1H-1**	11H-3	**0.0**	91.7	**0.0**	102.3
IIA	124.0	**10H-7, 0**	12H-7CC, 10	**93.4**	113.3	**102.5**	123.3	11H-3	**13H-3, 140**	91.7	**112.0**	102.3	**124.0**
IIB	143.0	12H-CC, 10	**14H-5, 95**	113.3	**129.9**	123.3	143.0	**13H-3, 140**	15H-2, 50	**112.0**	128.6	**124.0**	143.0
IIC	157.8	**14H-5, 95**	15H-7, 48	**129.9**	141.9	**143.0**	155.6	15H-2, 50	**16H-5, 30**	128.6	**142.4**	143.0	**157.8**
IIIA	265.4	16H-1, 0	25H-6, 80	141.9	234.9	158.3	265.6	**16H-5, 30**	**26X-3, 65**	**142.4**	**234.7**	**157.8**	**265.4**
IIIB	(367.9)*	25H-6, 80	33X-7CC, 38	234.9	312.3	265.6	349.2	**26X-3, 65**	**36X-CC, 37.5**	**234.7**	**329.2**	**265.4**	**367.9**

Notes: Bold intervals and depths define the unit boundaries; other intervals are recognized as part of units but do not contain the unit boundaries. * = bottom of deepest hole.

Unit/ subunit	Unit boundary depth (mcd)	Descriptions
I	102.3	Nannofossil ooze
IIA	124.0	Hematite-bearing clay, clay-bearing nannofossil ooze, and nannofossil clay
IIB	143.0	Nannofossil ooze, foraminifer-bearing nannofossil ooze, and clayey nannofossil ooze
IIC	157.8	Clay and nannofossil ooze with variable ash and clay
IIIA	265.4	Nannofossil ooze, clay-bearing nannofossil ooze, and nannofossil clay
IIIB	(367.9)*	Nannofossil ooze, nannofossil chalk, nannofossil clay, and ashy clay

Table T5. Stratigraphic positions of selected calcareous nannofossil datums, Site 1267. (**See table note.** Continued on next page.)

	Datum	Age (Ma)		Top of sample interval			Base of sample interval		
		Youngest	Oldest	Core, section, interval (cm)	Depth (mbsf)	Depth (mcd)	Core, section, interval (cm)	Depth (mbsf)	Depth (mcd)
				208-1267A-			208-1267A-		
B	*Emiliania huxleyi*	0.26	0.26	1H-1, 1	0.01	0.04	1H-1, 80	0.80	0.83
T	*Pseudoemiliania lacunosa*	0.46	0.46	1H-2, 90	2.40	2.43	1H-3, 90	3.90	3.93
B	*Gephyrocapsa parallela* (= reent. medium *G.*)	1.01	1.01	1H-5, 50	6.50	6.53	1H-6, 50	8.00	8.03
T	Large *Gephyrocapsa* spp.	1.22	1.22	2H-1, 120	10.10	10.77	2H-2, 65	11.05	11.72
B	Large *Gephyrocapsa* spp.	1.58	1.58	2H-3, 105	12.95	13.62	2H-4, 65	14.05	14.72
B	Medium *Gephyrocapsa* spp.	1.69	1.69	2H-5, 65	15.55	16.22	2H-6, 30	16.70	17.37
T	*Discoaster brouweri* and *D. triradiatus*	1.95	1.95	2H-CC	18.36	19.03	3H-1, 20	18.60	21.99
T	*Discoaster pentaradiatus*	2.52	2.52	3H-3, 140	22.80	26.19	3H-CC	28.31	31.70
T	*Discoaster tamalis*	2.83	2.83	3H-CC	28.31	31.70	4H-2, 110	30.40	36.02
T	*Reticulofenestra pseudoumbilicus*	3.82	3.82	5H-4, 40	42.30	47.19	5H-5, 40	43.80	48.69
T	*Amaurolithus* spp.	4.56	4.56	6H-1, 110	48.00	52.36	6H-2, 110	49.50	53.86
B	*Ceratolithus rugosus*	5.1	5.1	8H-6, 120	74.60	82.50	8H-7, 50	75.40	83.30
B	*Ceratolithus acutus*	5.37	5.37	9H-2, 120	78.10	87.24	9H-3, 120	79.60	88.74
T	*Nicklithus amplificus*	6.00	6.00	10H-1, 120	86.10	95.18	10H-2, 40	86.80	95.88
B	*Nicklithus amplificus*	6.84	6.84	10H-5, 40	91.30	100.38	10H-5, 120	92.10	101.18
B	*Amaurolithus primus*	7.39	7.39	10H-7, 10	93.50	102.58	10H-7, 100	94.40	103.48
B	*Discoaster loeblichii*	8.43	8.43	10H-7, 100	94.40	103.48	10H-CC	94.95	104.03
T	*Discoaster hamatus*	9.63	9.63	10H-2, 40	86.80	95.88	10H-3, 40	88.30	97.38
B	*Discoaster bellus* gr. (*D. hamatus*)	10.48	10.48	11H-3, 40	97.80	106.61	11H-5, 56	100.96	109.77
B	*Discoaster druggii*	22.82	22.82	11H-CC	103.87	112.68	12H-1, 80	104.70	114.76
T	*Reticulofenestra umbilicus* >14 µm	31.7	31.7	13H-3, 110	117.50	129.07	13H-4, 110	119.00	130.57
T	*Ericsonia formosa*	32.9	32.9	13H-CC	122.80	134.37	14H-1, 40	123.30	136.45
T	*Discoaster saipanensis*	34.0	34.0	14H-CC	132.70	145.85	15H-1, 76	133.16	146.86
T	*Chiasmolithus grandis*	37.1	37.1	15H-1, 76	133.16	146.86	15H-2, 100	134.90	148.60
T	*Nannotetrina* spp.	42.3	42.3	15H-3, 40	135.80	149.50	15H-4, 110	138.00	151.70
B	*Reticulofenestra umbilicus* >14 µm	42.5	42.5	15H-4, 110	138.00	151.70	15H-5, 110	139.50	153.20
T	*Nannotetrina fulgens*	43.4	43.4	15H-5, 110	139.50	153.20	15H-6, 110	141.00	154.70
T	*Discoaster sublodoensis*	47.2	47.2	15H-CC	141.89	155.59	16H-CC	150.92	167.32
B	*Nannotetrina* spp.	47.8	47.8	17H-2, 30	153.20	170.01	17H-3, 30	154.70	171.51
T	*Discoaster lodoensis*	48.0	48.0	17H-2, 30	153.20	170.01	17H-3, 30	154.70	171.51
T	*Tribrachiatus orthostylus*	51.0	51.0	18H-1, 20	161.10	179.27	18H-2, 30	162.70	180.87
B	*Discoaster lodoensis*	52.4	52.4	19H-CC	179.63	199.10	20H-1, 20	180.10	201.15
T	*Discoaster multiradiatus*	53.0	53.0	19H-CC	179.63	199.10	20H-1, 20	180.10	201.15
B	*Sphenolithus radians*	53.3	53.3	20H-3, 20	183.10	204.15	20H-3, 30	183.20	204.25
B	*Tribrachiatus orthostylus*	53.4	53.4	20H-5, 30	186.20	207.25	20H-6, 30	187.30	208.35
B	*Discoaster diastypus*	53.9	53.9	21H-4, 20	193.40	215.45	21H-5, 30	195.00	217.05
T	*Fasciculithus* spp.			22H-4, 40	203.17	227.15	22H-6, 10	205.87	229.85
	Decrease *Fasciculithus* spp.			22H-6, 60	206.37	230.35	22H-6, 105	206.82	230.80
B	Increase *Zygrhablithus bijugatus*			22H-6, 60	206.37	230.35	22H-6, 105	206.82	230.80
B	*Rhomboaster* spp.			22H-7, 20	207.47	231.45	22H-7, 26	207.53	231.51
B	*Discoaster multiradiatus*	56.2	56.2	24H-4, 120	223.60	251.19	24H-5, 83	224.73	252.32
B	*Discoaster nobilis*	56.5	56.5	24H-6, 100	225.98	253.57	24H-CC	226.62	254.21
B	*Heliolithus riedelii*	57.3	57.3	26X-3, 110	240.20	271.93	26X-5, 107	243.17	274.90
B	*Discoaster mohleri*	57.5	57.5	26X-6, 37	243.97	275.70	26X-7, 60	245.20	276.93
B	*Heliolithus kleinpellii*	58.2	58.2	26X-CC	245.75	277.48	27X-1, 41	245.31	278.54
B	*Sphenolithus anarrhopus*	58.4	58.4	27X-1, 41	245.31	278.54	27X-1, 112	246.02	279.25
B	*Heliolithus cantabriae*	58.8	58.8	27X-2, 70	247.10	280.33	27X-2, 115	247.55	280.78
B	*Fasciculithus pileatus*	59.3	59.3	28X-4, 45	259.45	292.25	28X-5, 30	260.80	293.60
B	*Fasciculithus tympaniformis*	59.7	59.7	28X-5, 30	260.80	293.60	28X-5, 110	261.60	294.40
B	*Sphenolithus primus*	60.6	60.6	28X-CC	261.97	294.77	29X-1, 23	264.33	296.67
B	*Chiasmolithus danicus*	64.2	64.2	29X-CC	273.22	305.56	30X-5, 20	279.90	312.91
B	*Cruciplacolithus tenuis* s.s.	64.5	64.5	30X-5, 20	279.90	312.91	30X-6, 60	281.80	314.81
B	*Cruciplacolithus primus*	64.8	64.8	31X-1, 99	284.29	318.69	31X-2, 60	284.90	319.30
B	*Micula prinsii*	65.4	65.4	31X-7, 133	292.63	327.03	31X-CC	292.86	327.26
B	*Micula murus*	66.2	66.2	32X-3, 40	296.30	332.31	32X-5, 100	299.90	335.91
				208-1267B-			208-1267B-		
B	*Emiliania huxleyi*	0.26	0.26	1H-CC	3.08	3.08	2H-CC	12.80	13.73
T	*Pseudoemiliania lacunosa*	0.46	0.46	1H-CC	3.08	3.08	2H-CC	12.80	13.73
T	Large *Gephyrocapsa* spp.	1.22	1.22	1H-CC	3.08	3.08	2H-CC	12.80	13.73
B	Medium *Gephyrocapsa* spp.	1.69	1.69	2H-CC	12.80	13.73	3H-1, 100	13.60	16.34
T	*Discoaster brouweri* and *D. triradiatus*	1.95	1.95	2H-CC	12.80	13.73	3H-1, 100	13.60	16.34
T	*Discoaster pentaradiatus*	2.52	2.52	3H-CC	19.67	22.41	4H-CC	31.94	37.15
T	*Discoaster tamalis*	2.83	2.83	3H-CC	19.67	22.41	4H-CC	31.94	37.15
T	*Reticulofenestra pseudoumbilicus*	3.82	3.82	5H-CC	40.70	45.84	6H-CC	50.71	56.65
T	*Amaurolithus* spp.	4.56	4.56	5H-CC	40.70	45.84	6H-CC	50.71	56.65

Table T5 (continued).

	Datum	Age (Ma) Youngest	Age (Ma) Oldest	Top of sample interval Core, section, interval (cm)	Top of sample interval Depth (mbsf)	Top of sample interval Depth (mcd)	Base of sample interval Core, section, interval (cm)	Base of sample interval Depth (mbsf)	Base of sample interval Depth (mcd)
B	*Ceratolithus acutus*	5.37	5.37	9H-CC	79.35	90.70	10H-CC	87.38	96.90
T	*Sphenolithus pseudoradians*	29.1	29.1	12H-CC	107.05	117.66	13H-CC	116.56	128.53
T	*Reticulofenestra umbilicus* >14 µm	31.7	31.7	13H-CC	116.56	128.53	14H-CC	126.01	139.48
T	*Ericsonia formosa*	32.9	32.9	14H-CC	126.01	139.48	15H-CC	135.62	150.03
T	*Discoaster saipanensis*	34.0	34.0	14H-CC	126.01	139.48	15H-CC	135.62	150.03
T	*Nannotetrina* spp.	42.3	42.3	15H-CC	135.62	150.03	16H-CC	145.33	160.71
B	*Reticulofenestra umbilicus* >14 µm	42.5	42.5	15H-CC	135.62	150.03	16H-CC	145.33	160.71
B	*Nannotetrina* spp.	47.8	47.8	16H-CC	145.33	160.71	17H-CC	155.47	172.55
T	*Discoaster lodoensis*	48.0	48.0	16H-CC	145.33	160.71	17H-CC	155.47	172.55
T	*Tribrachiatus orthostylus*	51.0	51.0	17H-CC	155.47	172.55	18H-CC	164.81	182.59
B	*Discoaster lodoensis*	52.4	52.4	19H-CC	174.53	193.25	20H-CC	184.10	205.14
T	*Discoaster multiradiatus*	53.0	53.0	19H-CC	174.53	193.25	20H-CC	184.10	205.14
B	*Sphenolithus radians*	53.3	53.3	19H-CC	174.53	193.25	20H-CC	184.10	205.14
B	*Tribrachiatus orthostylus*	53.4	53.4	19H-CC	174.53	193.25	20H-CC	184.10	205.14
T	*Fasciculithus* spp.			22H-CC	203.01	227.32	23H-CC	212.33	238.16
	Increase *Zygrhablithus bijugatus*			22H-CC	203.01	227.32	23H-CC	212.33	238.16
B	*Discoaster multiradiatus*	56.2	56.2	23H-CC	212.33	238.16	24H-CC	222.10	249.87
B	*Discoaster mohleri*	57.5	57.5	26X-CC	236.60	267.27	27X-CC	242.92	278.27
B	*Heliolithus kleinpellii*	58.2	58.2	27X-CC	242.92	278.27	28X-CC	252.75	288.09
B	*Fasciculithus pileatus*	59.3	59.3	28X-CC	252.75	288.09	29X-CC	262.03	296.64
B	*Fasciculithus tympaniformis*	59.7	59.7	28X-CC	252.75	288.09	29X-CC	262.03	296.64
B	*Chiasmolithus danicus*	64.2	64.2	30X-CC	273.12	306.86	31X-CC	280.58	315.83
	Cruciplacolithus tenuis s.s.	64.5	64.5	30X-CC	273.12	306.86	31X-CC	280.58	315.83
B	*Cruciplacolithus primus*	64.8	64.8	30X-CC	273.12	306.86	31X-CC	280.58	315.83
B	*Micula prinsii*	65.4	65.4	31X-CC	280.58	315.83	32X-CC	290.68	325.28
B	*Micula murus*	66.2	66.2	32X-CC	290.68	325.28	33X-CC	300.43	337.07
B	*Lithraphidites quadratus*	67.5	67.5	35X-CC	319.59	358.34	36X-1, 33	319.73	358.48

Note: T = top, B = bottom.

Table T6. Stratigraphic ranges and relative abundances for selected calcareous nannofossil taxa, Site 1267. (This table is available in an **oversized format.**)

Table T7. Stratigraphic positions of selected planktonic foraminiferal datums, Site 1267.

	Datum	Age (Ma) Youngest	Age (Ma) Oldest	Hole, core, section, interval (cm)	Depth (mbsf)	Depth (mcd)	Hole, core, section, interval (cm)	Depth (mbsf)	Depth (mcd)
				208-			208-		
T	*Globorotalia tosaensis*	0.61	0.61	1267B-1H-CC	3.08	3.08	1267A-1H-3, 32–34	3.32	3.35
T	*Globigerinoides obliquus*	1.30	1.30	1267A-1H-3, 32–34	3.32	3.35	1267A-1H-5, 32–34	6.32	6.35
T	*Globigerina apertura*	1.68	1.68	1267A-1H-CC	8.85	8.88	1267A-2H-1, 32–34	9.22	9.89
T	*Globigerinoides extremus*	1.91	1.91	1267A-2H-5, 32–34	15.22	15.89	1267A-2H-7, 32–34	17.72	18.39
B	*Globorotalia truncatulinoides*	2.03	2.03	1267A-2H-CC	18.36	19.03	1267A-3H-1, 32–34	18.72	22.11
	Pulleniatina reappearance	2.28	2.28	1267A-2H-CC	18.36	19.03	1267A-3H-1, 32–34	18.72	22.11
T	*Globoturborotalita woodi*	2.30	2.30	1267A-3H-3, 32–34	21.72	25.11	1267A-3H-5, 32–34	24.72	28.11
T	*Globigerina decoraperta*	2.70	2.70	1267A-3H-3, 32–34	21.72	25.11	1267A-3H-5, 32–34	24.72	28.11
T	*Dentoglobigerina altispira*	3.02	3.02	1267B-4H-CC	31.94	37.15	1267A-4H-5, 32–34	34.12	39.74
T	*Sphaeroidinellopsis seminulina*	3.18	3.18	1267A-4H-CC	36.29	41.91	1267A-5H-1, 32–34	37.72	42.61
B	*Globorotalia tosaensis*	3.35	3.35	1267A-5H-3, 32–34	40.72	45.61	1267B-5H-CC	40.70	45.84
T	*Neogloboquadrina acostaensis*	3.83	3.83	1267B-5H-CC	40.70	45.84	1267A-5H-5, 32–34	43.72	48.61
T	*Globorotalia plesiotumida*	4.15	4.15	1267A-5H-5, 32–34	43.72	48.61	1267A-6H-1, 32–34	47.22	51.58
T	*Hirsutella cibaoensis*	4.16	4.16	1267A-5H-CC	47.14	52.03	1267A-6H-3, 32–34	50.22	54.58
B	*Globorotalia crassaformis* s.l.	4.31	4.31	1267A-7H-3, 32–34	59.72	67.08	1267A-7H-5, 32–34	62.72	70.08
T	*Globoturborotalita nepenthes*	4.37	4.37	1267A-7H-7, 32–34	65.69	73.05	1267A-7H-CC	66.07	73.43
B	*Sphaeroidinella dehiscens* s.l.	4.94	4.94	1267A-8H-7, 32–34	75.22	83.12	1267A-8H-CC	75.62	83.52
B	*Globigerinoides conglobatus*	5.84	5.84	1267A-9H-CC	82.94	92.08	1267A-10H-1, 32–34	85.22	94.30
B	*Globorotalia tumida*	5.96	5.96	1267A-9H-3, 32–34	78.72	87.86	1267B-9H-CC	79.35	90.70
B	*Hirsutella cibaoensis*	7.91	7.91	1267A-10H-6, 32–34	92.72	101.80	1267A-10H-CC	94.95	104.03
B	*Globorotalia plesiotumida*	8.91	8.91	1267A-10H-6, 32–34	92.72	101.80	1267A-10H-CC	94.95	104.03
B	*Globigerinoides extremus*	8.94	8.94	1267A-10H-6, 32–34	92.72	101.80	1267A-10H-CC	94.95	104.03
T	*Globigerina euapertura*	23.03	23.03	1267A-12H-CC	113.30	123.36	1267B-13H-CC	116.56	128.53
T	*Subbotina angiporoides*	30.00	30.00	1267A-12H-CC	113.30	123.36	1267B-13H-CC	116.56	128.53
T	*Globigerinatheka index*	34.30	34.30	1267B-14H-CC	126.01	139.48	1267A-14H-CC	132.70	145.85
T	*Subbotina linaperta*	37.70	37.70	1267B-16H-CC	145.33	160.71	1267A-16H-CC	150.92	167.32
T	*Morozovella spinulosa*	38.10	38.10	1267A-15H-CC	141.89	155.59	1267B-16H-CC	145.33	160.71
T	*Acarinina bullbrooki*	40.50	40.50	1267B-15H-CC	135.62	150.03	1267A-15H-CC	141.89	155.59
B	*Globigerinatheka index*	42.90	42.90	1267B-15H-CC	135.62	150.03	1267A-15H-CC	141.89	155.59
T	*Morozovella aragonensis*	43.60	43.60	1267B-15H-CC	135.62	150.03	1267A-15H-CC	141.89	155.59
T	*Morozovella formosa*	50.80	50.80	1267B-18H-CC	164.81	182.59	1267A-18H-CC	170.69	188.86
B	*Morozovella aragonensis*	52.76	52.76	1267B-19H-CC	174.53	193.25	1267A-19H-CC	179.63	199.10
T	*Morozovella marginodentata*			1267B-21H-CC	193.50	216.32	1267A-21H-CC	198.96	221.01
T	*Morozovella lensiformis*			1267B-18H-CC	164.81	182.59	1267A-18H-CC	170.69	188.86
B	*Acarinina angulosa*	52.78	52.78	1267A-21H-CC	198.96	221.01	1267B-22H-CC	203.01	227.32
T	*Morozovella aequa*	52.89	52.89	1267B-19H-CC	174.53	193.25	1267A-19H-CC	179.63	199.10
B	*Morozovella formosa*			1267B-19H-CC	174.53	193.25	1267A-19H-CC	179.63	199.10
T	*Subbotina triangularis*	54.07	54.07	1267A-22H-7, 28–29	207.55	231.53	1267A-22H-7, 37–38	207.64	231.62
B	*Morozovella lensiformis*	53.68	53.68	1267B-20H-CC	184.10	205.14	1267A-20H-CC	188.46	209.51
T	*Subbotina velascoensis*	54.17	54.17	1267A-19H-CC	179.63	199.10	1267B-20H-CC	184.10	205.14
T	*Morozovella velascoensis*	54.31	54.31	1267A-22H-7, 37–38	207.64	231.62	1267A-22H-CC	208.96	232.94
T	*Morozovella acuta*	54.70	54.70	1267A-22H-7, 37–38	207.64	231.62	1267A-22H-CC	208.96	232.94
B	*Igorina broedermanni*	54.70	54.70	1267B-21H-CC	193.50	216.32	1267A-21H-CC	198.96	221.01
B	*Morozovella marginodentata*	54.34	54.34	1267A-21H-CC	198.96	221.01	1267B-22H-CC	203.01	227.32
T	*Stensioeina beccariiformis**	55.00	55.00	1267A-22H-7, 28–29	207.55	231.53	1267A-22H-7, 37–38	207.64	231.62
B	*Globanomalina australiformis*	55.50	55.50	1267A-22H-6, 130–131	207.07	231.05	1267A-22H-6, 148–149	207.25	231.23
B	*Morozovella subbotinae*	55.90	55.90	1267B-23H-CC	212.33	238.16	1267A-23H-CC	218.33	243.25
T	*Globanomalina pseudomenardii*	55.90	55.90	1267A-22H-CC	208.96	232.94	1267B-23H-CC	212.33	238.16
T	*Acarinina nitida* (= *A. acarinata*)	56.30	56.30	1267A-22H-CC	208.96	232.94	1267B-23H-CC	212.33	238.16
T	*Acarinina mckannai*	56.30	56.30	1267A-22H-CC	208.96	232.94	1267B-23H-CC	212.33	238.16
B	*Acarinina soldadoensis*	56.50	56.50	1267A-24H-CC	226.62	254.21	1267B-25H-CC	231.47	261.42
B	*Acarinina coalingensis* (= *triplex*)	56.50	56.50	1267A-23H-CC	218.33	243.25	1267B-24H-CC	222.10	249.87
B	*Morozovella aequa*	56.50	56.50	1267B-22H-CC	203.01	227.32	1267A-22H-6, 130–131	207.07	231.05
B	*Acarinina mckannai*	59.10	59.10	1267B-26X-CC	236.60	267.27	1267A-26X-CC	245.75	277.48
B	*Acarinina subsphaerica*	59.20	59.20	1267A-26X-CC	245.75	277.48	1267B-27X-CC	242.92	278.27
B	*Acarinina nitida*	59.20	59.20	1267A-26X-CC	245.75	277.48	1267B-27X-CC	242.92	278.27
B	*Globanomalina pseudomenardii*	59.20	59.20	1267B-28X-CC	252.75	288.09	1267A-28X-CC	261.97	294.77
B	*Morozovella velascoensis*	60.00	60.00	1267A-27X-CC	253.25	286.48	1267B-28X-CC	252.75	288.09
B	*Igorina albeari*	60.00	60.00	1267A-27X-CC	253.25	286.48	1267B-28X-CC	252.75	288.09
B	*Acarinina strabocella*	60.50	60.50	1267A-28X-CC	261.97	294.77	1267B-29X-CC	262.03	296.64
B	*Morozovella conicotruncata*	60.90	60.90	1267A-28X-CC	261.97	294.77	1267B-29X-CC	262.03	296.64
B	*Morozovella angulata*	61.00	61.00	1267B-29X-CC	262.03	296.64	1267A-29X-CC	273.22	305.56
B	*Praemurica uncinata*	61.20	61.20	1267A-29X-CC	273.22	305.56	1267B-30X-CC	273.12	306.86
B	*Globanomalina compressa*	63.00	63.00	1267B-30X-CC	273.12	306.86	1267B-31X-CC	280.58	315.83
B	*Praemurica inconstans*	63.00	63.00	1267B-30X-CC	273.12	306.86	1267B-31X-CC	280.58	315.83
B	*Subbotina triloculinoides*	64.50	64.50	1267A-31X-1, 90–91	284.20	318.60	1267A-31X-2, 60–61	284.90	319.30
T	*Parvularugoglobigerina eugubina*	64.90	64.90	1267A-31X-3, 30–31	285.60	320.00	1267A-31X-3, 50–51	285.80	320.20
B	*Parvularugoglobigerina eugubina*	64.97	64.97	1267A-31X-3, 70–71	286.00	320.40	1267A-31X-3, 74–75	286.04	320.44
T	*Abathomphalus mayaroensis*	65.00	65.00	1267A-31X-3, 70–71	286.00	320.40	1267A-31X-3, 74–75	286.04	320.44

Notes: T = top, B = bottom. * = benthic foraminifer datum.

Table T8. Stratigraphic ranges and relative abundances for selected planktonic foraminifer taxa, Site 1267. (This table is available in an **oversized format.**)

Table T9. Occurrences of selected benthic foraminifer taxa, Site 1267. (This table is available in an **oversized format.**)

Table T10. Magnetostratigraphic age-depth tie points, Site 1267.

Chron	Age (Ma) 1	Age (Ma) 2	Top: Hole, core, section, interval (cm)	Top: Depth (mbsf)	Top: Depth (mcd)	Bottom: Hole, core, section, interval (cm)	Bottom: Depth (mbsf)	Bottom: Depth (mcd)
			208-			208-		
C1n (o)	0.781	0.780	1267B-2H-2, 125	5.85	6.78	1267A-1H-6, 100	8.50	8.53
C1r.1n (y)	0.988	0.990	1267B-2H-3, 145	7.55	8.48	1267B-2H-4, 25	7.85	8.78
C1r.1n (o)	1.072	1.070	1267B-2H-4, 95	8.55	9.48	1267B-2H-5, 5	9.15	10.08
C2n (y)	1.785	1.770	1267A-2H-6, 40	16.80	17.47	1267B-3H-2, 120	15.30	18.04
C2n (o)	1.942	1.950	1267B-3H-3, 110	16.70	19.44	1267B-3H-4, 5	17.15	19.89
C2An.1n (y)	2.582	2.581	1267B-4H-2, 145	25.05	30.26	1267B-4H-3, 85	25.95	31.16
C2An.3n (y)	3.333	3.333	1267B-5H-4, 10	36.20	41.34	1267B-5H-4, 75	36.85	41.99
C2An.3n (o)	3.596	3.580	1267B-5H-6, 35	39.45	44.59	1267B-5H-6, 50	39.60	44.74
C12n (y)		30.479	1267B-13H-3, 130	111.90	123.87	1267B-13H-4, 65	112.70	124.67
C12n (o)		30.939	1267B-13H-4, 105	113.10	125.07	1267B-13H-4, 115	113.20	125.17
C13n (y)		33.058	1267B-14H-5, 90	123.96	137.43	1267A-14H-2, 30	124.70	137.85
C13n (o)		33.545	1267A-14H-4, 130	128.70	141.85	1267A-14H-5, 100	129.90	143.05
C20n (y)		42.536	1267B-16H-1, 65	136.75	152.13	1267A-15H-5, 100	139.40	153.10
C20n (o)		43.789	1267B-16H-2, 105	138.65	154.03	1267A-15H-6, 95	140.85	154.55
C21n (y)		46.264	1267A-16H-3, 60	145.50	161.90	1267A-16H-4, 25	146.65	163.05
C22n (o)		49.714	1267B-18H-3, 35	158.45	176.23	1267A-17H-7, 65	160.55	177.36
C25n (y)		55.904	1267A-24H-3, 15	221.05	248.64	1267A-24H-3, 95	221.85	249.44
C25n (o)		56.391	1267A-24H-5, 90	224.80	252.39	1267A-24H-6, 20	225.18	252.77
C26n (y)		57.554	1267B-27X-4, 130	240.20	275.55	1267B-27X-4, 135	240.25	275.60
C26n (o)		57.911	1267B-27X-6, 20	242.10	277.45	1267B-27X-6, 30	242.20	277.55
C27n (y)		60.920	1267B-30X-1, 90	264.20	297.94	1267A-29X-2, 105	266.65	298.99
C27n (o)		61.276	1267B-30X-3, 110	267.40	301.14	1267B-30X-3, 140	267.70	301.44
C28n (y)		62.499	1267B-30X-7, 45	272.75	306.49	1267A-30X-1, 75	274.45	307.46
C28n (o)		63.634	1267B-31X-3, 140	277.30	312.55	1267A-30X-5, 10	279.80	312.81
C29n (y)		63.976	1267A-30X-5, 105	280.75	313.76	1267B-31X-4, 140	278.80	314.05
C29n (o)		64.745	1267B-31X-5, 115	280.05	315.30	1267B-32X-2, 90	283.40	318.00
C30n (y)		65.578	1267A-31X-7, 125	292.55	326.95	1267B-33X-1, 60	291.20	327.84
C30n (o)		67.610	1267B-36X-2, 90	321.80	360.55	1267B-36X-2, 100	321.90	360.65
C31n (y)		67.735	1267B-36X-3, 120	323.60	362.35	1267B-36X-3, 140	323.80	362.55

Notes: o = old end of chron, y = young end of chron. 1 = ages as in Lourens et al. (in press), 2 = ages as in Cande and Kent (1995).

Table T11. Interstitial water analyses, Hole 1267A.

Core, section, interval (cm)	Depth (mcd)	pH	Alkalinity (mM)	Salinity	Cl (mM)	SO_4 (mM)	Na (mM)	Mg (mM)	Ca (mM)	K (mM)	B (µM)	Fe (µM)	Mn (µM)	Li (µM)	Ba (µM)	Sr (µM)	Si (µM)
208-1267A-																	
1H-5, 145–150	7.5	7.45	3.34	34.0	562	25.0	471	52.4	10.1	10.8	478	0.00	0.21	24.6	0.24	143	369
2H-5, 140–150	17.0	7.42	2.66	35.0	568	25.3	475	52.2	10.6	10.4	474	0.00	5.59	23.6	0.26	212	207
3H-5, 140–150	29.2	7.44	2.57	35.0	534	25.2	463	51.9	11.0	9.8	465	0.00	2.16	23.7	0.21	274	179
4H-4, 140–150	39.3	7.44	2.53	35.0	567	25.0	473	53.6	12.1	10.2	473	0.00	0.98	25.8	0.22	320	195
5H-5, 140–150	49.7	7.44	2.54	35.0	567	21.8	477	51.7	12.5	10.0	476	0.00	0.51	24.4	0.25	359	207
6H-5, 140–150	58.7	7.43	2.34	35.0	565	24.1	475	50.3	12.7	9.9	460	0.00	0.52	26.2	0.25	388	192
7H-5, 140–150	71.2	7.32	2.25	35.0	523	22.3	468	50.2	13.3	9.6	469	1.40	0.89	26.0	0.32	386	206
8H-5, 140–150	81.2	7.30	2.19	35.0	567	24.0	472	49.5	13.8	9.3	472	0.80	1.46	27.9	0.24	412	207
9H-3, 140–150	88.9	7.34	2.18	35.0	567	23.9	476	50.7	14.2	9.5	480	0.00	3.21	28.3	0.28	407	229
10H-5, 140–150	101.4	7.34	2.18	35.0	567	23.4	466	49.0	14.4	9.3	510	0.00	3.81	29.0	0.22	391	240
11H-5, 140–150	110.6	ND	ND	ND	ND	ND	467	48.7	16.6	9.2	711	2.15	1.34	28.8	0.47	397	365
13H-2, 140–150	127.9	7.41	2.01	35.0	565	22.2	476	47.8	16.2	9.2	530	0.00	0.35	31.2	0.24	359	267
16H-4, 140–150	164.2	7.47	1.86	35.0	564	22.7	481	47.0	18.3	8.6	512	0.14	0.61	32.2	0.30	325	333
17H-4, 140–150	174.1	7.42	1.83	35.0	564	23.4	473	45.9	18.7	8.5	464	0.00	0.17	35.3	0.28	322	385
18H-5, 140–150	186.5	7.37	1.81	35.0	563	22.9	475	46.7	19.3	8.3	471	0.00	0.28	33.1	0.25	316	486
19H-5, 140–150	196.8	7.41	1.79	34.5	566	20.6	472	47.2	19.0	8.6	453	0.00	0.23	35.5	0.27	302	509
23H-5, 140–150	240.7	7.38	1.52	35.0	569	22.6	465	44.3	21.2	8.2	442	0.00	0.67	36.4	2.83	275	704
25H-5, 140–150	264.7	7.38	1.46	35.0	565	21.9	470	43.9	22.4	8.4	465	0.00	0.84	39.1	0.35	273	672
26X-5, 140–150	275.2	7.28	1.78	35.0	567	22.2	470	43.0	23.2	8.0	446	0.00	0.96	40.1	0.35	279	651
27X-4, 140–150	284.0	7.36	1.81	35.0	560	21.5	459	42.0	22.7	7.4	460	0.16	3.54	40.1	0.38	263	545
28X-3, 140–150	291.7	7.36	1.77	35.0	569	21.7	465	42.8	23.7	7.3	471	0.00	5.20	40.7	0.42	264	468
32X-4, 140–150	334.8	7.40	1.17	34.5	568	21.7	478	40.8	26.9	7.1	502	0.00	8.72	39.8	0.51	252	370
33X-5, 140–150	346.8	7.39	1.29	35.5	565	21.6	471	53.6	26.6	6.9	498	0.00	9.62	40.4	0.43	255	338

Notes: ND = not determined.

Table T12. Sedimentary calcium carbonate concentrations, Site 1267.

Core, section, interval (cm)	Depth (mcd)	$CaCO_3$ (wt%)
208-1267A-		
1H-1, 72–73	0.75	87.8
1H-3, 72–73	3.75	94.6
1H-5, 72–73	6.75	93.6
2H-1, 72–73	10.29	91.0
2H-3, 72–73	13.29	93.9
2H-5, 72–73	16.29	92.5
3H-1, 72–73	22.51	93.2
3H-3, 72–73	25.51	93.6
3H-5, 72–73	28.51	95.0
4H-1, 72–73	34.24	94.0
4H-3, 72–73	37.14	95.6
4H-5, 72–73	40.14	94.6
5H-1, 72–73	43.01	91.6
5H-3, 72–73	46.01	95.0
5H-5, 72–73	49.01	95.1
6H-1, 72–73	51.98	94.7
6H-3, 72–73	54.98	97.0
6H-5, 72–73	57.98	95.1
7H-1, 72–73	64.48	95.6
7H-3, 72–73	67.48	94.8
7H-5, 72–73	70.48	89.1
8H-1, 72–73	74.52	94.5
8H-3, 72–73	77.52	95.0
8H-5, 72–73	80.52	94.9
9H-1, 72–73	85.26	92.3
9H-5, 72–73	91.26	76.9
10H-3, 72–73	97.70	85.1
10H-5, 72–73	100.70	86.7
11H-1, 72–73	103.93	75.3
11H-3, 72–73	106.93	27.2
11H-5, 72–73	109.93	41.3
13H-1, 72–73	125.69	83.6
13H-3, 72–73	128.69	82.1
13H-5, 72–73	131.69	90.9
14H-1, 72–73	136.77	90.3
14H-3, 72–73	139.77	82.7
14H-5, 72–73	142.77	71.5
15H-1, 72–73	146.82	51.7
15H-3, 72–73	149.82	52.0
15H-5, 72–73	152.82	60.1
16H-1, 72–73	159.02	90.6
16H-3, 72–73	162.02	89.5
16H-5, 55–56	164.85	88.6
17H-1, 72–73	168.93	93.0
17H-3, 72–73	171.93	83.0
17H-5, 72–73	174.93	90.9
18H-1, 72–73	179.79	93.8
18H-3, 72–73	182.79	93.5
18H-5, 72–73	185.79	94.4
19H-1, 72–73	190.59	94.8
19H-3, 72–73	193.59	93.6
19H-5, 72–73	196.15	95.4
20H-1, 72–73	201.67	93.8
20H-3, 72–73	204.67	93.6
20H-5, 77–78	207.72	92.7
21H-1, 72–73	212.17	92.6
21H-3, 72–73	214.47	89.2
21H-5, 72–73	217.47	92.4
21H-7, 72–73	220.47	94.1
22H-1, 72–73	223.60	91.3
22H-3, 72–73	225.97	93.8
22H-6, 90–90	230.65	92.6
22H-6, 100–100	230.75	90.5
22H-6, 110–110	230.85	92.9
22H-6, 120–120	230.95	87.2
22H-6, 125–125	231.00	89.2
22H-6, 130–130	231.05	83.2
22H-6, 135–135	231.10	90.1
22H-6, 140–140	231.15	89.1
22H-6, 142–142	231.17	89.6
22H-6, 144–144	231.19	86.5
22H-6, 148–148	231.23	79.6
22H-6, 150–150	231.25	76.0
22H-7, 2–2	231.27	67.0
22H-7, 4–4	231.29	59.5
22H-7, 6–6	231.31	57.6
22H-7, 8–8	231.33	57.1
22H-7, 10–10	231.35	52.7
22H-7, 12–12	231.37	46.6
22H-7, 14–14	231.39	43.9
22H-7, 16–16	231.41	38.8
22H-7, 18–18	231.43	27.1
22H-7, 20–20	231.45	2.9
22H-7, 22–22	231.47	2.5
22H-7, 24–24	231.49	1.1
22H-7, 26–26	231.51	0.9
22H-7, 28–28	231.53	0.7
22H-7, 30–30	231.55	1.7
22H-7, 32–32	231.57	1.4
22H-7, 35–35	231.60	79.6
22H-7, 40–40	231.65	77.8
22H-7, 45–45	231.70	84.0
22H-7, 50–50	231.75	85.2
22H-7, 60–60	231.85	83.4
22H-7, 70–70	231.95	86.5
23H-1, 72–73	234.04	92.1
23H-3, 72–73	237.04	89.1
23H-5, 72–73	240.04	94.1
24H-1, 72–73	246.21	92.0
24H-3, 72–73	249.21	92.8
24H-5, 72–73	252.21	89.1
25H-1, 72–73	258.05	84.2
25H-3, 72–73	261.05	93.6
25H-5, 72–73	264.05	88.5
26X-1, 72–73	268.55	86.6
26X-5, 72–73	274.55	89.5
27X-1, 72–73	278.85	82.2
27X-3, 72–73	281.85	82.7
27X-5, 72–73	284.85	85.1
28X-1, 53–54	287.83	84.7
28X-5, 72–73	294.02	82.6
29X-1, 72–73	297.16	80.3
29X-3, 72–73	300.16	80.9
29X-5, 72–73	303.16	77.1
30X-1, 72–73	307.43	76.9
30X-3, 72–73	310.43	76.6
32X-1, 72–73	329.63	79.0
33X-1, 74–75	340.19	73.6
33X-3, 70–71	343.13	63.1
33X-5, 74–75	346.17	83.2
208-1267B-		
23H-3, 0–0	230.53	91.2
23H-3, 10–10	230.63	88.5
23H-3, 20–20	230.73	88.8
23H-3, 30–30	230.83	89.8
23H-3, 40–40	230.93	90.6
23H-3, 45–45	230.98	89.3
23H-3, 50–50	231.03	87.1
23H-3, 55–55	231.08	90.4
23H-3, 60–60	231.13	89.9
23H-3, 65–65	231.18	84.1
23H-3, 68–68	231.21	79.8
23H-3, 70–70	231.23	77.8
23H-3, 72–72	231.25	70.1
23H-3, 74–74	231.27	56.6
23H-3, 76–76	231.29	56.4
23H-3, 78–78	231.31	53.2
23H-3, 80–80	231.33	53.7
23H-3, 82–82	231.35	48.1
23H-3, 84–84	231.37	42.2
23H-3, 86–86	231.39	38.1
23H-3, 88–88	231.41	20.5
23H-3, 90–90	231.43	6.2
23H-3, 92–92	231.45	5.3
23H-3, 94–94	231.47	1.8
23H-3, 96–96	231.49	0.9
23H-3, 98–98	231.51	1.2
23H-3, 100–100	231.53	1.4
23H-3, 102–102	231.55	52.1
23H-3, 104–104	231.57	80.1
23H-3, 106–106	231.59	81.0
23H-3, 108–108	231.61	81.6
23H-3, 110–110	231.63	78.3
23H-3, 115–115	231.68	83.9
23H-3, 120–120	231.73	87.1
23H-3, 130–130	231.83	83.5
23H-3, 140–140	231.93	86.0
23H-3, 150–150	232.03	87.6

Table T13. Age-depth control points, Site 1267. (**See table notes.** Continued on next two pages.)

	Datum	Type	Upper depth (mcd)	Lower depth (mcd)	Minimum age (Ma)	Maximum age (Ma)
B	*Emiliania huxleyi*	CN	0.04	0.83	0.26	0.26
T	*Pseudoemiliania lacunosa*	CN	2.43	3.93	0.46	0.46
T	*Globorotalia tosaensis*	PF	3.08	3.35	0.61	0.61
T	*Globigerinoides obliquus*	PF	3.35	6.35	1.30	1.30
B	*Gephyrocapsa parallela* (= reent. Medium *G.*)	CN	6.53	8.03	1.01	1.01
	C1n (o)	PMAG	6.78	8.53	0.781	0.781
	C1r.1n (y)	PMAG	8.48	8.78	0.988	0.988
T	*Globigerina apertura*	PF	8.88	9.89	1.68	1.68
	C1r.1n (o)	PMAG	9.48	10.08	1.072	1.072
T	Large *Gephyrocapsa* spp.	CN	10.77	11.72	1.22	1.22
B	Large *Gephyrocapsa* spp.	CN	13.62	14.72	1.58	1.58
T	*Globigerinoides extremus*	PF	15.89	18.39	1.91	1.91
B	Medium *Gephyrocapsa* spp.	CN	16.22	17.37	1.69	1.69
	C2n (y)	PMAG	17.47	18.04	1.785	1.785
B	*Globorotalia truncatulinoides*	PF	19.03	22.11	2.03	2.03
	Pulleniatina reappearance	PF	19.03	22.11	2.28	2.28
T	*Discoaster brouweri* and *D. triradiatus*	CN	19.03	21.99	1.95	1.95
	C2n (o)	PMAG	19.44	19.89	1.942	1.942
T	*Globoturborotalita woodi*	PF	25.11	28.11	2.30	2.30
T	*Globigerina decoraperta*	PF	25.11	28.11	2.70	2.70
T	*Discoaster pentaradiatus*	CN	26.19	31.70	2.52	2.52
	C2An.1n (y)	PMAG	30.26	31.16	2.582	2.582
T	*Discoaster tamalis*	CN	31.70	36.02	2.83	2.83
T	*Dentoglobigerina altispira*	PF	37.15	39.74	3.02	3.02
	C2An.3n (y)	PMAG	41.34	41.99	3.330	3.330
T	*Sphaeroidinellopsis seminulina*	PF	41.91	42.61	3.18	3.18
	C2An.3n (o)	PMAG	44.59	44.74	3.596	3.596
B	*Globorotalia tosaensis*	PF	45.61	45.84	3.35	3.35
T	*Neogloboquadrina acostaensis*	PF	45.84	48.61	3.83	3.83
T	*Reticulofenestra pseudoumbilicus*	CN	47.19	48.69	3.82	3.82
T	*Globorotalia plesiotumida*	PF	48.61	51.58	4.15	4.15
T	*Hirsutella cibaoensis*	PF	52.03	54.58	4.16	4.16
T	*Amaurolithus* spp.	CN	52.36	53.86	4.56	4.56
B	*Globorotalia crassaformis* s.l.	PF	67.08	70.08	4.31	4.31
T	*Globoturborotalita nepenthes*	PF	73.05	73.43	4.37	4.37
B	*Ceratolithus rugosus*	CN	82.50	83.30	5.1	5.1
B	*Sphaeroidinella dehiscens* s.l.	PF	83.12	83.52	4.94	4.94
B	*Ceratolithus acutus*	CN	87.24	88.74	5.37	5.37
B	*Globorotalia tumida*	PF	87.86	90.70	5.96	5.96
B	*Globigerinoides conglobatus*	PF	92.08	94.30	5.84	5.84
T	*Nicklithus amplificus*	CN	95.18	95.88	6.00	6.00
B	*Nicklithus amplificus*	CN	100.38	101.18	6.84	6.84
B	*Hirsutella cibaoensis*	PF	101.80	104.03	7.91	7.91
B	*Globorotalia plesiotumida*	PF	101.80	104.03	8.91	8.91
B	*Globigerinoides extremus*	PF	101.80	104.03	8.94	8.94
B	*Amaurolithus primus*	CN	102.58	103.48	7.39	7.39
B	*Discoaster loeblichii*	CN	103.48	104.03	8.43	8.43
B	*Discoaster bellus* gr. (*D. hamatus*)	CN	106.61	109.77	10.48	10.48
B	*Discoaster druggii*	CN	112.68	114.76	22.82	22.82
T	*Globigerina euapertura*	PF	123.36	128.53	23.03	23.03
T	*Subbotina angiporoides*	PF	123.36	128.53	30.00	30.00
	C12n (y)	PMAG	123.87	124.67	30.479	30.479
	C12n (o)	PMAG	125.07	125.17	30.939	30.939
T	*Reticulofenestra umbilicus* >14 m	CN	129.07	130.57	31.7	31.7
T	*Ericsonia formosa*	CN	134.37	136.45	32.9	32.9
	C13n (y)	PMAG	137.43	137.85	33.058	33.058
T	*Globigerinatheka index*	PF	139.48	145.85	34.30	34.30
	C13n (o)	PMAG	141.85	143.05	33.545	33.545
T	*Discoaster saipanensis*	CN	145.85	146.86	34.0	34.0
T	*Chiasmolithus grandis*	CN	146.86	148.60	37.1	37.1
T	*Nannotetrina* spp.	CN	149.50	151.70	42.3	42.3
T	*Acarinina bullbrooki*	PF	150.03	155.59	40.50	40.50
B	*Globigerinatheka index*	PF	150.03	155.59	42.90	42.90
T	*Morozovella aragonensis*	PF	150.03	155.59	43.60	43.60
B	*Reticulofenestra umbilicus* >14 m	CN	151.70	153.20	42.5	42.5
	C20n (y)	PMAG	152.13	153.10	42.536	42.536
T	*Nannotetrina fulgens*	CN	153.20	154.70	43.4	43.4
	C20n (o)	PMAG	154.03	154.55	43.789	43.789

Table T13 (continued).

	Datum	Type	Upper depth (mcd)	Lower depth (mcd)	Minimum age (Ma)	Maximum age (Ma)
T	*Morozovella spinulosa*	PF	155.59	160.71	38.10	38.10
T	*Discoaster sublodoensis*	CN	155.59	167.32	47.2	47.2
T	*Subbotina linaperta*	PF	160.71	167.32	37.70	37.70
	C21n (y)	PMAG	161.90	163.05	46.264	46.264
B	*Nannotetrina* spp.	CN	170.01	171.51	47.8	47.8
T	*Discoaster lodoensis*	CN	170.01	171.51	48.0	48.0
	C22n (o)	PMAG	176.23	177.36	49.714	49.714
T	*Tribrachiatus orthostylus*	CN	179.27	180.87	51.0	51.0
T	*Morozovella formosa*	PF	182.59	188.86	50.80	50.80
B	*Morozovella aragonensis*	PF	193.25	199.10	52.76	52.76
T	*Morozovella aequa*	PF	193.25	199.10	52.89	52.89
T	*Subbotina velascoensis*	PF	199.10	205.14	54.17	54.17
B	*Discoaster lodoensis*	CN	199.10	201.15	52.4	52.4
T	*Discoaster multiradiatus*	CN	199.10	201.15	53.0	53.0
B	*Sphenolithus radians*	CN	204.15	204.25	53.3	53.3
B	*Morozovella lensiformis*	PF	205.14	209.51	53.68	53.68
B	*Tribrachiatus orthostylus*	CN	207.25	208.35	53.4	53.4
B	*Discoaster diastypus*	CN	215.45	217.05	53.9	53.9
B	*Igorina broedermanni*	PF	216.32	221.01	54.70	54.70
B	*Acarinina angulosa*	PF	221.01	227.32	52.78	52.78
B	*Morozovella marginodentata*	PF	221.01	227.32	54.34	54.34
B	*Morozovella aequa*	PF	227.32	231.05	56.50	56.50
B	*Globanomalina australiformis*	PF	231.05	231.23	55.50	55.50
T	*Subbotina triangularis*	PF	231.53	231.62	54.07	54.07
T	*Stensioeina beccariiformis*	BF	231.53	231.62	55.0	55.0
T	*Morozovella acuta*	PF	231.62	232.94	54.70	54.70
T	*Globanomalina pseudomenardii*	PF	232.94	238.16	55.90	55.90
T	*Acarinina nitida* (= *A. acarinata*)	PF	232.94	238.16	56.30	56.30
T	*Acarinina mckannai*	PF	232.94	238.16	56.30	56.30
B	*Morozovella subbotinae*	PF	238.16	243.25	55.90	55.90
B	*Acarinina coalingensis* (= *triplex*)	PF	243.25	249.87	56.50	56.50
	C25n (y)	PMAG	248.64	249.44	55.904	55.904
B	*Discoaster multiradiatus*	CN	251.19	252.32	56.2	56.2
	C25n (o)	PMAG	252.39	252.77	56.391	56.391
B	*Discoaster nobilis*	CN	253.57	254.21	56.5	56.5
B	*Acarinina soldadoensis*	PF	254.21	261.42	56.50	56.50
B	*Acarinina mckannai*	PF	267.27	277.48	59.10	59.10
B	*Heliolithus riedelii*	CN	271.93	274.90	57.3	57.3
	C26n (y)	PMAG	275.55	275.60	57.554	57.554
B	*Discoaster mohleri*	CN	275.70	276.93	57.5	57.5
	C26n (o)	PMAG	277.45	277.55	57.911	57.911
B	*Acarinina subsphaerica*	PF	277.48	278.27	59.20	59.20
B	*Acarinina nitida*	PF	277.48	278.27	59.20	59.20
B	*Heliolithus kleinpellii*	CN	277.48	278.54	58.2	58.2
B	*Sphenolithus anarrhopus*	CN	278.54	279.25	58.4	58.4
B	*Heliolithus cantabriae*	CN	280.33	280.78	58.8	58.8
B	*Morozovella velascoensis*	PF	286.48	288.09	60.00	60.00
B	*Igorina albeari*	PF	286.48	288.09	60.00	60.00
B	*Globanomalina pseudomenardii*	PF	288.09	294.77	59.20	59.20
B	*Fasciculithus pileatus*	CN	292.25	293.60	59.3	59.3
B	*Fasciculithus tympaniformis*	CN	293.60	294.40	59.7	59.7
B	*Acarinina strabocella*	PF	294.77	296.64	60.50	60.50
B	*Morozovella conicotruncata*	PF	294.77	296.64	60.90	60.90
B	*Sphenolithus primus*	CN	294.77	296.67	60.60	60.6
B	*Morozovella angulata*	PF	296.64	305.56	61.00	61.00
	C27n (y)	PMAG	297.94	298.99	60.920	60.920
	C27n (o)	PMAG	301.14	301.44	61.276	61.276
B	*Praemurica uncinata*	PF	305.56	306.86	61.20	61.20
B	*Globanomalina compressa*	PF	306.86	315.83	63.00	63.00
B	*Praemurica inconstans*	PF	306.86	315.83	63.00	63.00
B	*Chiasmolithus danicus*	CN	305.56	312.91	64.20	64.2
	C28n (y)	PMAG	306.49	307.46	62.499	62.499
	C28n (o)	PMAG	312.55	312.81	63.634	63.634
B	*Cruciplacolithus tenuis* s.s.	CN	312.91	314.81	64.50	64.5
	C29n (y)	PMAG	313.76	314.05	63.976	63.976
	C29n (o)	PMAG	315.30	318.00	64.745	64.745
B	*Cruciplacolithus primus*	CN	318.69	319.30	64.8	64.8
B	*Subbotina triloculinoides*	PF	318.60	319.30	64.50	64.50
T	*Parvularugoglobigerina eugubina*	PF	320.00	320.20	64.90	64.90

Table T13 (continued).

	Datum	Type	Upper depth (mcd)	Lower depth (mcd)	Minimum age (Ma)	Maximum age (Ma)
B	*Parvularugoglobigerina eugubina*	PF	320.40	320.44	64.97	64.97
T	*Abathomphalus mayaroensis*	PF	320.40	320.44	65.00	65.00
	C30n (y)	PMAG	326.95	327.84	65.578	65.578
B	*Micula prinsii*	CN	327.03	327.26	65.40	65.40
B	*Micula murus*	CN	332.31	335.91	66.20	66.20
	C30n (o)	PMAG	360.55	360.65	67.610	67.610
	C31n (y)	PMAG	362.35	362.55	67.735	67.735

Notes: T = top, B = bottom. o = oldest, y = youngest. PF = planktonic foraminifers, CN = calcareous nannoplankton, PMAG = paleomagnetic reversals, BF = benthic foraminifers. This table is also available in **ASCII.**

Table T14. Age model, linear sedimentation rates, and mass accumulation rates, Site 1267.

Age (Ma)	Depth (mcd)	LSR	Growth factor	Corrected LSR	Dry density (g/cm^3)	$CaCO_3$ (wt%)	Total MAR (g/cm^2/k.y.)	$CaCO_3$ MAR (g/cm^2/k.y.)	Noncarbonate MAR (g/cm^2/k.y.)
1	8.73	8.73	1.15	7.59	0.95	92.0	0.72	0.666	0.058
2	20.42	11.69	1.15	10.16	1.10	92.4	1.11	1.031	0.084
3	37.13	16.70	1.15	14.53	1.15	93.9	1.68	1.575	0.102
4	49.58	12.46	1.15	10.83	1.17	94.3	1.27	1.197	0.072
5	79.31	29.72	1.15	25.85	1.15	94.9	2.96	2.811	0.152
6	95.53	16.22	1.15	14.11	1.14	84.6	1.61	1.360	0.247
7	101.51	5.98	1.15	5.11	1.09	85.4	0.56	0.478	0.081
8	103.45	1.94	1.15	1.65	1.11		0.18		
9	104.54	1.09	1.15	1.10	1.30	75.3	0.14	0.107	0.035
10	106.35	1.81	1.15	1.53					
11	107.39	1.04	1.15	0.91	1.08	27.2	0.10	0.027	0.071
12	107.90	0.51	1.15	0.44					
13	108.38	0.48	1.15	0.42					
14	108.89	0.51	1.15	0.44					
15	109.43	0.54	1.15	0.47					
16	110.00	0.57	1.15	0.50	1.25	41.3	0.06	0.026	0.037
17	110.60	0.60	1.15	0.52					
18	111.20	0.61	1.15	0.53		87.4			
19	111.82	0.62	1.15	0.54					
20	112.46	0.64	1.15	0.55					
21	113.12	0.67	1.15	0.58					
22	113.84	0.72	1.15	0.62					
23	114.66	0.81	1.15	0.71					
24	115.58	0.92	1.15	0.80	1.25		0.10		
25	116.60	1.02	1.15	0.88					
26	117.72	1.12	1.15	0.97	1.29		0.13		
27	118.95	1.23	1.15	1.07					
28	120.30	1.36	1.15	1.18					
29	121.79	1.49	1.15	1.30	1.38		0.18		
30	123.43	1.64	1.15	1.42	1.32		0.19		
31	125.34	1.91	1.15	1.66					
32	130.61	5.27	1.15	4.58	1.28	82.9	0.59	0.486	0.100
33	137.04	6.43	1.15	5.59	1.28	90.6	0.72	0.650	0.067
34	146.00	8.96	1.15	7.79	1.39	77.1	1.09	0.837	0.249
35	147.17	1.17	1.15	1.02	1.39	51.7	0.14	0.073	0.068
36	147.59	0.42	1.15	0.37					
37	148.03	0.44	1.15	0.38					
38	148.50	0.47	1.15	0.41					
39	148.98	0.48	1.15	0.42					
40	149.46	0.48	1.15	0.42					
41	149.94	0.48	1.15	0.42	1.34	52.0	0.06	0.029	0.027
42	150.96	1.02	1.15	0.89	0.99	0.0	0.09	0.000	0.088
43	153.04	2.08	1.15	1.81	1.33	60.1	0.24	0.145	0.096
44	154.86	1.82	1.15	1.58					
45	157.83	2.97	1.15	2.58	1.41		0.36		
46	161.46	3.63	1.15	3.16	1.16	90.6	0.37	0.332	0.034
47	165.93	4.47	1.15	3.89	1.29	88.3	0.50	0.445	0.059
48	170.76	4.83	1.15	4.20	1.19	93.0	0.50	0.464	0.035
49	174.58	3.82	1.15	3.32	1.28	83.3	0.42	0.354	0.071
50	177.39	2.81	1.15	2.44	1.30	90.9	0.32	0.289	0.029
51	179.27	1.88	1.15	1.64					
52	194.14	14.87	1.15	12.93	1.32	94.0	1.71	1.605	0.102
53	201.00	6.86	1.15	5.97	1.31	95.4	0.78	0.748	0.036
54	217.77	16.77	1.15	14.59	1.32	92.4	1.93	1.779	0.146
55	231.50	13.73	1.15	11.94	1.32	63.1	1.58	0.997	0.583
56	249.98	18.48	1.15	16.07	1.40	65.4	2.24	1.467	0.777
57	266.74	16.76	1.15	14.57	1.40	88.3	2.04	1.801	0.238
58	277.67	10.92	1.15	9.50	1.42	86.4	1.35	1.169	0.184
59	285.00	7.34	1.15	6.38	1.37	82.2	0.87	0.718	0.155
60	294.41	9.41	1.15	8.18	1.37	85.0	1.12	0.951	0.168
61	299.12	4.71	1.15	4.10	1.38	80.3	0.57	0.454	0.111
62	304.64	5.52	1.15	4.80	1.33	79.0	0.64	0.503	0.134
63	309.48	4.84	1.15	4.21	1.29	76.9	0.54	0.418	0.126
64	314.01	4.52	1.15	3.93	1.36	76.6	0.53	0.409	0.125
65	320.42	6.41	1.15	5.58	1.45		0.81		
66	330.58	10.16	1.15	8.84	1.38	79.0	1.22	0.961	0.256
67	348.67	18.09	1.15	15.73	1.48	76.3	2.32	1.770	0.551

Notes: LSR = linear sedimentation rate, MAR = mass accumulation rate. This table is also available in ASCII.